3-in-1 Nanotherapeutic Strategies for Ovarian Cancer

Emma Durocher

Thesis submitted to the University of Ottawa in partial fulfillment of the requirements for the Masters of Science degree in Cellular and Molecular Medicine

Department of Cellular and Molecular Medicine

Faculty of Medicine

University of Ottawa, Ontario Canada

Abstract

Among gynecological cancers, ovarian cancer causes the most fatalities. Currently, cisplatin is a potent chemotherapy used for treatment. However, cisplatin efficacy remains limited due to chemotherapy resistance. DNA repair and altered metabolism are two resistance mechanisms that prevent effective cytotoxicity. Olaparib and metformin have improved cisplatin sensitivity by targeting these two mechanisms, respectively. Although previous studies have demonstrated that cisplatin combined with either olaparib or metformin have shown stronger efficacy than a single drug alone, non-selective distribution causes systemic toxicity, thus preventing full benefit. In this context, cancer nanotechnology has several advantages, including targeted drug delivery. Therefore, we hypothesized that the combination of cisplatin, olaparib, and metformin encapsulated into a single nanoparticle (NP) will improve overall survival in ovarian cancer compared to free drugs in combination. We first developed cisplatin and metformin conjugates for increased encapsulation into polymeric NPs. The synergistic ratio between cisplatin, olaparib, and metformin was identified using CompuSyn and Synergy Finder software. Self-assembly PLGA-PEG NPs were synthesized, encapsulating the cisplatin polymers, olaparib, and metformin derivatives. Final NP formulations were selected based on the most optimal values in terms of size, morphology, polydispersity index, surface charge, and encapsulation efficiency. Preliminary evidence using flow cytometry and western blot analysis demonstrated the individual drug efficacy in the triple combination NP following endosomal escape in SKOV-3 cells. Initial NP cytotoxicity studies were conducted using low cisplatin concentrations given the synergistic combination with olaparib and metformin. Taken together, the results provide insight into novel nanotherapeutic strategies for improving ovarian cancer treatment.

Acknowledgements

I'd like to first thank my supervisor, Dr. Suresh Gadde, for the continuous support throughout my Masters. Thank you for teaching and guiding me these past 2 years and being available for all my questions. It has been a pleasure working in your lab. Thank you to CIHR, University of Ottawa, and INTBIOTECH for funding this research. Additionally, I'd like to thank the University of Ottawa flow cytometry core facilities.

I would also like to thank my TAC members, Dr. Barbara Vanderhyden and Dr. Shawn Beug for the supportive advice and scientific discussion at every meeting. I'd also like to thank all the lab members, particularly Michelle Gandelman and Esha Gahunia, for all the fun times we have had in the lab. Additionally, I'd like to thank Redaet Daniel for all the help and moral support you provided me during this degree. I am very grateful to have worked alongside you all.

Lastly, I'd like to thank my family and friends for their constant encouragement, unconditional love, and support. Thank you for always reassuring and inspiring me to continue. To Sam, I am incredibly lucky and thankful to have you by my side every day.

Table of Contents

List of Abbreviations

AA	Adipic acid
ACN	Acetonitrile
AMPK	AMP-activated protein kinase
ATM	Ataxia telangiectasia mutated kinase
ATR	Ataxia telangiectasia and Rad3 related kinase
BRCA	Breast Cancer gene
CBTA	Cyclobutane-1,2,3,4-tetracarboxylic dianhydride
CI	Combination index
Cis	Cisplatin
CTR1	Copper transporter
DCM	Dichloromethane
DIC	N,N'-diisopropylcarbodiimide
DICD	1,12-diisocyanatododecane
DMAP	4-dimethylaminopyridine
DMEM	Dulbecco's Modification of Eagle's Medium
DMF	Dimethylformamide
DMSO	Dimethyl sulfoxide
DNA-PK	DNA-dependent protein kinase
Dox	Doxorubicin
DTB	4,4'-dithiodibutyric acid
EE	Encapsulation efficiency
EPR	Enhanced permeability and retention
ESI-MS	Electrospray ionisation mass spectrometry
GSH	Glutathione
GSSG	Oxidized glutathione
GST	Glutathione S-transferase
H2AX	H2A histone family member X
HCl	Hydrochloric acid
HPLC	High pressure liquid chromatography

HSA	Highest single agent
IC50	Half-maximal inhibitory concentration
ICP-MS	Inductively coupled plasma mass spectrometry
KRAS	Kirsten rat sarcoma viral oncogene homolog
Met	Metformin
MFI	Median fluorescence intensity
mTOR	Mammalian target of rapamycin
MTT	3-(4,5-Dimethylthiazol-2-yl)-2,5-Diphenyltetrazolium Bromide
MWCO	Molecular weight cut off
NMR	Nuclear magnetic resonance
NP	Nanoparticle
OCT1	Organic cation transporter 1
OD	Optical density
Ola	Olaparib
PAR	Poly-ADP ribose
PARP	Poly-ADP ribose polymerase
PBS	Phosphate buffered saline
PDI	Polydispersity index
PEG	Polyethylene glycol
PIMA	Poly(isobutylene-alt-maleic anhydride)
PLGA	Poly lactic-co-glycolic acid
ppb	Parts per billion
RB	Round bottom
ROS	Reactive oxygen species
RPMI	Roswell Park Memorial Institute
TEM	Transmission electron microscopy
TLC	Thin layer chromatography
Tx	Treatment

List of Figures

1.0 Introduction

1.1 Ovarian cancer

Among gynecological cancers, ovarian cancer is the leading cause of death in women[1]. Approximately 3000 women were diagnosed with ovarian cancer in 2023 in Canada (300,000 worldwide)[2,3]. Unfortunately after diagnosis, the five-year survival rate is approximately 55% for these patients[4]. This can be attributed to the fact that about 75% of patients only start to exhibit ovarian cancer symptoms at an advanced stage once the cancer has metastasized into the peritoneal cavity. Ultimately, current treatment options are not adequate at eradicating the disease, thus explaining the high mortality[1,5].

1.1.1 Histological subtypes

Ovarian cancer encompasses a group of related cancers that all originate in the ovaries or nearby organs, such as the fallopian tubes or the mesothelium lining the peritoneal cavity[1]. The most common type, accounting for roughly 90% of cases, is epithelial ovarian cancer[6,7]. Epithelial ovarian cancer can be subclassified into five groups based on histology, which include high-grade serous carcinoma, low-grade serous carcinoma, endometrioid carcinoma, mucinous carcinoma, and clear cell carcinoma[6]. Serous carcinoma, the most common histotype, is characterized by glandular or papillary morphology similar to fallopian tube epithelium[1]. Endometrioid carcinoma consists of endometrioid-like glands resembling cancer of the uterus, whereas mucinous carcinoma resembles endocervical glands or gastrointestinal epithelium. The fourth type, clear cell carcinoma, shares both serous and endometrioid morphology[1]. In addition to morphological and histological differences, similar and distinct mutations and amplifications have been reported contributing to variable genetic landscapes between subtypes. For example, p53 mutations are

most commonly characteristic of type II tumors (high-grade serous carcinoma), whereas most type I tumors (low-grade serous, endometrioid, mucinous, and clear cell carcinoma) display wildtype p53[1,6,8]. Additional distinct driving genetic alterations of high-grade serous carcinoma are mutations in *BRCA1* and *BRCA2* genes[1,6,8]. In contrast, KRAS mutations are predominantly found in type I tumors, with low occurrences in type II tumors[1,8]. These genetic differences can affect the efficacy of second line targeted therapies.

1.2 Current treatment options

1.2.1 Cytoreductive surgery

Current treatment strategies for epithelial ovarian cancer include cytoreductive surgery, which removes as much of the cancer as possible leaving minimal residual disease, followed by chemotherapy and sometimes maintenance therapy[1]. Several retrospective studies have been conducted highlighting the correlation between reduction in mass size by cytoreductive surgery and survival[9–11]. Cytoreductive surgery aims to remove the bulk of the tumor, namely the cells furthest from oxygen supply and non-proliferating cells that have the greatest potential of becoming chemoresistant. In this regard, remaining microscopic cell masses are hopefully susceptible to subsequent chemotherapy treatment[5].

1.2.2 Chemotherapy

Chemotherapy options include platinum, anthracycline, and taxane-based agents, with the current standard of care consisting of carboplatin and paclitaxel. Paclitaxel, a taxane-based agent, works by targeting microtubules, thereby halting cell division[5]. As part of the platinum-based chemotherapeutic options, carboplatin, an analogue of cisplatin, is currently the standard in clinic,

due to its ability to achieve equivalent cell killing efficacy with less emetogenic and nephrotoxicity than cisplatin[5]. However, the focus of this thesis is to prevent the toxicities associated with chemotherapy using nanotechnology. Therefore, cisplatin was selected as the chemotherapy of interest. The anticancer effects of cisplatin were first discovered by Rosenberg and colleagues in 1961 and the chemotherapy has since been in clinical use for several decades[12,13]. Cisplatin is a DNA damaging drug that works via alkylation. Cisplatin uptake by cells occurs either via passive diffusion or facilitation by the copper transporter CTR1 due to a chloride ion concentration gradient across the cell membrane[5,13]. Once inside, cisplatin [$Pt(NH_3)_2Cl_2$] undergoes aquation in the cytoplasm, causing the chloride atoms to become displaced by hydroxyl functional groups, which thus activates the platinum compound. Activated cisplatin [$Pt(NH_3)_2(OH_2)_2$] becomes an electrophile and travels into the nucleus where it can target nucleophilic agents such as purine bases in DNA[13]. The most common intrastrand crosslink active cisplatin can form with DNA is a 1,2-guanine-guanine adduct, representing about 90% of adduct formation (**Figure 1**)[13]. Cisplatin-DNA adduct formation prevents sufficient DNA replication, ultimately inhibiting cell division and resulting in cell death.

Following DNA double strand breaks, serine-threonine kinases, specifically ataxia telangiectasia mutated (ATM), ataxia telangiectasia and Rad3 related (ATR), and DNA-dependent protein kinase (DNA-PK) activate and phosphorylate H2A histone family member X (H2AX) adjacent to the damage[14,15]. Phosphorylation of H2AX on serine 139 is commonly referred to as γH2AX. γH2AX acts as an upstream apoptotic marker given its positive correlation with DNA damage[16]. Several lines of evidence suggest γH2AX signals for repair proteins to reverse DNA damage and acts as a potential docking site for these proteins[14,15]. Nonetheless, aberrant DNA fragmentation leading to hyperphosphorylation of H2AX can cause cell death.

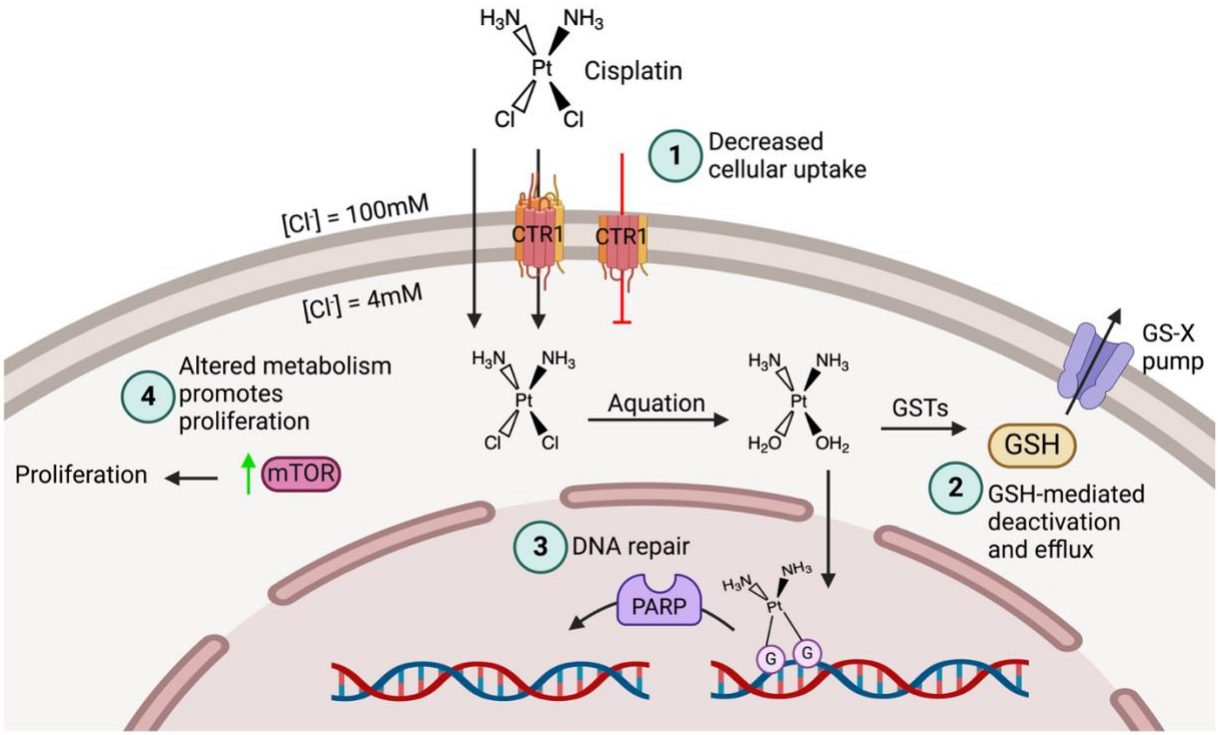
Cisplatin
1 Decreased cellular uptake
CTR1
CTR1
[Cl-] = 100mM
[Cl-] = 4mM
Aquation
GSTs
GS-X pump
GSH
2 GSH-mediated deactivation and efflux
4 Altered metabolism promotes proliferation
Proliferation
mTOR
3 DNA repair
PARP

Figure 1. Cisplatin mechanism of action and possible resistance pathways. Cisplatin enters the cells either by passive diffusion or through the CTR1 transporter due to the chloride ion concentration difference across the cell membrane. Once inside, cisplatin undergoes aquation and crosses into the nucleus where it forms adducts with DNA, the most common being a 1,2-guanine-guanine adduct. Resistance mechanisms are labelled 1-4, with mechanisms 1 and 2 falling under category 1 and mechanisms 3 and 4 in category 2. (1) Excision of the N-terminal domain on CTR1 prevents facilitated cisplatin uptake. (2) GSTs catalyze the conjugation of GSH to active cisplatin, which promotes efflux via GS-X pumps. (3) DNA repair of cisplatin DNA adducts prevent cell death. (4) Upregulated mTOR levels confers an altered metabolism that promotes proliferation. Created with BioRender.com. CTR1, copper transporter; GSTs, glutathione S-transferases; GSH, glutathione; GS-X pump, ATP-dependent glutathione S-conjugate pumps; mTOR, mammalian target of rapamycin; PARP, poly-ADP ribose polymerase.

Of the chemotherapeutic agents corresponding to anthracyclines, doxorubicin has been used to treat ovarian cancer when platinum agents are no longer effective[17]. There are two main mechanisms by which doxorubicin exerts anti-cancer effects: 1) intercalation into DNA and 2) generation of free radicals[18]. Doxorubicin enters cells via diffusion and once inside, the drug's high affinity for the cytoplasm proteasome causes interaction. This complex is then translocated into the nucleus in which doxorubicin now has higher affinity for DNA, resulting in disassociation from the proteasome and intercalation into DNA[19]. This event causes disruption of topoisomerase-II-mediated DNA repair, preventing alleviation of the DNA supercoils generated during DNA replication[18,19]. Prior to entering the nucleus, doxorubicin can also undergo oxidation in the cytoplasm to form an unstable metabolite known as semiquinone[18]. The conversion of semiquinone back to doxorubicin produces reactive oxygen species (ROS). ROS can have deleterious effects on cells including lipid and membrane oxidation, DNA damage and apoptosis[18,19]. Ultimately, doxorubicin causes sustained damage resulting in cell death.

1.3 Relapse occurrence

Several clinical trials have evaluated cisplatin efficacy in the context of ovarian cancer treatment, and all reveal greater survival in patient groups who received either cisplatin alone or in combination with other therapeutics[20–22]. However, following the initial course of treatment, generally 70% of ovarian cancer patients diagnosed at late stage are shown to relapse[23,24]. Depending on the length of time to relapse, patients are classified as either platinum-sensitive or platinum-resistant. For platinum-resistant relapsed ovarian cancer, other non-platinum agents, such as doxorubicin and gemcitabine, are required. However, patients experience only minimal

(approximately less than 20%) response rates[17]. Ultimately, cisplatin efficacy remains limited due to the development of resistance and systemic, non-selective distribution.

1.4 Platinum-based chemotherapy resistance

1.4.1 Mechanisms prior to adduct formation

To simplify the variety of platinum resistance mechanisms, they can be divided into 2 main categories: 1) mechanisms that prevent the cytotoxic adduct formation and 2) mechanisms that prevent cell death following adduct formation[5]. Mechanisms related to reduced drug influx and increased deactivation and efflux can be grouped into category 1, while mechanisms involved in DNA damage repair and inhibition of apoptosis fall into category 2 (**Figure 1**)[5]. Firstly, studies have shown that CTR1 knockout results in diminished cellular uptake of cisplatin, conferring resistance to the chemotherapy[13,25]. However, acquired cisplatin resistance does not occur due to the loss of CTR1 expression. Instead, it was proposed that the lack of glycosylation of CTR1 promotes excision of the N-terminal domain causing the loss of facilitated transport function[25,26]. The membrane bound domain remains present, thereby suggesting CTR1 change in activity results in resistance development as opposed to change in expression.

Furthermore, platinum resistance can also develop via glutathione-mediated deactivation and efflux[27,28]. Given its electrophilic nature, active cisplatin is not limited to reacting only with nucleophilic purine bases. Other cellular nucleophiles, such as glutathione (GSH), can also interact with platinum-based agents[27,28]. GSH covalently binds to cisplatin forming a GSH-cisplatin conjugate for cellular detoxification. This conjugation reaction is catalyzed by glutathione S-transferase (GST) enzymes[27,29,30]. The conjugate product is then shuttled out of the cell via ATP-dependent glutathione S-conjugate pumps, thereby enhancing cisplatin efflux[28]. Overexpression

of GSTs in cisplatin resistant cells has been reported[29,31,32]. A study conducted by Lewis and colleagues showed that GSH and GST were 1.4-fold and 2.9-fold higher in ovarian adenocarcinoma cells from a patient with developed cisplatin resistance compared to cells from a chemosensitive patient[32]. Some strategies have been investigated to diminish GSH-mediated cisplatin deactivation by employing combination therapy with GST inhibitors[29,33]. Although inhibiting GSTs improved cisplatin sensitivity in resistant cells, platinum resistance is multifactorial and not the result of just one mechanism. Other pathways can also contribute to resistance when one mechanism is diminished.

1.4.2 Mechanisms post adduct formation

Resistance can also occur after a cisplatin-DNA adduct has been formed, preventing the apoptotic outcome. One of these key resistance mechanisms is the ability to repair damaged DNA. Of the DNA repair pathways, the nucleotide excision repair system is particularly responsible for reversing the damage caused by platinum to allow normal DNA replication to proceed[34]. Poly ADP-ribose polymerase 1 (PARP-1) is an enzyme involved in this pathway that works by detecting single strand breaks in DNA via the zinc-finger domain[34,35]. PARP-1 then signals for the recruitment of proteins to the site of damage and catalyzes a poly ADP ribose (PAR) polymer chain onto the proteins, thus activating them to repair DNA[34,35]. After this catalytic reaction, PARP-1 loses affinity for DNA, allowing other repair complex enzymes to take over. Poly ADP-ribose glycohydrolase restores PARP-1's ability to detect and repair other sites of DNA damage[34]. Ultimately, this repair pathway prevents aberrant DNA damage that would trigger apoptosis.

Moreover, cisplatin induced apoptosis can be inhibited by other active pathways with greater proliferation effects, thus contributing to cisplatin resistance. Ovarian cancer cells have

been shown to have an altered metabolism, which can contribute to accelerated proliferation[36,37]. The mammalian target of rapamycin (mTOR) protein is the common metabolic regulator for these pathways[37]. Previous studies have shown that mTOR is highly expressed in advanced-stage ovarian tumors, thereby positively regulating tumor proliferation and cell cycle progression[38,39]. In a growth-promoting tumor microenvironment, mTOR upregulates the anabolic production of proteins, lipids, and nucleotides, thereby downregulating catabolism[40]. With this metabolic switch, mTOR inhibits autophagy. Upstream in the pathway, AMP-activated protein kinase (AMPK) is a negative regulator of mTOR, which promotes autophagy initiation. However, the constitutive activation of mTOR overrides those signals[40]. Some trials have investigated the use of mTOR inhibitors as an addition to chemotherapy to enhance sensitivity. However, poor outcomes, specifically lack of survival improvement and severe toxicities have been reported[41,42]. Therefore, new strategies are required to suppress the mTOR pathway for autophagy regulation. Overall, there are several mechanisms of platinum resistance that can occur at different stages of the adduct formation. These active pathways prevent patients from achieving full benefit from chemotherapy, which thus demonstrates the requirement for new therapeutic options to overcome resistance.

1.5 Systemic distribution

In addition to platinum resistance, systemic non-selective distribution causes low tolerability and severe toxicities, ultimately causing additional harm to patients[43]. Patients on long-term cisplatin use have reported side effects, including but not limited to vomiting, nausea, nephrotoxicity, and myelosuppression as well as damage to healthy tissue[43]. The current standard practice of care is to administer chemotherapy through intravenous infusions. Since cisplatin first needs to travel through the bloodstream to reach the tumor, this provides cisplatin accessibility to

other off target organs[44]. This not only causes the undesirable side effects but also prevents full infusion from targeting the tumor. In contrast, cisplatin given through intraperitoneal injections has been shown to result in higher drug accumulation at the site of the tumor and cause less systemic toxicity[45]. This is explained by bypassing the bloodstream as the mode of distribution and injecting directly into the peritoneal cavity, the location of the disease at diagnosis[1]. However, few patients receive intraperitoneal chemotherapy in addition to intravenous administration. Delivery complications and drug tolerability prevent intraperitoneal injections from being a favourable route of administration[44]. Therefore, different strategies for improving cisplatin targetability via intravenous administration is required to limit toxic effects.

1.6 Combination therapy

Improving clinical use of cisplatin for the treatment of ovarian cancer thus requires lowering drug resistance and serious side effects. Firstly, previous studies have demonstrated that combination therapy with two or more drugs has shown stronger efficacy with decreased resistance development and increased overall survival than single drug alone[46–48].

1.6.1 Targeted agents

Olaparib is an FDA approved small molecule drug that functions as a PARP inhibitor. Olaparib inhibits PARP-1 from detecting and repairing single strand breaks in DNA[49]. Olaparib induced PARP-1 inhibition has been shown to promote caspase-3 expression, which is a cysteine protease[50]. Cleavage of caspase-3 by initiator caspases activates caspase-3, which can then cleave PARP-1, demonstrating a clear marker of apoptosis[51–53]. When PARP-1 is inhibited, the single strand breaks in DNA can no longer be repaired, causing double strand breaks to arise. Another

DNA repair pathway, known as homologous recombination, which specializes in repairing double strand breaks, then becomes activated[54]. The *BRCA1* and *BRCA2* genes encode proteins, particularly tumor suppressors, that are involved in homologous recombination repair[55]. However, mutations in the *BRCA1* or *BRCA2* gene are found in roughly 20% of epithelial ovarian cancer patients[56]. As a result, some ovarian cancer patients have deficient homologous recombination repair systems, rendering them incapable of repairing double strand breaks. Therefore, inhibiting PARP-1 in BRCA-deficient ovarian cancer results in synthetic lethality, since two DNA repair pathways are substantially impaired[49]. Ultimately, combining olaparib with cisplatin treatment allows for increased potential for persistent cisplatin-DNA adducts to cause cell death. Several preclinical and clinical studies have explored the combined use of cisplatin and olaparib for the treatment of ovarian cancer. Due to favourable results, olaparib has been added to the treatment regimen as a maintenance therapy for ovarian cancer patients[46–48].

Furthermore, metformin is a clinically approved antidiabetic drug that has been recently reported to have anticancer effects. Several studies have used metformin to sensitize ovarian cancer cells to cisplatin by indirectly increasing AMPK activation[58,60]. Specifically, metformin enters the cells through the organic cation transporter 1 (OCT1) and inhibits respiratory complex chain I part of the electron transport chain of the mitochondria[57]. This inhibition prevents the conversion of ADP to ATP, resulting in increased AMP:ATP and ADP:ATP ratios. This low energy state triggers activation of AMPK by phosphorylation, thereby inhibiting mTOR, resulting in increased autophagy and decreased proliferation[58–60]. Since inhibiting mTOR has proven to be difficult, targeting AMPK, a protein upstream, may provide better autophagic outcomes.

Previous studies have combined cisplatin with either olaparib or metformin to demonstrate improved cell killing ability[46,47,61–63]. A study conducted by Gao and colleagues showed greater

inhibitory effects when olaparib was combined with cisplatin in two different ovarian cancer cell lines compared to when olaparib was combined with paclitaxel, a taxane-based chemotherapy[47]. Additionally, the combination of cisplatin with olaparib demonstrated a dose-reduction index of greater than 1[47]. Furthermore, a phase I trial conducted by Balmaña and colleagues revealed no dose-limiting toxicities when the doses of olaparib and cisplatin were lowered from 100-200mg and 75mg/m^2 to 50mg and 60mg/m^2, respectively[46]. This regimen also revealed an overall response rate of 43%[46]. Preclinical studies also demonstrated enhanced cell death when cisplatin was combined with metformin[61,62]. Particularly, Ricci and colleagues were able to partially reverse cisplatin resistance with combined cisplatin metformin treatment in vivo[63]. Ultimately, combination therapy has been shown to improve chemotherapy resistance in ovarian cancer patients and is thus standard treatment practice for this multifaceted disease.

1.6.2 Advantages

In addition to reducing the possibility of drug resistance, combination therapy has several benefits. For example, combination therapies can achieve maximum efficacy while minimizing doses due to synergistic antitumor effects[64]. As a result, combination therapy can result in less systemic toxicity since drug exposure is not occurring at concentrations above the therapeutic index. Moreover, combining different agents allows for targeting of multiple pathways. Since there are several metabolic, genomic, and environmental factors, amongst others that contribute to the progression of ovarian cancer, targeting just one is not sufficient for eradicating this complex disease.

1.6.3 Limitations

Although there has been great progress in combination therapy for the treatment of ovarian cancer, there are multiple drawbacks that remain. Various drugs used in combination can have different physicochemical properties, such as polarity, solubility, or size, that can all affect pharmacokinetics[65]. For example, the physicochemical differences between cisplatin, olaparib, and metformin warrant different routes of administration. It is standard practice to deliver cisplatin through intravenous infusions, whereas both olaparib and metformin are dosed orally[66,67]. Given these administration differences, the rate and sites of absorption and tissue distribution can vary. For example, cisplatin preferentially accumulates in the kidneys and liver, whereas the highest concentrations of metformin are found predominantly in the gut[66,67]. Additionally, drug polarity will dictate the potential protein interaction in the bloodstream, contributing to further disturbances to tissue distribution. When dosed at 10μg/mL, the plasma protein binding to olaparib is roughly 82%[68]. Consequentially, the predicted drug concentrations will differ from the actual concentrations that reach the tumor. As a result, drug synergy at the site of the tumor will be lost[65]. Therefore, in the clinic, it is difficult to find an optimal dosing schedule that ensures synergistic antitumor effects of multiple drugs in combination. Lastly, certain drug combinations can cause enhanced side effects due to the different toxicity profiles of single drugs in combination[65]. If we can achieve synergistic doses in the tumor by specifically delivering there, we can overcome the limitations of combination therapies.

1.7 Nanotechnology

To improve targeted distribution of drug combinations, nanoparticle delivery systems can provide huge benefits. Nanoparticles (NPs) are nanometer-sized particles that can have a vast array

of purposes[65]. They can be composed from a wide range of materials rendering NPs with different properties for different objectives, such as diagnosis, drug delivery, and vaccine development.

1.7.1 Different platforms

Among the plethora of developed NP platforms, certain systems have been well established for drug delivery purposes, including but not limited to liposomal and polymeric formulations (**Figure 2**)[65]. Liposomal NPs generally consist of either single or bilayer lipid membrane structures with an aqueous core, providing the loading capability of both hydrophilic and hydrophobic drugs. They have a spherical morphology and can assume a variety of sizes. Typical components include both natural and synthetic lipids as well as cholesterol to optimize rigidity (**Figure 2**)[65]. Several drug delivery studies employing liposomes have attained phase III clinical trials and post-trial approval[69–71].

Polymeric NPs are another versatile platform for drug delivery. These NPs normally consist of biodegradable and biocompatible polymers and co-polymers with both hydrophilic and hydrophobic properties[65]. Owing to the interplay between hydrophobic and hydrophilic interactions, polymeric NPs form through self-assembly methods producing a hydrophobic core surrounded by a hydrophilic exterior. Hydrophilic polymers form the outer sheath of NPs protecting against aggregation of hydrophobic polymers and conferring NP stability[65]. Similar to liposomes, polymeric NPs have a spherical appearance and can load both hydrophobic and hydrophilic drugs. Polymeric NPs can also vary in size, while on average ranging around 100nm[72,73]. Other attractive characteristics include controlled drug release, better drug encapsulation, and scalability (**Figure 2**)[65,74]. Polymeric NP formulations are also entering clinical

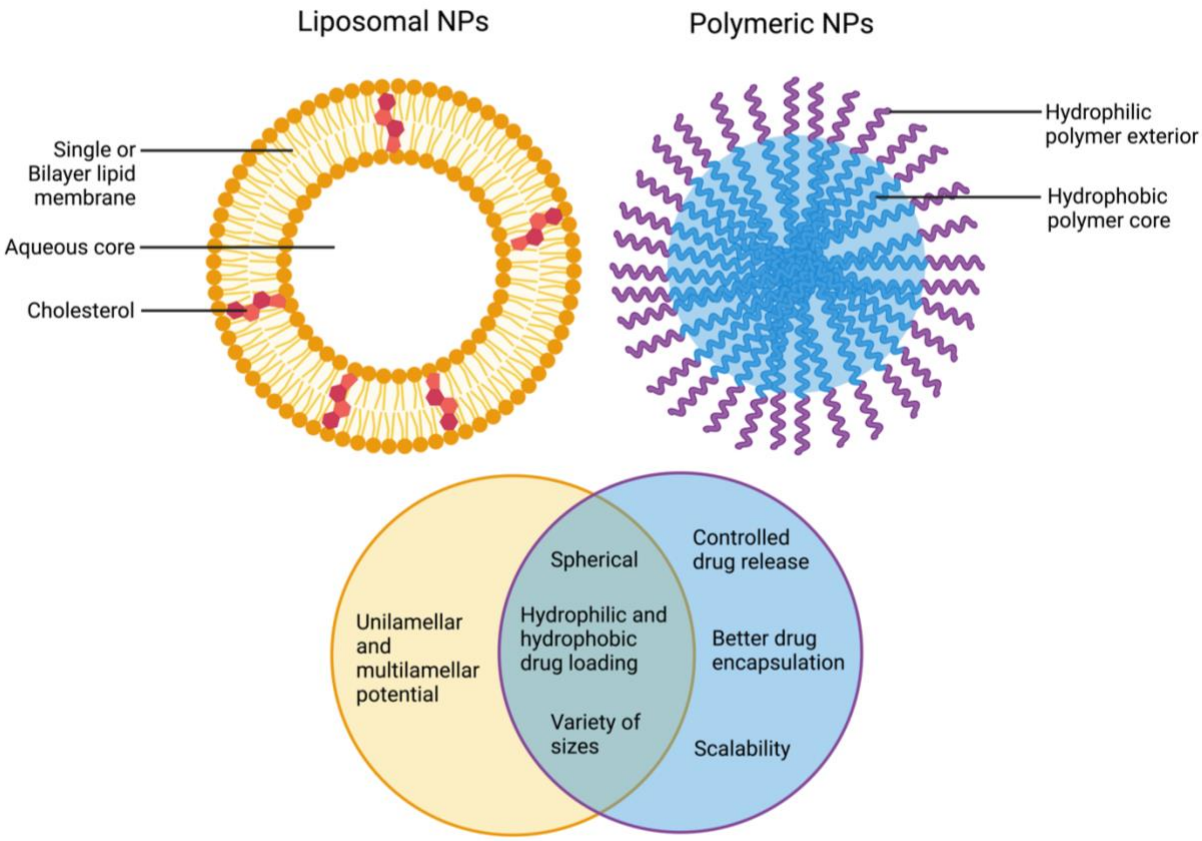
Liposomal NPs
Polymeric NPs
Single or
Bilayer lipid
membrane
Aqueous core
Cholesterol
Hydrophilic
polymer exterior
Hydrophobic
polymer core
Unilamellar
and
multilamellar
potential
Spherical
Hydrophilic and
hydrophobic
drug loading
Variety of
sizes
Controlled
drug release
Better drug
encapsulation
Scalability

Figure 2. Liposomal versus polymeric nanoparticles (NPs). The differences in NP composition are highlighted from the different structures. Similar and unique NP properties are outlined in the Ven diagram between liposomal and polymeric NPs. Created with BioRender.com.

trials, particularly for cancer treatment[75]. Given the provided advantages, polymeric NPs were selected as the drug delivery system for this thesis.

1.7.2 Tunable characteristics

One advantage of polymeric NPs is tunable physicochemical characteristics for optimizing ideal properties for specific applications. Particle size, size distribution (denoted as polydispersity index, PDI) and surface charge can heavily influence tissue distribution, protein interaction in the bloodstream, and cellular entry. For example, extremely small NPs (<8nm) are capable of glomerular filtration and are readily cleared from the body[76]. Conversely, NPs of larger sizes (>200nm) can be recognized as foreign entities and subsequently removed by the immune system. NPs within the size range of 8-200nm thus have increased chances of cellular uptake and tumor penetration[72,77]. Narrow size distribution, ideally PDI<0.2, can also ensure uniform NP behaviour given the size consistency of particles in solution. Moreover, the end functional group on the surface of polymeric NPs can dictate neutral, negative, or positive charge. This surface chemistry causes affinity for differing protein identity and quantity during transport, creating unique protein coronas surrounding NPs[72,78,79]. For example, positively charged NPs have been shown to bind albumin, whereas negatively charged particles preferentially bind IgG[78]. Therefore, the composition including polymer molecular weights and end functional groups, can be adjusted to optimize for ideal values.

1.7.3 Improved pharmacokinetics

In the context of cancer treatment, NPs can be used to encapsulate drugs, forming a drug delivery system with multiple advantages. Firstly, encapsulating multiple drugs inside one

nanocarrier (2-in-1 or 3-in-1) causes overlapping pharmacokinetic properties, ensuring identical absorption and distribution of drugs in combination[65]. However, one key clause to this advantage is that NPs can only encapsulate drugs of a similar nature. Hydrophilic drugs experience great difficulty in encapsulation, given that polymeric NP platforms possess a hydrophobic core[65]. Researchers have overcome this challenge by using chemical modification to enhance the hydrophobicity of existing drugs to create prodrugs that are more amenable to encapsulation while retaining normal pharmacological activity[65,80–82]. For example, Dhar and colleagues synthesized a Pt(IV) prodrug conjugate for NP encapsulation for prostate cancer treatment[82]. They showed that their cisplatin-loaded NP was significantly superior to free, unencapsulated cisplatin[82].

1.7.4 Controlled loading, release, and synergy

Another strong benefit of NP platforms for multidrug delivery is the ratiometric loading of more than one drug[65]. The maximum efficacy of multiple drugs in combination is strongly impacted by the drug-to-drug ratio at the tumor. Encapsulating multiple drugs into one NP system (2-in-1 or 3-in-1) ensures the synergistic drug ratios are retained from NP synthesis to intracellular uptake by the tumor cells[65]. Drug synergy is defined as the effect of two drugs in combination being greater than the additive effect. This concept was derived from the median-effect equation (fraction affected + fraction unaffected = 1) and is referred to as the Chou Talalay method[83]. This method is well established in combination therapeutic research settings to determine synergy. Obtaining a synergistic effect is highly dependent on concentration[84,85]. Therefore, regulating the ratiometric drug loading inside a single NP ensures synergistic concentrations are reaching the tumor at the same time. Clinical evidence proving synergistic benefit in patients was obtained from phase III trials with VYXEOS, the only dual-drug liposome chemotherapy with FDA-approval for

newly diagnosed therapy-related acute myeloid leukemia[86]. VYXEOS is a liposome containing daunorubicin and cytarabine at a synergistic 1:5 molar ratio designed for prolonged exposure to leukemia cells in the bone marrow[87]. Clinical data revealed 1-year overall survival was greater with VYXEOS (42%) compared to current treatment (28%)[88].

In addition to efficient drug loading, NPs can regulate the controlled release of drugs depending on the composition of the delivery system and cellular requirement[65]. Sengupta and colleagues demonstrated the temporal release of first an anti-angiogenesis agent entrapped in the outer compartment and subsequently a chemotherapy agent encapsulated in the inner core of a lipid-polymer hybrid NP[89]. This allowed for first vascular dysregulation followed by improved penetration of chemotherapy in solid tumors[89]. The sequential release of these agents affects overall efficacy given that targeting specificity is dependent on the tumor compartment.

Controlled release can also be triggered in response to certain stimuli. For example, poly lactic-co-glycolic acid (PLGA) and polyethylene glycol (PEG) are biocompatible and biodegradable polymers commonly used to synthesize polymeric NP systems[90]. These polymers display differential structural stability when exposed to either neutral or acidic/basic pH. In neutral conditions, such as the bloodstream, PLGA-PEG NPs are highly stable, whereas, in acidic conditions, such as the tumor microenvironment, the close ester bonds found in PLGA are subjected to degradation[91]. Therefore, NP systems composing of PLGA-PEG polymers can control drug release at appropriate cellular targets.

In addition to pH stimuli, NP platforms have been developed that are GSH-responsive[27,92,93]. Ling and colleagues synthesized cysteine-based poly (disulfide amide) polymers to accompany Pt(IV) conjugate encapsulation in a lipid-PEG NP[27]. These cysteine-based polymers have high disulfide content that can react with GSH causing reduction of the disulfide bonds. This

reaction scavenges GSH, which can inhibit GSH-mediated cisplatin deactivation and efflux[27]. They revealed a pronounced reduction in the reduced GSH to oxidized glutathione (GSSG) ratio following treatment with the Pt(IV), cysteine-based polymer NP as opposed to free cisplatin in both cisplatin-sensitive and cisplatin-resistant cell lines. This was accompanied by enhanced apoptosis following NP treatment in both cell lines[27]. Incorporating a GSH-responsive feature into cisplatin NP formulations creates a more sophisticated platform for reducing drug resistance.

1.7.5 Targeted delivery

NP delivery systems promote both passive and active targeted drug delivery, thereby decreasing serious side effects by minimizing systemic distribution to healthy organs[65]. As a result, therapeutic efficacy is enhanced due to maximized drug exposure in the tumors. In the context of cancer nanomedicine, NPs preferentially target and accumulate in tumors due to the enhanced permeability and retention effect (EPR)[94,95]. The EPR effect is an example of NP passive targetability. The rapid development of vasculature around tumors results in defective vessel wall formation, allowing for enhanced permeability of NPs out of the vasculature and into tumor cells. Once inside the tumor environment, they are retained due to poor lymphatic drainage[94,95]. Although this concept requires further investigation, the proposed outcome remains true. Active targeted delivery to specific cell surface receptors can also be achieved with appropriate ligand conjugation to the NP surface[65]. Lastly, NPs protect drugs against degradation and prevent plasma protein interactions in the bloodstream. In turn, lower drug concentrations can be loaded into NPs as drug payload to the tumor is increased[65].

1.8 Previous NP formulations

To summarize, NP delivery systems provide extensive advantages at improving existing therapy limitations. Several approaches at formulating optimal nanocarrier platforms encapsulating different small molecule drugs for ovarian cancer treatment have been explored[96,97]. Particularly, multiple researchers have encapsulated cisplatin in a single drug-loaded polymeric NP and showed great inhibition of tumor growth and better tolerability than free cisplatin treatment[96,97]. Under the supervision of Paula Hammond, Mensah and colleagues developed a layer-by-layer liposomal NP encapsulating both cisplatin and olaparib for ovarian cancer treatment[98]. They used an emulsion technique to load hydrophilic cisplatin and hydrophobic olaparib in the liposomal core and bilayer, respectively[98]. This allowed for modular release of first olaparib followed by cisplatin. They reported significant tumor regression and moderated systemic toxicity in orthotopic xenograft-bearing mice treated with the layer-by-layer NP compared to free dual drug combination[98]. Although promising results were achieved, clinical translation remains limited due to upscaling challenges with this NP synthesis technique, thus requiring better reproducible formulations.

Another study conducted by Faramarzi and colleagues improved the weak bioavailability of metformin by employing a PLGA-PEG nanocarrier for drug delivery[99]. They demonstrated cell viability reduction potential accompanied by upregulated mRNA expression levels of apoptotic markers such as caspase-3 through in vitro studies[99]. Limited studies have reported NP-mediated delivery of metformin combined with cisplatin; however, treatment was indicated for other cancers, namely colorectal and non-small cell lung cancer[100,101]. Further testing for ovarian cancer application is required.

1.9 Rationale and hypothesis

Resistance to platinum-based chemotherapy and systemic toxicities remain the greatest obstacles in achieving remission. Multidrug-loaded NPs can provide huge benefits to circumvent existing therapeutic limitations by targeting therapies to tumors for blockade of multiple resistance mechanisms[65]. Although a variety of studies have explored multidisciplinary approaches involving nanotechnology for effective cancer therapy development, greater advancements remain an unmet medical need. Based on an extensive literature review, only single and dual drug-loaded NPs have been explored for ovarian cancer therapy[96–99]. Given the complexity of the disease, a triple-drug NP formulation may provide more favourable outcomes, with a better chance of obtaining a prolonged survival phenotype. It is hypothesized that the combination of cisplatin, olaparib, and metformin encapsulated into a single NP will improve overall survival in ovarian cancer compared to free drugs in combination. Encapsulating all three drugs in a single NP will allow for overlapping pharmacokinetic profiles and cause uniform entry into the cells. **Figure 3** outlines the proposed triple drug NP mechanism. We began testing this hypothesis using the two following objectives:

Objective 1. Develop and optimize a 3-in-1 NP formulation containing cisplatin, olaparib, and metformin.

Objective 2. Determine the in vitro efficacy of the triple drug NP.

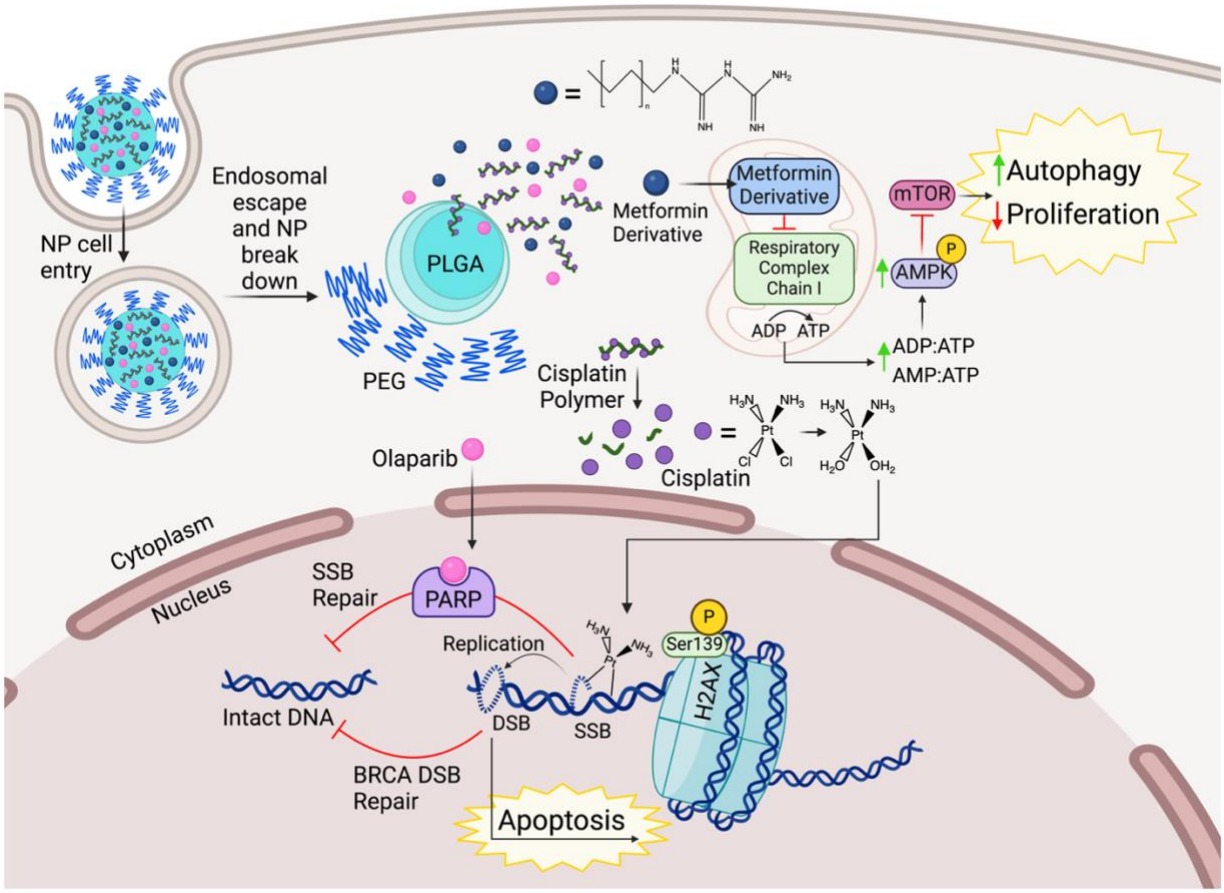
NP cell entry
Endosomal escape and NP break down
PLGA
PEG
Metformin Derivative
Metformin Derivative
Respiratory Complex Chain I
ADP ATP
ADP:ATP
AMP:ATP
AMPK
P
mTOR
Autophagy
Proliferation
Cisplatin Polymer
Cisplatin
Olaparib
Cytoplasm
Nucleus
SSB Repair
PARP
Replication
Ser139
H2AX
Intact DNA
DSB
SSB
BRCA DSB Repair
Apoptosis

Figure 3. Mechanism of triple-drug-NP treatment upon entry in ovarian cancer cells. NP enters through the endocytic pathway before undergoing endosomal escape and breakdown of the PLGA-PEG polymers, releasing metformin derivative, cisplatin polymer, and olaparib. The metformin derivative (blue circle) inhibits respiratory complex chain I in the mitochondria, thereby increasing the ratio of ADP and AMP to ATP, leading to AMPK activation, inhibition of mTOR and ultimately increased autophagy and decreased cell proliferation. Cisplatin polymer is reduced releasing cisplatin (purple circle). Cisplatin undergoes aquation, before crossing into the nucleus to form DNA adducts. Ser139 on H2AX becomes phosphorylated following adjacent DNA damage. Olaparib (pink circle) binds to and cleaves PARP preventing SSB repair of cisplatin induced DNA damage. PARP inhibition coupled with mutated BRCA DSB repair causes synthetic lethality, leading to apoptosis. Created with BioRender.com. NP, nanoparticle; PLGA-PEG, poly lactic-co-glycolic acid polyethylene glycol; AMPK, AMP-activated protein kinase; mTOR, mammalian target of rapamycin; H2AX, H2A histone family member X; PARP, poly-ADP ribose polymerase; SSB, single strand break; BRCA, Breast Cancer gene; DSB, double strand break.

2.0 Materials and Methods

2.1 Materials

Cisplatin (Cis) was purchased from Sigma Aldrich (Cat # 479306-5G). Olaparib (Ola), metformin (Met) and doxorubicin (Dox) were purchased from Selleckchem (Cat # S1060, # S1950, # S1208, respectively).

2.2 Drug synthesis and characterization

All synthesis products were characterized by either nuclear magnetic resonance (NMR) using a Bruker AVANCE II 400, inductively coupled plasma mass spectrometry (ICP-MS, as described in section 2.7.2 for cisplatin encapsulation efficiency), and/or electrospray ionisation mass spectrometry (ESI-MS). For NMR preparation, all products were dissolved using deuterated solvents in thin-walled glass vials. Products analyzed by ESI-MS were prepared by dissolving in acetonitrile (ACN) at 10µg/mL and filtered.

2.2.1 Synthesis and characterization of oxoplatin [$PtCl_2(NH_3)_2OH_2$]

Cisplatin (496.2mg, 1.65 mmol) was added to a 50mL round bottom (RB) flask with water (3mL). 30% hydrogen peroxide (16mL, BioShop) was added, the temperature was set at 75°C, and the reaction proceeded for 4 hours. The reaction was then stopped, cooled at room temperature, and placed in the 4°C fridge overnight to help precipitate. The solution was filtered through 5µm filter paper in a glass funnel to collect product. The product was then washed separately with water and diethyl ether and then left to dry again for roughly 1 hour after each wash. The product was collected in a 20mL glass vial (VWR) and placed on the vacuum for 3 days. Oxoplatin was collected in 49.6% (273.6mg) yield.

2.2.2 Synthesis and characterization of DTB Polymer

All cisplatin polymers are named using the linker moiety connecting cisplatin units. 4,4'-dithiodibutyric acid (DTB, 35.56mg, 0.15mmol, Sigma Aldrich, Cat # C15605-10G) in DMSO (1mL) was added to a 20mL vial. N,N'-diisopropylcarbodiimide (DIC, 5µL, 3 equiv., Alfa Aesar, Cat # A19292) was added as a coupling reagent for ester bond formation. The reaction mixture was stirred for approximately 4-5 minutes before adding 4-dimethylaminopyridine (DMAP, 54.68mg, 3 equiv., Alfa Aesar, Cat # A13016), a nucleophilic catalyst for ester reactions. Oxoplatin (50mg, 1 equiv.) in DMSO was added to the reaction. The reaction mixture was heated to 70°C and proceeded overnight. After cooling the reaction mixture, the solution was lyophilized using a FreeZone 1L Benchtop Freeze Dry System (Labconco, Kansas City, Missouri, USA) for 6 days to remove the solvent by sublimation. The resulting precipitate was dissolved in methanol for dialysis preparation to remove unreacted reagents. Dialysis was performed using SnakeSkin dialysis tubing (3500 Da MWCO, Thermo Fisher, Cat # 68035) in methanol (roughly 2L) for 24 hours. The polymer solution inside the tubing was transferred to a 20mL vial before rotary evaporation of the excess methanol. The water bath was set at 30°C and pressure reached about 20mbar. The resulting precipitate was then kept at -20°C in preparation for subsequent lyophilization for 3 days. Product was stored at 4°C. ^{1}H NMR (400 MHz, DMSO-d6): δ 5.46 (d, NH3), 4.27 (hept, NH3), 2.65 (t, CH2), 2.34 (t, CH2), 1.83 (p, CH2). ^{13}C NMR (101 MHz, DMSO-d6) δ 169.32, 165.30, 153.44, 45.00, 42.43, 37.14, 32.61, 23.31, 21.70, 20.32. The percent of platinum measured by ICP-MS is 10% (w/w).

2.2.3 Synthesis and characterization of AA Polymer

Adipic acid (AA, 21.8mg, 0.15mmol, Sigma Aldrich) in DMSO (1mL) was added to a 20mL vial followed by DIC (5µL, 3 equiv.). After 4-5 minutes, DMAP (54.68mg, 3 equiv.) was added followed by oxoplatin (50mg, 1 equiv.). Reaction followed the same procedure as described

for DTB Polymer in section 2.2.2. AA Polymer yield was 93.4mg. ^{1}H NMR (400 MHz, DMSO-d6): δ 5.49 (d, NH3), 4.38 (m, NH3), 2.23 (d, CH2), 1.48 (d, CH2). ^{13}C NMR (101 MHz, DMSO-d6) δ 169.72, 156.78, 153.57, 63.07, 44.89, 42.37, 40.66, 34.04, 24.60, 23.30, 21.67, 20.33. The percent of platinum measured by ICP-MS is 14% (w/w).

2.2.4 Synthesis and characterization of CBTA Polymer

Oxoplatin (49.4mg, 0.15mmol) was mixed with cyclobutane-1,2,3,4-tetracarboxylic dianhydride (CBTA, 30.4mg, 1 equiv., Sigma Aldrich, Cat # 161330-5G) in an RB flask. DMSO (3mL) was used for dissolution. Reaction was heated to 60°C and proceeded for 24 hours. Reaction mixture was cooled to room temperature, transferred to a 15mL conical tube, and placed at -80°C. Lyophilization was performed to remove the solvent. Excess methanol was added to the resulting precipitate to dissolve unreacted cyclobutane-1,2,3,4-tetracarboxylic dianhydride. The solution was sonicated and once the precipitate separated from the solvent, the solvent was decanted. Residual methanol was evaporated using a rotary evaporator. The product was stored at room temperature. ^{1}H NMR of CBTA Polymer (300 MHz, DMSO-d6): δ 12.52 (s, OH), 6.20 (s, NH3), 3.29 (s, CH). The percent of platinum measured by ICP-MS is 27% (w/w).

2.2.5 Synthesis and characterization of PIMA Polymer

Poly(isobutylene-alt-maleic anhydride) (PIMA, approximately 25mg, 4.2μmol, Sigma Aldrich, Cat # 531278-250G) and oxoplatin (approximately 50mg, 40 equiv.) were combined in a 20mL vial with dimethylformamide (DMF, 1mL). Reaction was set to 55°C and proceeded for 24 hours. Reaction was stopped and placed at 4°C overnight. Acetone was added to the reaction mixture and the solution was transferred to a 15mL conical tube for centrifugation. Solvent was decanted and the precipitate was kept at 4°C before lyophilization. The product was stored at room temperature. ^{1}H NMR of PIMA Polymer (400 MHz, DMSO-d6): δ 12.21 (s, OH), 8.06 (m, NH3),

2.88 (d, CH), 2.57 (d, CH2), 0.92 (s, CH3). The percent of platinum measured by ICP-MS is 40% (w/w).

2.2.6 Synthesis and characterization of Cis Octyl

Oxoplatin (121.2mg, 0.36mmol) was added to a 20mL vial in DMF (2.2mL). Octyl isocyanate (383µL, 6 equiv., Sigma Aldrich, Cat # 329746-5G) was then added. Reaction was closed and proceeded for 24 hours at room temperature. Reaction was stopped and DMF was evaporated using a rotary evaporator with the water bath set at 60-70°C. Ice cold diethyl ether was added, and solution was sonicated to force unreacted octyl isocyanate dissolution. Once precipitate separated from solvent, diethyl ether was decanted. A 1:1 mixture of ice-cold diethyl ether and dichloromethane (DCM) was added, and the process of sonicating and decanting was repeated. The precipitate was placed on the vacuum for 3 days. The yellow solid product was stored at room temperature. Cis Octyl was collected in 76.1% (177.4mg) yield. ^{1}H NMR of Cis Octyl (400 MHz, DMSO-d6): δ 6.75 (s, 6H, NH3), 3.26 (s, 4H, CH2), 2.86 (d, 4H, CH2), 1.34 (s, 4H, CH2), 1.21 (s, 16H, CH2), 0.90 (m, 6H, CH3). ^{195}Pt NMR in DMSO-d6 δ: 1283. ESI-MS calculated for m/z 643.22, found 667.2115 [M + H + Na].

2.2.7 Synthesis and characterization of Cis OD

Oxoplatin (102.8mg, 0.31mmol) in DMF (2mL) and octadecyl isocyanate (642µL, 6 equiv., Sigma Aldrich, Cat # 305405-5G) were added to a 20mL vial. The synthesis followed the same reaction procedure as described for Cis Octyl in section 2.2.6. Cis OD was collected in 89.5% (254mg) yield. ^{1}H NMR of Cis OD (400 MHz, DMSO-d6): δ 6.68 (s, 6H, NH3), 3.31 (s, 4H, CH2), 1.52 (q, 4H, CH2), 1.23 (s, 60H, CH2), 0.85 (m, 6H, CH3). ESI-MS calculated for m/z 923.54, found 924.5355 [M + H].

2.2.8 Synthesis and characterization of Cis DICD

Oxoplatin (49.4mg, 0.15mmol) was dissolved in DMF (2mL) in a 20mL vial. 1,12-diisocyanatododecane (DICD, 48μL, 1.2 equiv., Sigma Aldrich, Cat # 341762-5G) was added to the oxoplatin solution. The reaction mixture was stirred at room temperature and proceeded for 48 hours. The synthesis followed the same reaction procedure as described for Cis Octyl in section 2.2.6. ^{1}H NMR of Cis DICD (400 MHz, DMSO-d6): δ 7.95 (s, NH), 3.31 (s, CH2), 2.89 (s, CH2), 2.73 (d, CH2), 1.23 (s, NH3). The percent of platinum measured by ICP-MS is 18% (w/w).

2.2.9 Synthesis and characterization of Dox Polymer

Doxorubicin (100mg, 0.17mmol) and poly(isobutylene-alt-maleic anhydride) (25.9mg, 0.025 equiv.) were combined in a 20mL vial with DMF (2mL). Reaction mixture was closed and stirred at room temperature for 48 hours. Reaction was stopped and solution was dialysed in methanol (about 2L) using SnakeSkin dialysis tubing (3500 Da MWCO) to remove unreacted doxorubicin. Fresh methanol was replaced 3 times. Dox Polymer solution was collected in a clean 20mL vial and excess methanol was evaporated using a rotary evaporator before lyophilizing the precipitate. The red solid product was stored at 4°C. Dox Polymer yield was 107.5mg. ^{1}H NMR of Dox Polymer (400 MHz, DMSO-d6): δ 13.28 (s, OH), 12.36 (s, OH), 7.94 (d, CH), 7.80 (s, CH), 7.68 (t, CH), 5.46 (m, OH), 5.30 (s, CH), 4.96 (t, OH), 4.89 (t, CH), 4.57 (d, CH2), 4.18 (q, CH), 4.00 (s, CH3), 3.56 (s, CH), 3.52 (s, CH), 3.32 (s, NH2), 2.95 (m, CH2), 2.33 (s, CH2), 2.14 (d, CH2), 1.82 (m, CH2), 1.16 (m, CH3), 0.89 (m, CH3).

Amount of doxorubicin attached to Dox Polymer was measured by absorbance given its chromophore nature. A standard curve was first generated. Doxorubicin was dissolved in DMSO at a concentration of 0.5mg/mL and was serially diluted until 0.004mg/mL. The concentrations were added to a black 96-well plate with a clear flat bottom (Sigma Aldrich). Absorbance was measured at 485nm using a BioTek Synergy Neo2 Microplate Reader (Agilent). Optical density

(OD) values were plotted against amount of doxorubicin (mg) to obtain a linear relationship. Dox Polymer was dissolved in DMSO at 1mg/mL and serially diluted to 0.125mg/mL. Each concentration was plated in triplicate in the 96-well plate. Amount of doxorubicin in the Dox Polymer concentrations was calculated using the corresponding OD values and equations generated from the standard curve. Percent doxorubicin in Dox Polymer measured by absorbance is roughly 75%.

2.2.10 Synthesis and characterization of C_{16}-Met

Hexadecylamine (about 200mg, 0.83mmol, Sigma Aldrich, Cat # H7408-500G) and dicyandiamide (about 250mg, 4 equiv., Sigma Aldrich, Cat # D76609-25G) were added to an RB flask. 2M hydrochloric acid (HCl, 8mL) was added. A reflux condenser was equipped to the RB flask to cool the produced vapour back to the reaction vessel. Reaction was heated to 100°C for 24 hours. The reaction mixture cooled to room temperature before filtering through 5μm filter paper in a glass funnel. The precipitate was washed with excess water and diethyl ether to remove unreacted dicyandiamide and hexadecylamine, respectively. The resulting product was scraped into a clean 20mL vial and left to air dry before storing at 4°C. ^{1}H NMR of (400 MHz, DMSO-d6): δ 8.29 (s, 4H, NH), 2.97 (s, 2H, CH2), 1.76 (t, 2H, NH2), 1.25 (m, 28H, CH2), 0.87 (m, 3H, CH3). ^{13}C NMR (101 MHz, DMSO-d6) δ 155.57, 154.45, 38.71, 31.29, 28.93, 28.84, 28.70, 28.54, 26.94, 25.83, 22.09, 13.96. ESI-MS calculated for m/z 325.32, found 326.3284 [M + H].

2.2.11 Synthesis and characterization of C_6-Met

Hexylamine (789μL, 5.9mmol, Sigma Aldrich, Cat # 8.04326.0100) and dicyandiamide (1.996g, 4 equiv.) were combined in a 100mL RB flask with 2M HCl (16mL). Reaction was set at 100°C and proceeded for 24 hours. The reaction was stopped and cooled at room temperature for 2 hours. Precipitate appeared and the flask was placed in the 4°C fridge overnight. The solution

was transferred to 20mL vials and placed at -80°C before lyophilization. After freeze drying, excess diethyl ether was added to each vial to remove unreacted hexylamine. After washing, the solvent was removed, and the product was left to air dry covered. Thin layer chromatography (TLC) was performed to confirm product was distinct from reagents. Briefly, both reagents and product were dabbed onto aluminium-based TLC paper (Silicycle, Cat # TLA-R10011B-323) using capillary tubes (Chemglass Life Sciences). Mobile phase consisted of 10% methanol in chloroform. TLC paper was placed in a small amount of mobile phase and reagents and product travelled up the paper. Iodine powder staining revealed distinct formations on the TLC paper. White solid product was stored at 4°C. ^{1}H NMR (400 MHz, DMSO-d6): δ 10.18 (s, 4H, NH), 7.86 (s, 2H, NH2), 2.74 (s, 2H, CH2), 1.52 (q, 2H, CH2), 1.28 (d, 6H, CH2), 0.86 (m, 3H, CH3). ^{13}C NMR (101 MHz, DMSO-d6) δ 155.66, 154.50, 38.72, 30.75, 26.89, 25.55, 21.92, 13.87.

2.3 Dox Polymer – metformin binding studies

The ability of the available carboxylic acid group on the Dox Polymer to hydrogen bond with guanidine groups on metformin and metformin derivatives was assessed using absorbance. Dox Polymer was combined with either metformin or C_{16}-Met, each at a concentration of 1mg/mL in 1:1 DMSO:Water, at a 1:0.1 (v/v) ratio increasing to a 1:3 (v/v) ratio. Equivalent ratios were also made using Dox Polymer with solvent to act as a control. All combinations were plated in a black 96-well plate with a clear flat bottom. Absorbance was measured using a microplate reader across a range of wavelengths (300-700nm), measuring at 5nm increments. OD values at 350nm were adjusted to the measurement of Dox Polymer alone to normalize starting absorbance value. All measurements were adjusted using the same reference difference. OD values measured at 545nm (approaching the point of equilibrium) were plotted against Dox Polymer concentration

when combined with either metformin, C_{16}-Met or solvent. The observed linear relationship for each condition was plotted and an equation was determined.

2.4 Cell culture

Human epithelial SKOV-3 cells (ATCC, Manassas, Virginia, United States) were cultured in McCoy's 5A medium (Cedarlane, Cat # 30-2007) supplemented with 10% heat inactivated fetal bovine serum (FBS, Corning), and 1% penicillin/streptomycin/L-Glutamine (Corning). ID8;p53$^{-/-}$;BRCA1$^{-/-}$ (provided by Dr. Vanderhyden) derived from spontaneously transformed ovarian surface epithelial cells from C57BL/6 mice were cultured in 1x Dulbecco's Modification of Eagle's Medium (DMEM, Wisent) supplemented with 1x Insulin-Transferrin-Selenium (ITS-G, Gibco – Thermo Fisher), 4% heat inactivated FBS, and 1% penicillin/streptomycin/L-Glutamine. Cisplatin-sensitive (A2780-S, provided by Dr. Beug) and cisplatin-resistant (A2780-CP, provided by Dr. Tsang) cells were derived from human endometrioid ovarian carcinoma. Both A2780 cells were cultured in 1x Roswell Park Memorial Institute (RPMI) 1640 medium (Wisent) supplemented with 0.5% Amphotericin B (250µg/mL, Thermo Fisher), 10% heat inactivated FBS, and 0.5% penicillin/streptomycin/L-Glutamine. Cells were grown in humidified incubators at 37°C with 5% CO_2 and split every 2-3 days.

2.5 MTT assays to determine drug synergy

Synergistic drug ratios were determined by MTT assays. Seeding densities were first optimized to ensure final absorbance values were within a linear range. SKOV-3, ID8;p53$^{-/-}$;BCRA1$^{-/-}$, and A2780-S and A2780-CP cells were seeded at 1000 cells/well, 500 cells/well, and 2000 cells/well, respectively in 96-well plates. Cells grew overnight and were incubated with various concentrations of cisplatin, olaparib, metformin and all possible combinations. The plates were then incubated for 72 hours. Drug media was replaced with 10µL of MTT reagent (3-(4,5-

Dimethylthiazol-2-yl)-2,5-Diphenyltetrazolium Bromide, Alfa Aesar, Cat # L11939) (5mg/mL in 1x phosphate buffered saline, PBS) and 90µL of phenol red free culture media (Wisent); taken from a master mix preparation. The plate was covered in tin foil and incubated for 30 minutes. Cells were then lysed with 100µL DMSO and placed on a plate shaker for 15 minutes. Purple formazan crystals were detected by optical density using a microplate reader at 570nm. Background absorbance was also detected at 630nm. No treatment (Tx) cell group was assumed to be 100% viable. Percent cell viability and cytotoxicity were calculated by subtracting background absorbance and using the averages of 3 technical replicates using the following equations:

$$\%\ Cell\ viability = \left(\frac{sample}{No\ Tx}\right) * 100$$

$$\%\ Cytotoxicity = \left(\frac{(No\ Tx - sample)}{No\ Tx}\right) * 100$$

Percent cytotoxicity values were inputted into either CompuSyn software (New Jersey, USA) or Synergy Finder (Helsinki, Finland), two independent synergy calculating software. CompuSyn software generates combination index (CI) values by using the Chou Talalay method to calculate synergy. CI < 1 is indicative of a synergistic concentration ratio between two or more agents in terms of cytotoxicity, whereas CI > 1 indicates an antagonistic relationship at specific concentration ratios[83]. Synergy Finder uses the highest single agent (HSA) reference method, in which synergy is denoted when the expected combination effect is greater than the highest effect of both individual drugs at the same concentrations[102].

2.6 Polymeric NP synthesis

Polymeric NPs were synthesized using previously described self-assembly nanoprecipitation methods[103,104]. Briefly, PLGA-PEG (50kDa – 5kDa MW, 75:25 L:G ratio,

methyl terminated, PolySciTech, Cat # AK148) was dissolved in ACN at a concentration of 10mg/mL. 1mM solutions of DTB and AA Polymers were prepared in DMF. Percent platinum values determined by ICP-MS were utilized to adjust for appropriate amount of drug-polymer that was equivalent to 1mM of pure cisplatin. 30mg/mL solution of olaparib and 8mg/mL solutions of C_{16}-Met and C_6-Met in DMSO were all prepared. Single, dual, and triple drug NPs were synthesized using these drug solutions in different combinations. All formulations followed the same procedure irrespective of number of drugs. PLGA-PEG, cisplatin drug-polymer, olaparib, and metformin derivative were added to a 1.5mL microcentrifuge tube (VWR) maintaining a (v/v) ratio of 3:1 polymer:total drug content. The ratio between cisplatin polymer, olaparib, and metformin derivative was 1:2.5:2.5 (v/v/v). The polymer and drug solution was lightly vortexed before adding dropwise to water, respecting an organic to aqueous phase ratio of 1:10 (v/v). NPs were spun to allow self-assembly on a multi-position stir plate at approximately 600rpm for 2 hours at room temperature. NP solutions were then filtered and concentrated using centrifugation. Solutions were transferred to 50mL centrifugal filter conical tubes (100kDa MWCO, VWR, Cat # MAP100C38) and centrifuged at roughly 3000rpm for 10 minutes. NPs were washed with 0.5mL sterile water between the first 2 out of 5 rounds of centrifugation. Once concentrated NPs were 1-10% of the starting volume (including the aqueous phase), they were collected in fresh microcentrifuge tubes and stored at 4°C for further characterization and in vitro testing. Empty NPs were synthesized using the same outlined method, except drug volumes were replaced by solvent (DMF and/or DMSO) alone.

2.7 NP characterization

2.7.1 Transmission electron microscopy

NP morphology was determined using transmission electron microscopy (TEM). A single droplet of concentrated NPs was added to carbon-coated copper grids (400 mesh, Ted Pella, Cat # 01822). Using forceps, excess solution that did not attach to the grid was wicked off onto filter paper. NPs were then negatively stained with uranyl acetate (Electron Microscopy Sciences, Cat # 22409), blotted again, and washed with water. Grids were allowed to dry for at least 24 hours before imaging. Electron micrographs were taken using a JEM-1400Flash TEM (120kv) system.

2.7.2 Size, polydispersity index, surface charge, and encapsulation efficiency

NP size, polydispersity index (PDI) and surface charge (zeta potential) were all measured by dynamic light scattering using a ZetaSizer Nano Series machine (Malvern Panalytical, United Kingdom). To prepare samples, 10µL of concentrated NPs were diluted in 1mL sterile water in polystyrene cuvettes (Fisher Scientific) for size and PDI measurements and folded capillary cells (Malvern Panalytical) for surface charge determination. Three sets of five measurements each were recorded at 25°C.

Cisplatin encapsulation efficiency (EE) was determined by ICP-MS. Briefly, NP samples (20-100µL) were digested with 70% nitric acid for 2 hours at 90°C. Samples were then cooled and 0.5mL hydrogen peroxide was added. Samples were diluted in water to a final volume of 250mL, for a final nitric acid concentration of 0.5-2%. A calibration curve was first established using known platinum parts per billion (ppb) concentrations. NP data was compared back to the calibration curve for platinum ppb determinations.

Olaparib EE was measured by high pressure liquid chromatography (HPLC). A standard curve was first prepared using free olaparib. A 0.5mg/mL solution of olaparib was made in a 4:6 ratio of Water:DMSO. Serial dilutions were performed until 0.03125mg/mL. Samples were loaded in 2mL glass vials fitted with glass inserts into the Dionex UltiMate 3000 HPLC machine (Thermo

Fisher). Samples were first mixed before injecting 50µL through a reversed-phase 5µm C_{18} column (250x4.6mm, Thermo Fisher, Cat # 063197), in a column oven heated to 37°C. The mobile phase consisted of water and ACN, both with 0.01% trifluoroacetic acid (Sigma Aldrich), which passed through with a gradient of increasing ACN, with a flow rate of 1mL/min. The eluate was detected using a UV-Vis Diode Array Detector (Thermo Fisher) at 254nm. HPLC data was then processed to determine the area under the curve (mAU*min), which was plotted against amount of olaparib injected (mg) to generate a linear relationship. NP samples were prepared by breaking open 37.5µL concentrated NPs in 50µL DMSO. Digests were placed on a plate shaker for 30 minutes at room temperature. Samples were then immediately loaded into the HPLC machine and run using the same protocol described. Amount of olaparib was calculated using the standard curve equation.

2.7.3 NP stability studies

NP size and PDI stability in various conditions was assessed by dynamic light scattering using the ZetaSizer. Firstly, size and PDI were measured directly upon synthesis completion. NPs were then stored at 4°C. After 60 days of storage, size and PDI were measured again to determine storage stability. As a surrogate for blood serum stability, NP size and PDI were measured following incubation with either 0, 5, or 10% FBS in sterile water at both 25°C and 37°C. Each solution contained 1% NPs. Measurements were taken at 0-, 4-, and 24-hour time points.

2.7.4 Drug release kinetics

Release of cisplatin from the drug-polymer and NP was assessed using dialysis technique in response to pH stimuli. NPs (50µL) were mixed with 1x PBS (50µL) calibrated to either pH 7.4 or 5.5 using acetic acid (Anachemia) for adjustments. Both NP suspension conditions were added to dialysis membrane-lined buckets (20kDa MWCO, Thermo Fisher, Cat # 88402) placed in 15mL conical tubes filled with 1x PBS (14mL) set to the equivalent pH (3 replicates for each condition).

Tubes were placed on a gentle plate shaker, incubated at 37°C. At 24-, 48-, and 72-hour time points, PBS from the different conditions was collected and analyzed for platinum content by ICP-MS, following the same procedure outlined for EE determination in section 2.7.2.

2.8 Flow cytometry H2AX assays

To assess the ability of NP encapsulated cisplatin polymers to successfully release active cisplatin inside cells to cause DNA damage, γH2AX was measured by flow cytometry. SKOV-3 cells were seeded at $2x10^5$ cells per well in 6-well plates and incubated overnight. Cells were then treated with free cisplatin (positive control), DTB-NP, AA-NP, DTB-Ola-C_{16}-Met-NP, E-NP (Empty-NP), or left untreated (negative control) for 24 hours. Cells were then washed with 1x PBS and incubated with 0.05% trypsin/0.53mM EDTA (Corning). Detached cells were collected, using complete medium to neutralize trypsin, into 15mL conical tubes and centrifuged at 1000rpm for 5 minutes at 4°C. Supernatant was discarded, and cell pellet was resuspended and washed with 1x PBS and centrifuged again at 300g for 6 minutes. Supernatant was discarded again, and cell pellet was dislodged by light vortexing while adding ice cold 70% ethanol dropwise to fix and permeabilize the cells. Cells were incubated at -20°C for 60 minutes. Cells were then centrifuged and washed with cell staining buffer (BioLegend, Cat # 420201) 3 times before resuspending at a final concentration of roughly 10^6 cells/100µL. Cells were stained with 5µL of FITC anti-H2A.X Phospho (Ser139) antibody (25µg/mL, BioLegend, Cat # 613403) for 1 hour covered from light at room temperature. Unbound antibody was removed by 2 more washes with cell staining buffer. Cell suspensions were then analyzed by the LSR Fortessa (BD Biosciences, California USA). The median fluorescence intensity (MFI) of the second peak from 2 independent replicates was analyzed and plotted as a bar graph.

2.9 Protein extraction and western blot

For protein extraction, cells were washed with cold 1x PBS and collected into 1.5mL microcentrifuge tubes using cell scrapers (Fisher Scientific). Samples were centrifuged and cells were resuspended in 50μL RIPA lysis buffer (1M NaF, 1M β-glycerophosphate, 1M dithiothreitol, 1mg/mL leupeptin, 1mg/mL aprotinin, 0.2M benzamide, 150mM NaCl, 50mM Tris, 0.1% SDS, 1% Triton X-100, 0.5% sodium deoxycholate, pH 8.0, 1% pepstatin (1mg/mL), 1% phenylmethylsulfonyl fluoride (0.1M), and 0.625% sodium orthovanadate (100mM)), vortexed, and placed at -80°C until ready for western blotting. Before blotting, lysates were thawed and centrifuged at max speed for 10 minutes at 4°C to pellet cell debris. Protein concentration was quantified using a Bradford Lowry Reagent (Bio-Rad, Mississauga, Ontario, Canada). 20μg of protein lysate were loaded and separated on a 10% polyacrylamide gel and subsequently transferred to a polyvinylidene difluoride (PVDF) membrane (Bio-Rad). Membranes were blocked in either 5% bovine serum albumin (BSA, Sigma Aldrich) or skim milk in 1x tris-buffered saline with 0.1% Tween-20 (TBST) for 1 hour at room temperature. Membranes were washed 3 times for 5 minutes with TBST before incubating with primary antibody overnight at 4°C. Three washes were performed again before horseradish peroxidase (HRP) conjugated secondary antibody incubation for 1 hour at room temperature. Membranes were washed 3 more times before imaging using a 1:1 (v/v) ratio of Clarity Western enhanced chemiluminescence and peroxide solutions (Bio-Rad, Cat # 1705061) using a ChemiDoc MP Imaging System (Bio-Rad). Primary and secondary antibodies used include: phospho-AMPKα (Thr172) (1:1000 in BSA, Cell Signaling Technology, Cat # 2535S), AMPKα (1:1000 in BSA, Cell Signaling Technology, Cat # 5831S), PARP (1:1000 in milk, Cell Signaling Technology, Cat # 9542S), cleaved PARP (Asp214) (1:1000 in milk, Cell Signaling Technology, Cat # 9541S), Caspase-3 (1:1000 in milk, Cell Signaling Technology, Cat # 9662S), cleaved Caspase-3 (Asp175) (1:1000, Cell Signaling Technology, Cat

9664T), GAPDH (1:1000, Thermo Fisher, Cat # MA5-15738), anti-rabbit IgG, HRP-linked (1:2000, Cell Signaling Technology, Cat # 7074S), and anti-mouse IgG, HRP-linked (1:2000, Cell Signaling Technology, Cat # 7076S).

2.10 Cell viability

Cell viability following NP treatment was assessed using MTT assays as previously described in section 2.5.

2.11 Statistical analysis

Data is presented as means ± standard error of the mean (SEM). Three technical replicates were performed for every biological replicate. Where appropriate, statistical analysis was performed using GraphPad prism. Statistical analyses conducted include paired Student's t tests and simple linear and nonlinear regression analysis. Statistical significance was defined as $p < 0.05$.

3.0 Results

3.1 Cisplatin, doxorubicin, and metformin prodrug and derivative library reveals successfully synthesized products

Non-selective distribution of cisplatin contributes to serious systemic toxicities in patients. Encapsulating cisplatin inside a NP to promote targeted delivery provides an attractive option to improve cisplatin therapy. However, the hydrophilicity of cisplatin prevents efficient loading into the NP hydrophobic core. Various cisplatin prodrugs were synthesized to increase hydrophobicity without altering pharmacological effects. Firstly, each prodrug synthesis required hydroxyl groups functionalized to the axial positions of cisplatin (Oxoplatin synthesis) for reactivity with different dicarboxylic acids, dianhydrides and cyanates. Each prodrug conjugate possesses a different purpose, increasing the therapeutic options. DTB Polymer contains a disulfide bond in the linker moiety connecting cisplatin units together for GSH scavenging potential (**Figure 4A**). AA Polymer was created to serve as a control for DTB Polymer, thereby mimicking the structure, except lacking the disulfide bond (**Figure 5A**). Alternatively, CBTA Polymer and PIMA Polymer contain available carboxylic acid groups for non-covalent binding of hydrogen donating drugs, such as metformin, for increased encapsulation inside NPs (**Figure 6A and C**). Small molecule cisplatin prodrugs, Cis Octyl and Cis OD, were also synthesized for non-polymeric options, using cyanates with varying hydrocarbon chain lengths. Cis DICD was created as a synthetically similar polymer prodrug to the small molecule conjugates Cis Octyl and Cis OD for comparison of cyanate functional groups (**Figure 7A**). All structures were confirmed by ^{1}H NMR and/or ^{13}C NMR, revealing pure correctly synthesized structures (**Figures 4-7**).

(A)

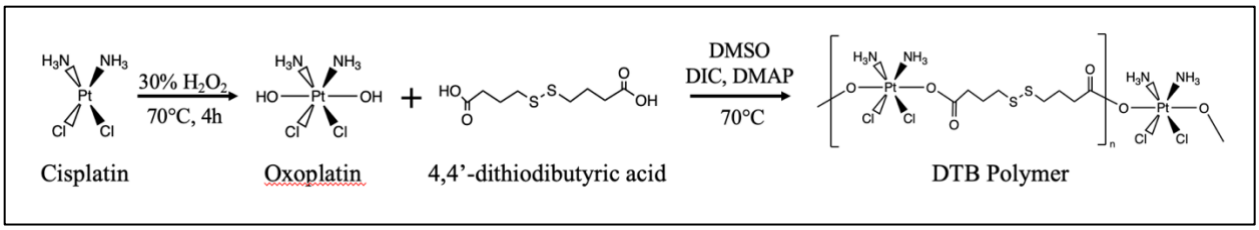
30% H2O2
70°C, 4h
DMSO
DIC, DMAP
70°C
Cisplatin
Oxoplatin
4,4'-dithiodibutyric acid
DTB Polymer

(B)

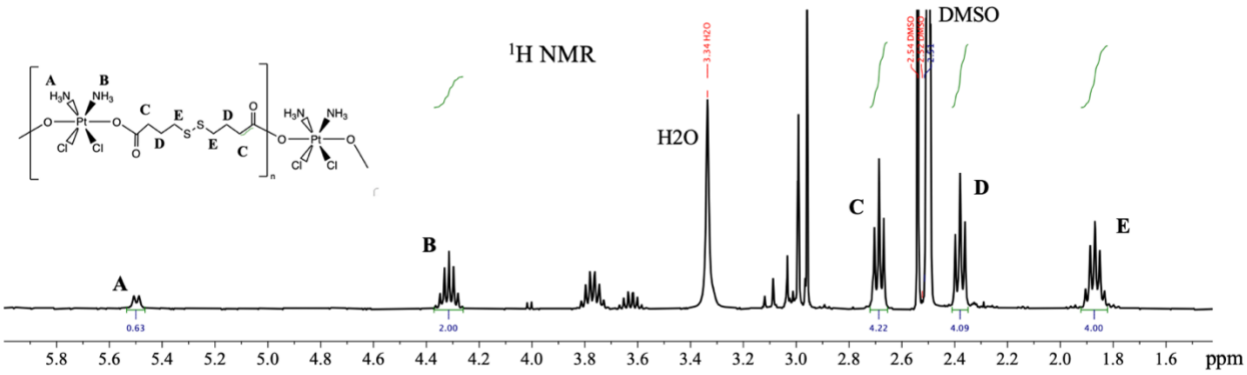
1H NMR
H2O
DMSO
A
B
C
D
E
0.63
2.00
4.22
4.09
4.00
ppm

(C)

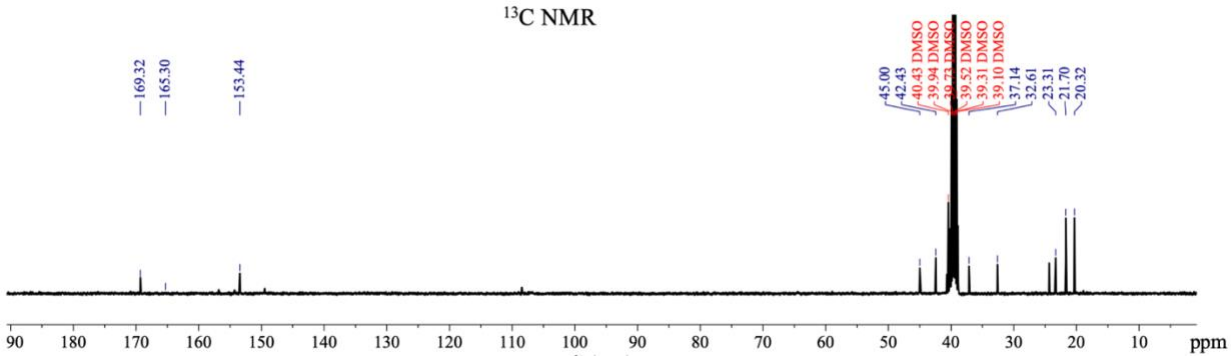
13C NMR
169.32
165.30
153.44
45.00
42.43
40.43 DMSO
39.94 DMSO
39.73 DMSO
39.52 DMSO
39.31 DMSO
39.10 DMSO
37.14
32.61
23.31
21.70
20.32
ppm

Figure 4. Synthesis and characterization of DTB Polymer conjugate. (A) Synthetic scheme of DTB Polymer. Cisplatin reacted with 30% hydrogen peroxide (H_2O_2) at 70°C for 4 hours to form oxoplatin. Oxoplatin reacted with 4,4'-dithiodibutyric acid in DMSO with DIC and DMAP activators at 70°C to form DTB polymer. (B) ^{1}H NMR spectrum in DMSO-d6. Peaks corresponding to specific hydrogens in the compound are identified using alphabetical labeling. (C) ^{13}C NMR spectrum in DMSO-d6. DMSO, dimethyl sulfoxide; DIC, N,N'-diisopropylcarbodiimide; DMAP, 4-dimethylaminopyridine; NMR, nuclear magnetic resonance; ppm, parts per million.

(A)

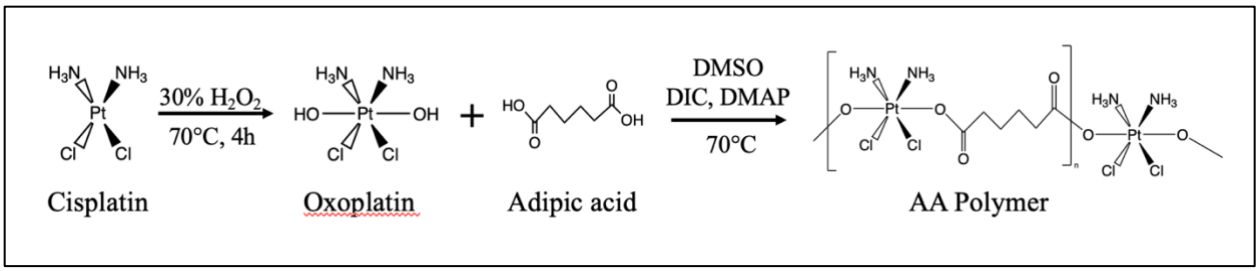
30% H2O2
70°C, 4h
DMSO
DIC, DMAP
70°C
Cisplatin
Oxoplatin
Adipic acid
AA Polymer

(B)

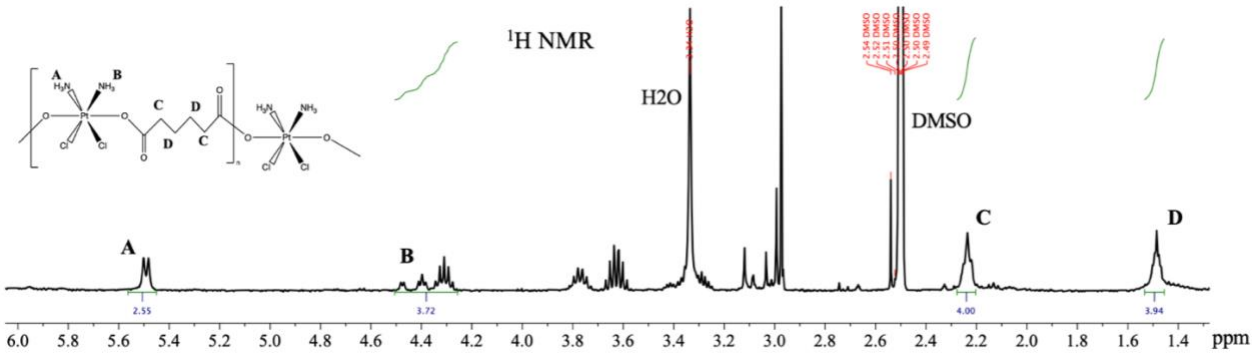
1H NMR
H2O
DMSO
A
B
C
D
2.55
3.72
4.00
3.94
ppm

(C)

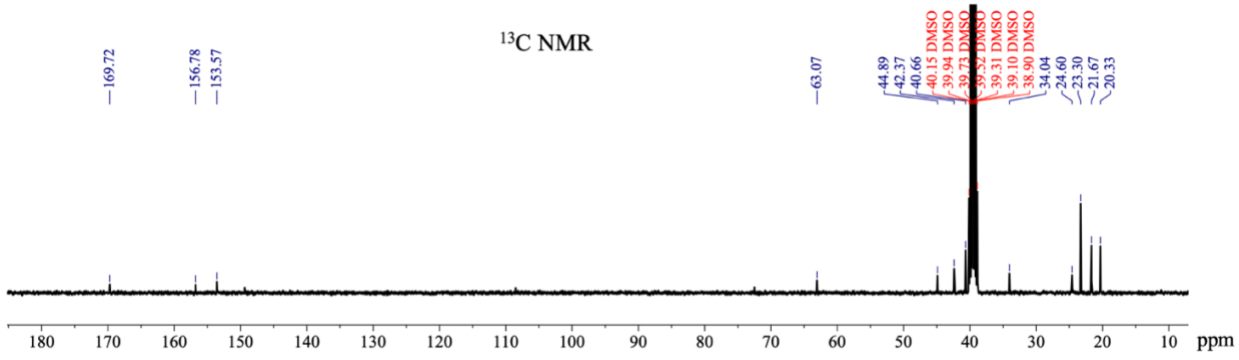
13C NMR
169.72
156.78
153.57
63.07
44.89
42.37
40.66
40.15 DMSO
39.94 DMSO
39.73 DMSO
39.52 DMSO
39.31 DMSO
39.10 DMSO
38.90 DMSO
34.04
24.60
23.30
21.67
20.33
ppm

Figure 5. Synthesis and characterization of AA Polymer conjugate. (A) Synthetic scheme of AA Polymer. Cisplatin reacted with 30% hydrogen peroxide (H_2O_2) at 70°C for 4 hours to form oxoplatin. Oxoplatin reacted with adipic acid with DIC and DMAP activators at 70°C to form AA polymer. (B) ^{1}H NMR spectrum in DMSO-d6. Peaks corresponding to specific hydrogens in the compound are identified using alphabetical labeling. (C) ^{13}C NMR spectrum in DMSO-d6. DMSO, dimethyl sulfoxide; DIC, N,N'-diisopropylcarbodiimide; DMAP, 4-dimethylaminopyridine; NMR, nuclear magnetic resonance; ppm, parts per million.

(A)

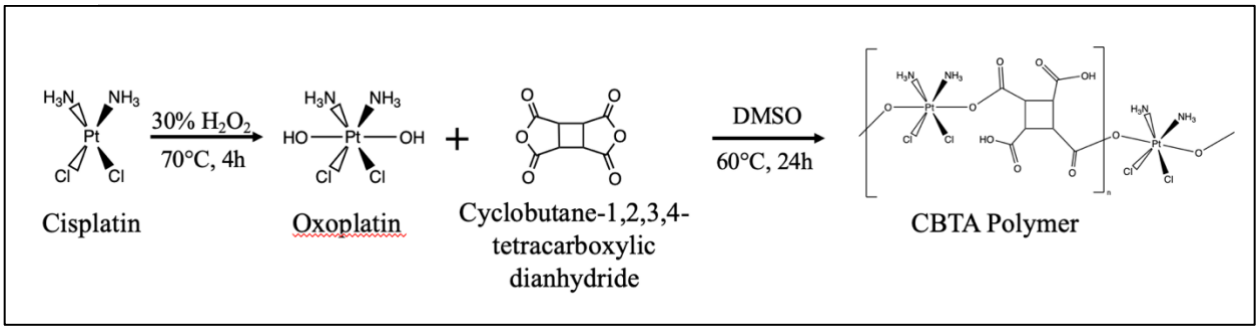
30% H2O2
70°C, 4h
DMSO
60°C, 24h
Cisplatin
Oxoplatin
Cyclobutane-1,2,3,4-tetracarboxylic dianhydride
CBTA Polymer

(B)

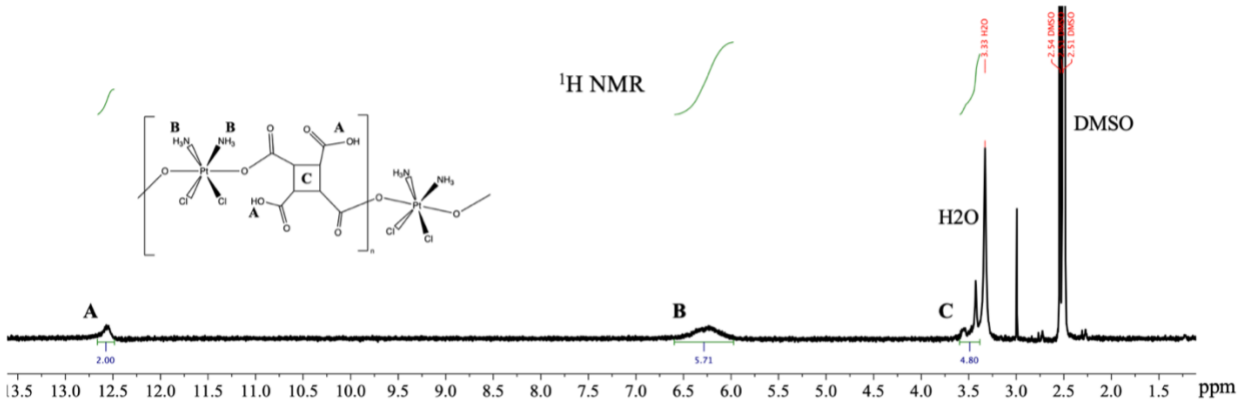
1H NMR
DMSO
H2O
A
B
C
2.00
5.71
4.80
ppm

(C)

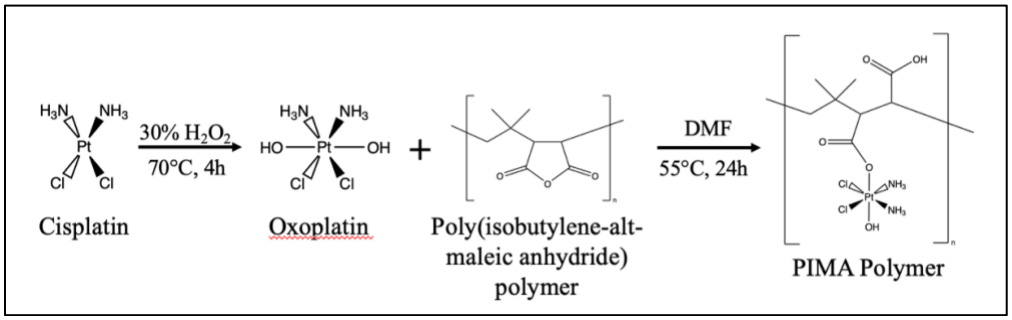
30% H2O2
70°C, 4h
DMF
55°C, 24h
Cisplatin
Oxoplatin
Poly(isobutylene-alt-maleic anhydride) polymer
PIMA Polymer

(D)

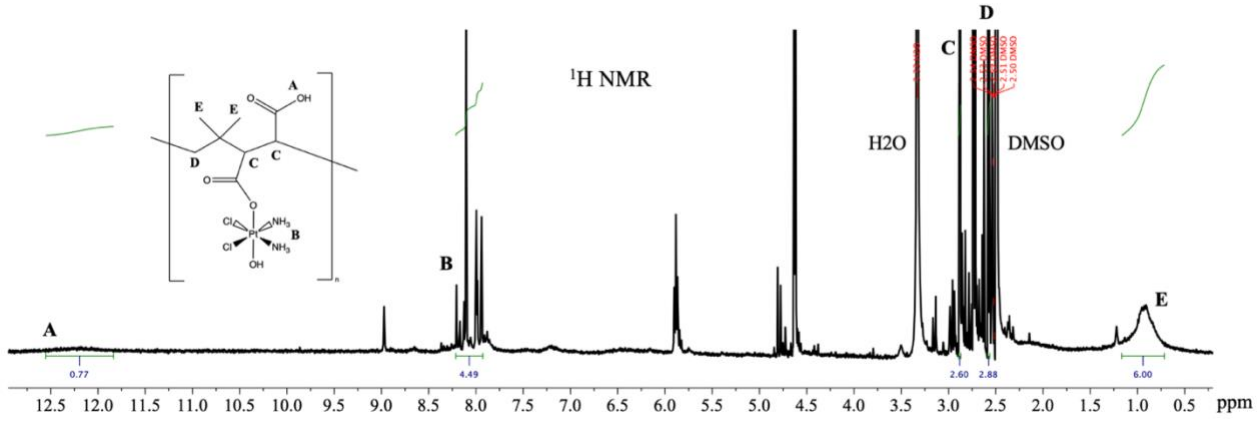
1H NMR
H2O
DMSO
A
B
C
D
E
0.77
4.49
2.60
2.88
6.00
ppm

Figure 6. Synthesis and characterization of additional cisplatin polymer conjugates. (A) Synthetic scheme of CBTA Polymer. Cisplatin reacted with 30% hydrogen peroxide (H_2O_2) at 70°C for 4 hours to form oxoplatin. Oxoplatin reacted with cyclobutane-1,2,3,4-tetracarboxylic dianhydride in DMSO at 60°C for 24 hours to form CBTA polymer. (B**)** ^{1}H NMR spectrum of CBTA Polymer in DMSO-d6. (C) Synthetic scheme of PIMA Polymer. The same starting oxoplatin reaction was performed. Oxoplatin reacted with poly(isobutylene-alt-maleic anhydride) polymer in DMF at 55°C for 24 hours to form PIMA polymer. (D) ^{1}H NMR spectrum of PIMA Polymer in DMSO-d6. Peaks corresponding to specific hydrogens in the compound are identified using alphabetical labeling in both polymer NMR spectra. DMSO, dimethyl sulfoxide; NMR, nuclear magnetic resonance; DMF, dimethylformamide; ppm, parts per million.

(A)

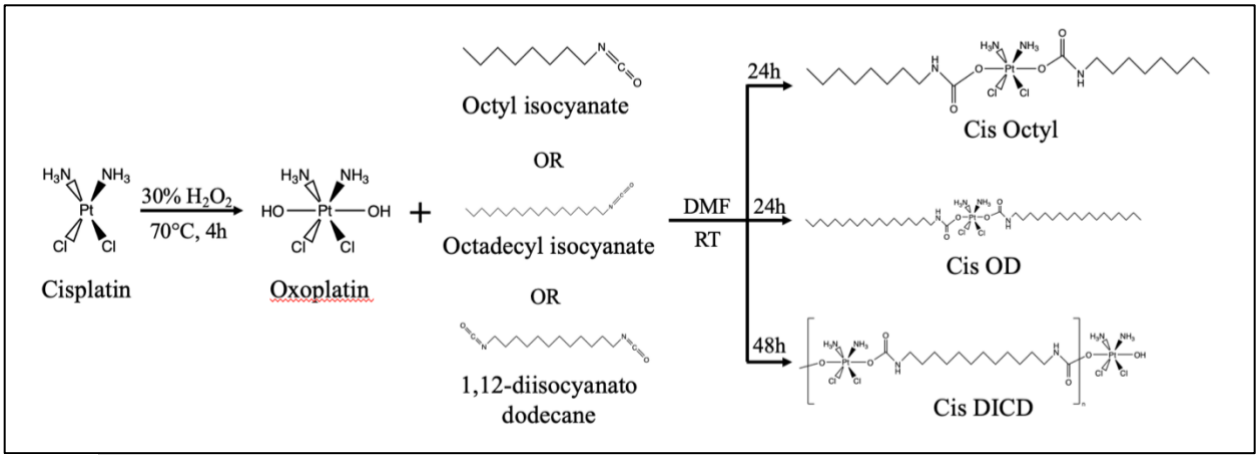
Cisplatin
30% H2O2
70°C, 4h
Oxoplatin
Octyl isocyanate
OR
Octadecyl isocyanate
OR
1,12-diisocyanato dodecane
DMF
RT
24h
Cis Octyl
24h
Cis OD
48h
Cis DICD

(B)

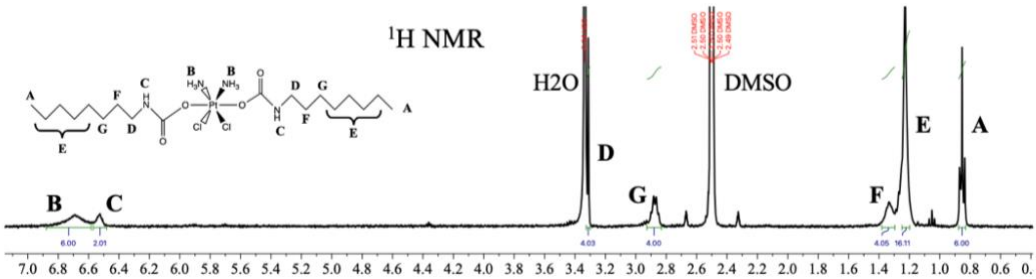
1H NMR
H2O
DMSO
A
B
C
D
E
F
G
ppm

(C)

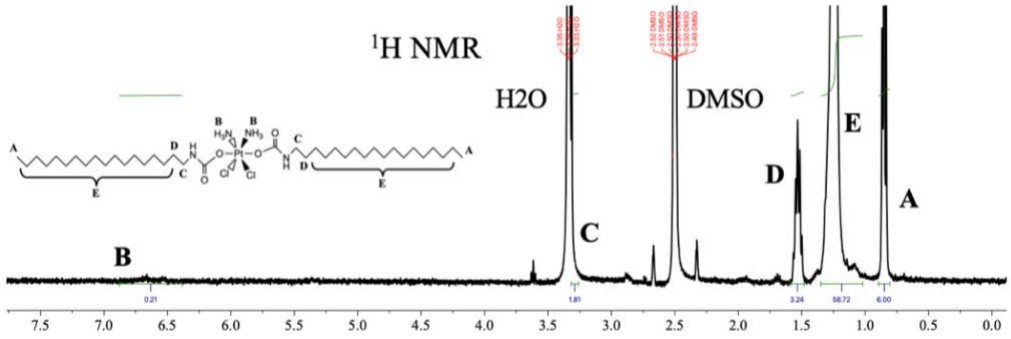
1H NMR
H2O
DMSO
A
B
C
D
E
ppm

(D)

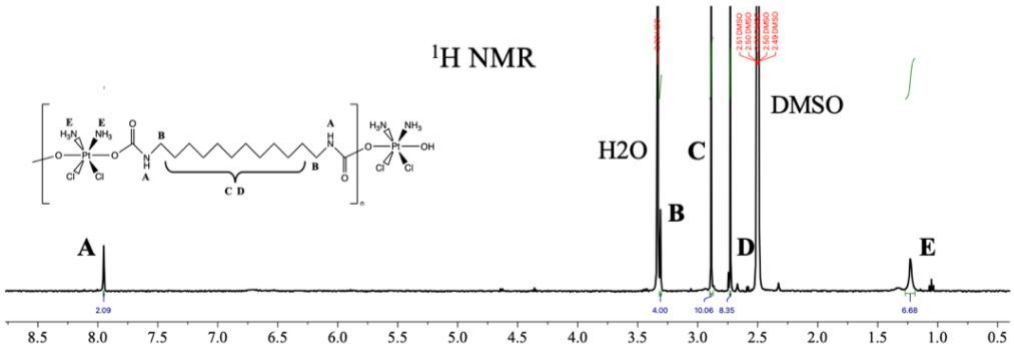
1H NMR
H2O
DMSO
A
B
C
D
E
ppm

Figure 7. Synthesis and characterization of cisplatin conjugates formed with cyanate reagents. (A) Synthetic scheme of Cis Octyl, Cis OD and Cis DICD. Cisplatin reacted with 30% hydrogen peroxide (H_2O_2) at 70°C for 4 hours to form oxoplatin. Oxoplatin reacted with either octyl isocyanate, octadecyl isocyanate or 1,12-diisocyanatododecane in DMF at RT for either 24 or 48 hours to form Cis Octyl, Cis OD, or Cis DICD, respectively. (B) ^{1}H NMR spectrum of Cis Octyl in DMSO-d6. (C) ^{1}H NMR spectrum of Cis OD in DMSO-d6. (D) ^{1}H NMR spectrum of Cis DICD in DMSO-d6. Peaks corresponding to specific hydrogens in the compound are identified using alphabetical labeling in all 3 NMR spectra. DMF, dimethylformamide; RT, room temperature; NMR, nuclear magnetic resonance; DMSO, dimethyl sulfoxide; ppm, parts per million.

To expand the scope of these prodrug conjugates to other classes of chemotherapeutics, Dox Polymer was synthesized, containing doxorubicin and the same polymer backbone used for PIMA Polymer synthesis. Therefore, the synthesis product, Dox Polymer, also contains an available carboxylic acid for additional drug binding (**Figure 8A**). Dox Polymer structure and purity were confirmed by ^{1}H NMR (**Figure 8B**).

Similar to cisplatin, metformin is also hydrophilic, thus posing the same encapsulation limitation. To increase metformin loading into PLGA-PEG NPs, two different metformin derivatives, C_{16}-Met and C_{6}-Met, were synthesized to create structures with varying hydrocarbon chain lengths to optimize for best encapsulation, while maintaining structural similarity to metformin (**Figure 9A and 10A**). Both C_{16}-Met and C_{6}-Met were characterized by ^{1}H NMR and ^{13}C NMR (**Figure 9B and 10B**).

(A)

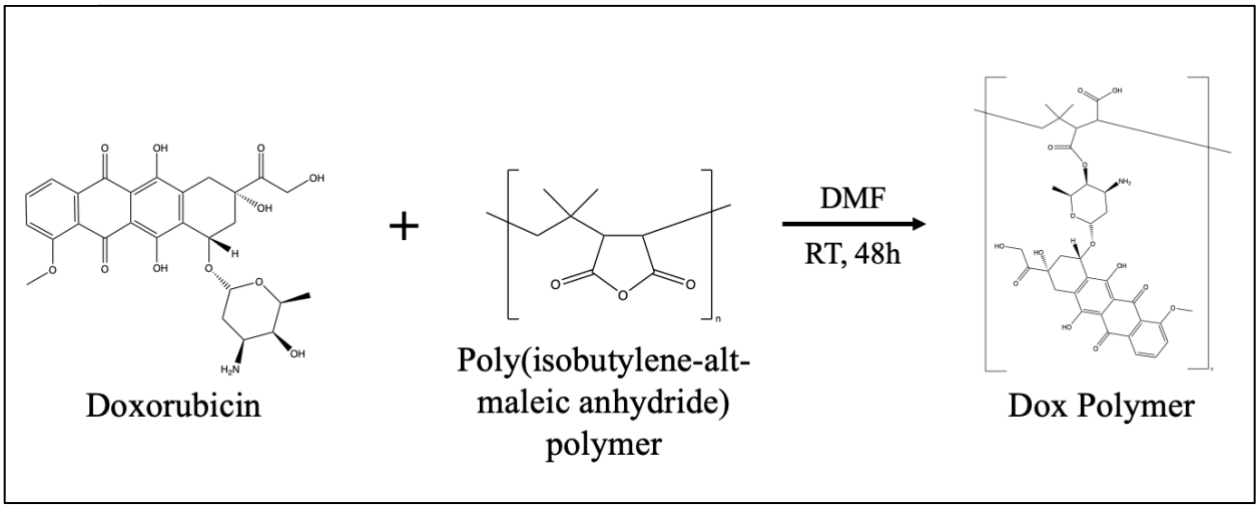
DMF
RT, 48h
Doxorubicin
Poly(isobutylene-alt-maleic anhydride) polymer
Dox Polymer

(B)

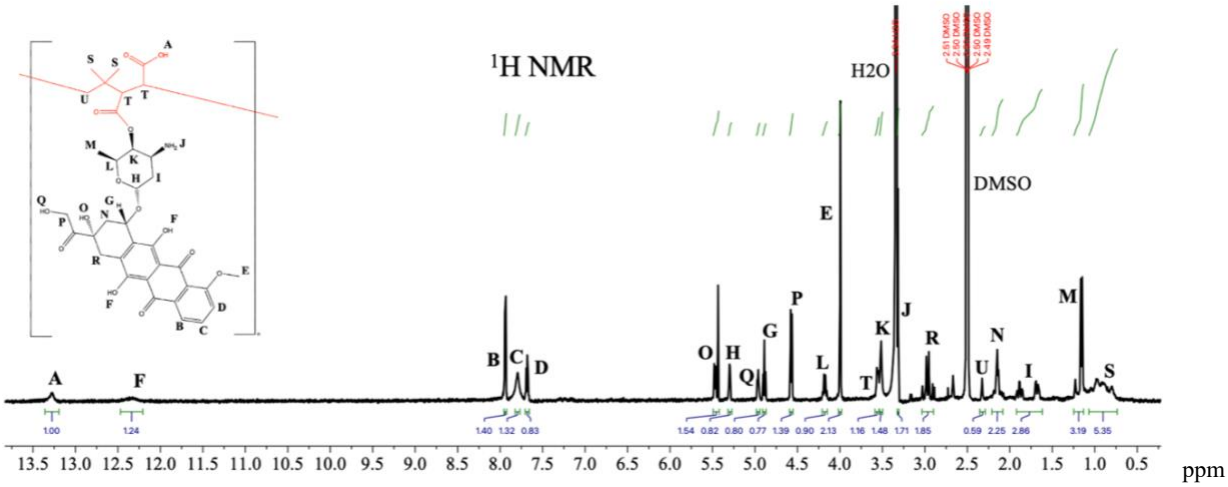
^{1}H NMR
H2O
DMSO
ppm

Figure 8. Synthesis and characterization of Dox Polymer prodrug. (A) Synthetic scheme of Dox Polymer. Doxorubicin reacted with poly(isobutylene-alt-maleic anhydride) polymer in DMF at RT for 48 hours to form Dox Polymer. (B) ^{1}H NMR spectrum in DMSO-d6. Peaks corresponding to specific hydrogens in the compound are identified using alphabetical labeling. DMF, dimethylformamide; RT, room temperature; NMR, nuclear magnetic resonance; DMSO, dimethyl sulfoxide; ppm, parts per million.

(A)

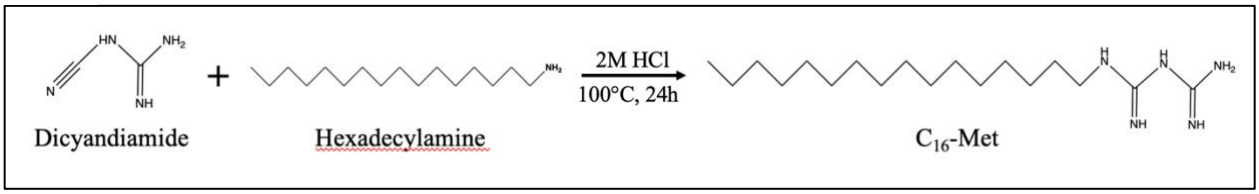
2M HCl
100°C, 24h
Dicyandiamide
Hexadecylamine
C_{16}-Met

(B)

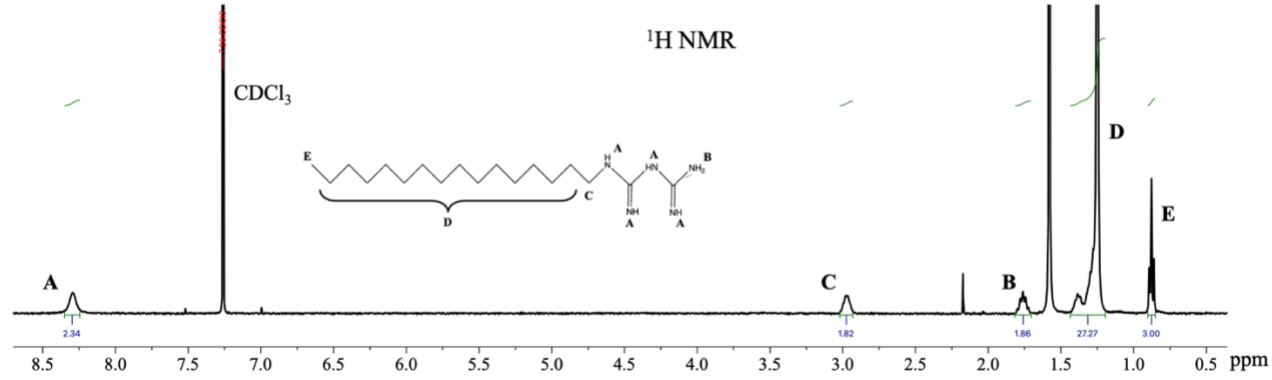
^{1}H NMR
$CDCl_3$
A
B
C
D
E
2.34
1.82
1.86
27.27
3.00
ppm

(C)

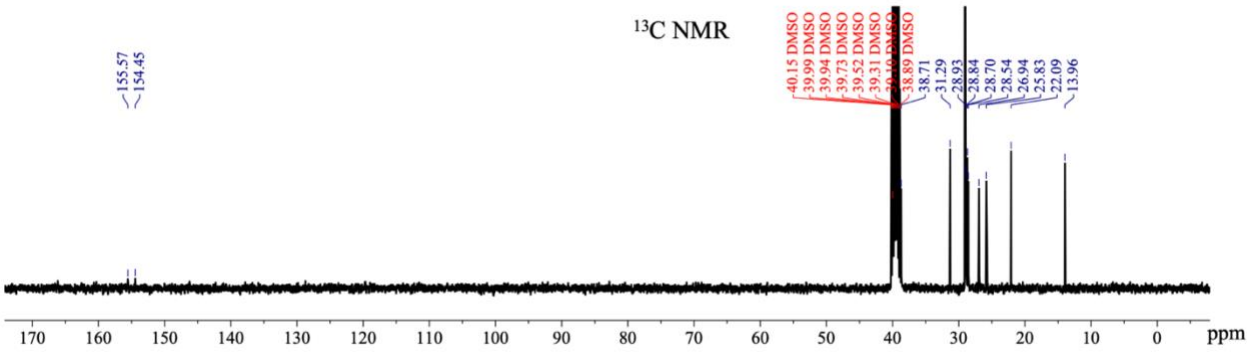
^{13}C NMR
155.57
154.45
40.15 DMSO
39.99 DMSO
39.94 DMSO
39.73 DMSO
39.52 DMSO
39.31 DMSO
38.89 DMSO
38.71
31.29
28.93
28.84
28.70
28.54
26.94
25.83
22.09
13.96
ppm

Figure 9. Synthesis and characterization of C_{16}-Met derivative. (A) Synthetic scheme of C_{16}-Met derivative. Dicyandiamide reacted with hexadecylamine in 2M HCl at 100°C for 24 hours to form C_{16}-Met. (B) ^{1}H NMR spectrum in $CDCl_3$. Peaks corresponding to specific hydrogens in the compound are identified using alphabetical labeling. (C) ^{13}C NMR spectrum in DMSO-d6. HCl, hydrochloric acid; NMR, nuclear magnetic resonance; $CDCl_3$, chloroform-D; DMSO, dimethyl sulfoxide; ppm, parts per million.

(A)

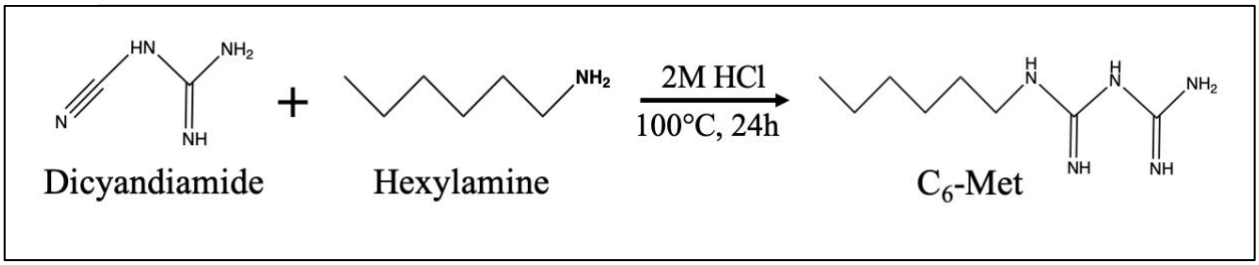
HN
NH2
N
NH
NH2
2M HCl
100°C, 24h
H
N
NH
NH2
Dicyandiamide
Hexylamine
C6-Met

(B)

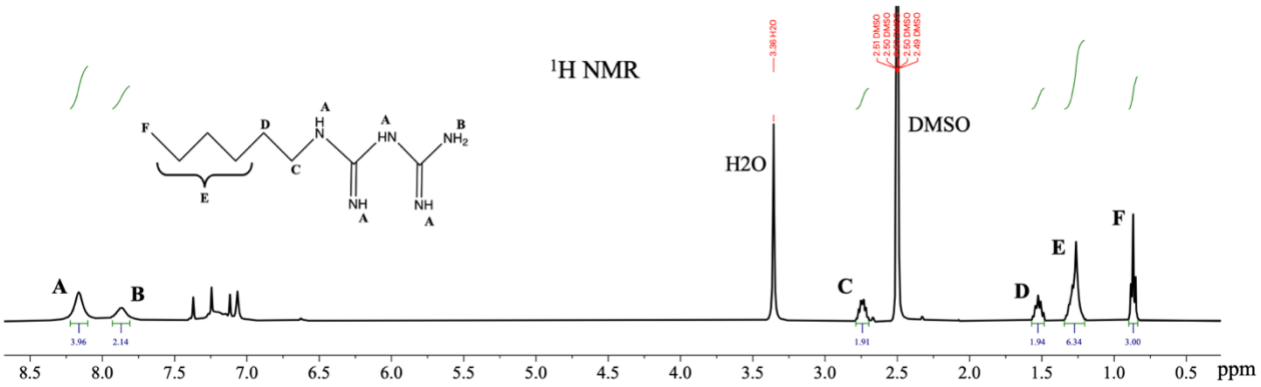
1H NMR
H2O
DMSO
A
B
C
D
E
F
8.5
8.0
7.5
7.0
6.5
6.0
5.5
5.0
4.5
4.0
3.5
3.0
2.5
2.0
1.5
1.0
0.5
ppm

(C)

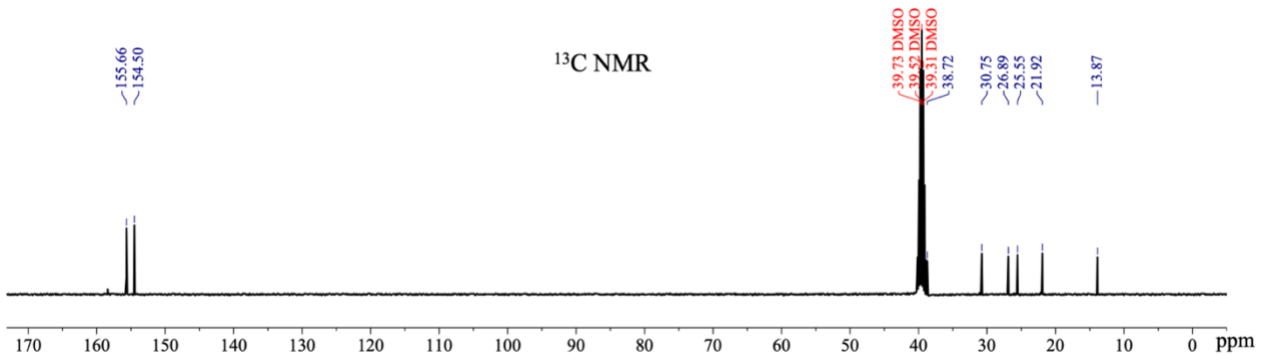
13C NMR
155.66
154.50
39.73 DMSO
39.52 DMSO
39.31 DMSO
38.72
30.75
26.89
25.55
21.92
13.87
170
160
150
140
130
120
110
100
90
80
70
60
50
40
30
20
10
0
ppm

Figure 10. Synthesis and characterization of C_6-Met derivative. (A) Synthetic scheme of C_6-Met derivative. Dicyandiamide reacted with hexylamine in 2M HCl at 100°C for 24 hours to form C_6-Met. (B) ^{1}H NMR spectrum in DMSO-d6. Peaks corresponding to specific hydrogens in the compound are identified using alphabetical labeling. (C) ^{13}C NMR spectrum in DMSO-d6. HCl, hydrochloric acid; NMR, nuclear magnetic resonance; DMSO, dimethyl sulfoxide; ppm, parts per million.

3.2 Metformin and C_{16}-Met bind to Dox Polymer

CBTA Polymer, PIMA Polymer and Dox Polymer all contain carboxylic acid functional groups due to a ring opening reaction of the dianhydride reagent (**Figure 11A**). The ability of doxorubicin to absorb light across a range of wavelengths was exploited to determine the binding capability of the carboxylic acid present in Dox Polymer to guanidine groups on metformin and C_{16}-Met (**Figure 11B**). Dox Polymer was combined with increasing amounts of metformin or C_{16}-Met, and the absorbance spectra was measured across a wavelength range of 300-700nm. Data was compared to Dox Polymer combined with increasing amounts of solvent (1:1 Water:DMSO) as a control. OD values measured at 545nm (approaching the point of equilibrium) were plotted against the change in Dox Polymer concentration due to the addition of increasing metformin, C_{16}-Met or solvent volumes. The rate at which the Dox Polymer – metformin and Dox Polymer – C_{16}-Met absorbance spectra reaches the point of equilibrium was slower than the control. Additionally, Dox Polymer – metformin and Dox Polymer – C_{16}-Met did not absorb as much light compared to control, suggesting metformin and C_{16}-Met are indirectly altering doxorubicin absorption (**Figure 11C**). Taken altogether, the data suggests that both metformin and C_{16}-Met are binding to Dox Polymer. Since this determination is difficult to model with the cisplatin polymers (CBTA and PIMA Polymers) that create available carboxylic acids, it is assumed the binding capability is translatable to these polymers as well.

(A)

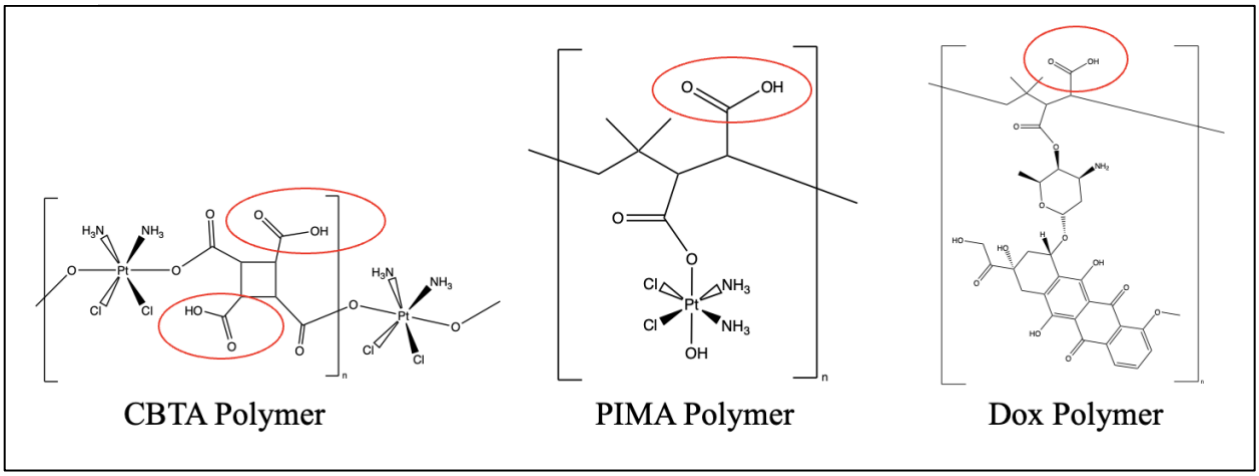
CBTA Polymer
PIMA Polymer
Dox Polymer

(B)

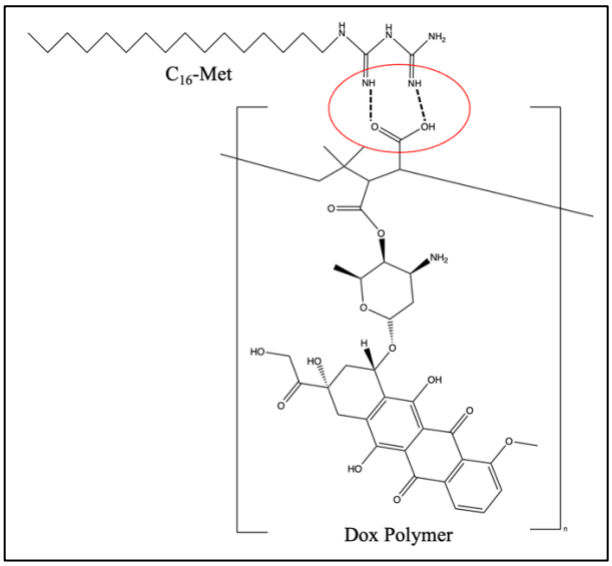
C16-Met
Dox Polymer

(C)

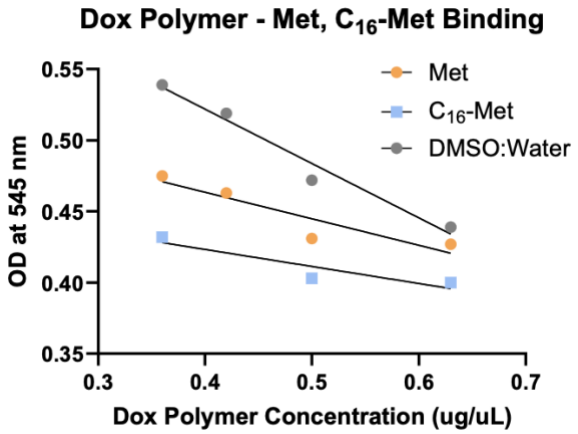
Dox Polymer - Met, C16-Met Binding
Met
C16-Met
DMSO:Water
OD at 545 nm
0.55
0.50
0.45
0.40
0.35
0.3
0.4
0.5
0.6
0.7
Dox Polymer Concentration (ug/uL)

Figure 11. Dox Polymer – metformin binding. (A) Schematic representation of available carboxylic acid (COOH) functional groups on CBTA, PIMA and Dox Polymers. COOH group highlighted by red circles. (B) Schematic representation of C_{16}-Met hydrogen bonding with the available carboxylic acid on Dox Polymer. Hydrogen bonds are denoted by dotted lines. Hydrogen bonding event is highlighted by the red circle. (C) Suggested bonding of metformin and C_{16}-Met to Dox Polymer. Dox polymer concentration was measured at 545nm, approaching the point of equilibrium, when combined with either metformin, C_{16}-Met, or solvent control (1:1 DMSO:Water). Simple linear regression analysis was performed revealing the following equations for met, C_{16}-Met and DMSO:Water, respectively: $y=-0.1864x + 0.5380$, $y=-0.1197x + 0.4711$ and $y=-0.3818x + 0.6746$ (n=1).

3.3 Cisplatin, metformin, and olaparib combinations display synergy in various ovarian cancer cell lines

To determine cell viability following single agent treatment with cisplatin and olaparib and various combinations between the two for 72 hours, MTT assays were performed. Most combination treatments resulted in lower cell viability compared to either single agent across all 4 cell lines (**Figure 12**). The data presented in **figure 12** was inputted into either Synergy Finder or CompuSyn software to determine the synergistic ratio between cisplatin and olaparib across the four cell lines, SKOV-3, ID8;$p53^{-/-}$;$BRCA1^{-/-}$, A2780-S, and A2780-CP (**Figure 13**). Synergy Finder uses the HSA reference method to calculate synergy, in which a positive synergy score indicates a synergistic relationship. The identified concentration ranges for both cisplatin and olaparib that demonstrated synergy in combination were at the lower end, indicating a synergistic relationship can be achieved while minimizing the concentration of each drug (**Figure 13A**). CompuSyn uses the established Chou Talalay method for synergy calculation, in which CI values < 1 indicate synergy. The concentration ranges corresponding to $CI<1$ corroborate the data obtained from Synergy Finder (**Figure 13B**).

The concentration ratio between cisplatin and metformin and between olaparib and metformin that demonstrated synergy in SKOV-3 cells were also identified using the same outlined methods (**Figure 14**). Altogether, the data suggests both dual drug combinations displayed synergy with specific concentration ranges. To determine the synergistic relationship between all three cisplatin, olaparib, and metformin in combination, a final synergy study was conducted and optimized to obtain concentration ranges demonstrating $CI<1$ calculated by CompuSyn software (**Figure 15**). Collectively, the presented synergy data helps guide the NP synthesis to ensure drug encapsulation maintains the identified synergistic concentration ratios.

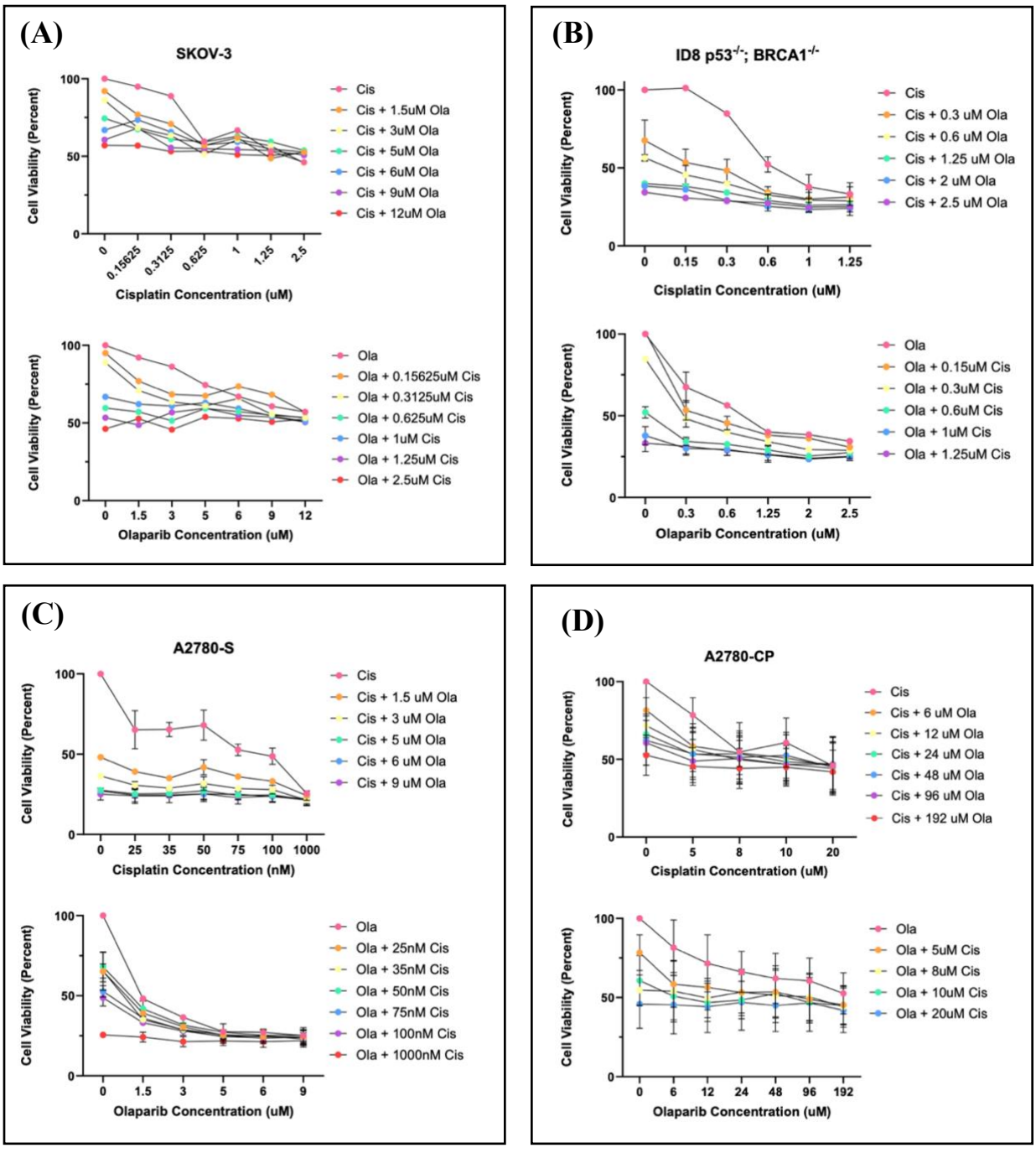
(A)
SKOV-3
Cell Viability (Percent)
Cis
Cis + 1.5uM Ola
Cis + 3uM Ola
Cis + 5uM Ola
Cis + 6uM Ola
Cis + 9uM Ola
Cis + 12uM Ola
Cisplatin Concentration (uM)
Ola
Ola + 0.15625uM Cis
Ola + 0.3125uM Cis
Ola + 0.625uM Cis
Ola + 1uM Cis
Ola + 1.25uM Cis
Ola + 2.5uM Cis
Olaparib Concentration (uM)
(B)
ID8 p53-/-; BRCA1-/-
Cis
Cis + 0.3 uM Ola
Cis + 0.6 uM Ola
Cis + 1.25 uM Ola
Cis + 2 uM Ola
Cis + 2.5 uM Ola
Cisplatin Concentration (uM)
Ola
Ola + 0.15uM Cis
Ola + 0.3uM Cis
Ola + 0.6uM Cis
Ola + 1uM Cis
Ola + 1.25uM Cis
Olaparib Concentration (uM)
(C)
A2780-S
Cis
Cis + 1.5 uM Ola
Cis + 3 uM Ola
Cis + 5 uM Ola
Cis + 6 uM Ola
Cis + 9 uM Ola
Cisplatin Concentration (nM)
Ola
Ola + 25nM Cis
Ola + 35nM Cis
Ola + 50nM Cis
Ola + 75nM Cis
Ola + 100nM Cis
Ola + 1000nM Cis
Olaparib Concentration (uM)
(D)
A2780-CP
Cis
Cis + 6 uM Ola
Cis + 12 uM Ola
Cis + 24 uM Ola
Cis + 48 uM Ola
Cis + 96 uM Ola
Cis + 192 uM Ola
Cisplatin Concentration (uM)
Ola
Ola + 5uM Cis
Ola + 8uM Cis
Ola + 10uM Cis
Ola + 20uM Cis
Olaparib Concentration (uM)

Figure 12. Cell viability following single agent and combination treatment with cisplatin and olaparib. (A) SKOV-3 (n=1), (B) ID8 $p53^{-/-}$; $BRCA1^{-/-}$ (n=2), (C) A2780-S (n=2), and (D) A2780-CP (n=2) cell viability following treatment with cisplatin, olaparib and the two agents in combination for 72 hours plotted either against cisplatin concentration (top) or olaparib concentration (bottom). Data measured by MTT assays. Data presented as means ± SEM. Cis, cisplatin; Ola, olaparib.

(A)

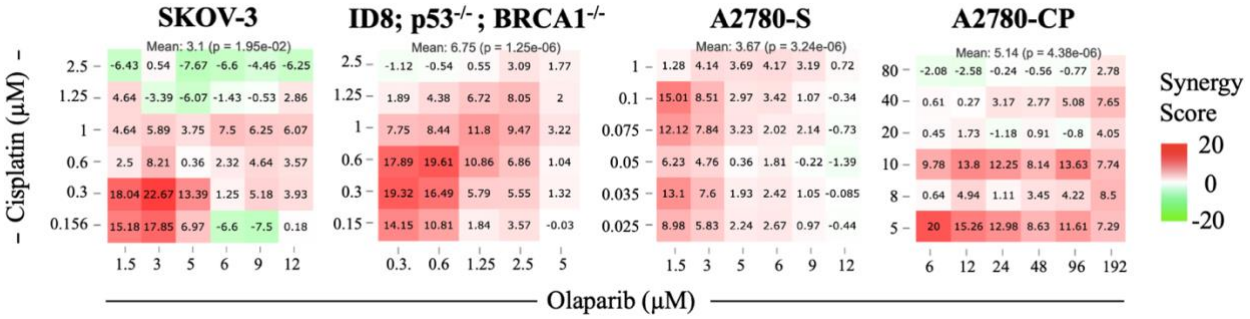

(B)

	SKOV-3	ID8; p53$^{-/-}$; BRCA1$^{-/-}$	A2780-S	A2780-CP
Cisplatin : Olaparib (μM)	0.156-0.6 : 1.5-5	0.15-1.25 : 0.3-2.5	0.025-0.1 : 1.5-6	5-40 : 6-192
Combination Index	0.60 – 0.89	0.59 – 0.96	0.52 – 0.96	0.38 – 0.98

Figure 13. Synergistic ratios between cisplatin and olaparib across different ovarian cancer cell lines. MTT data was inputted into either (A) Synergy Finder or (B) CompuSyn to obtain synergy scores and combination index (CI) values, respectively for SKOV-3 (n=1), ID8 $p53^{-/-}$; $BRCA1^{-/-}$ (n=2), A2780-S (n=2) and A2780-CP (n=2) cells. The synergy scores were calculated using the HSA reference model. CompuSyn calculates CI values using the Chou Talalay method. HSA, highest single agent.

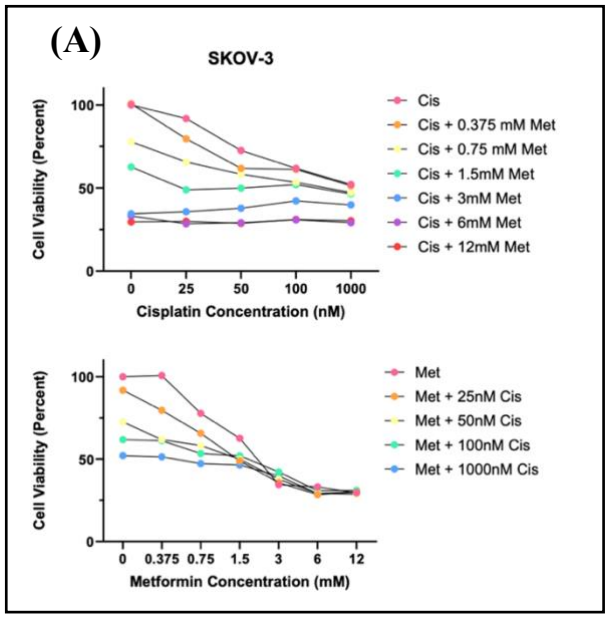

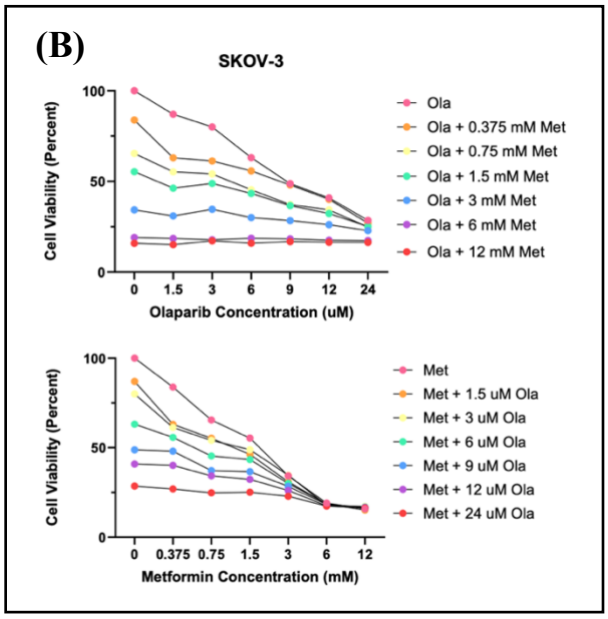

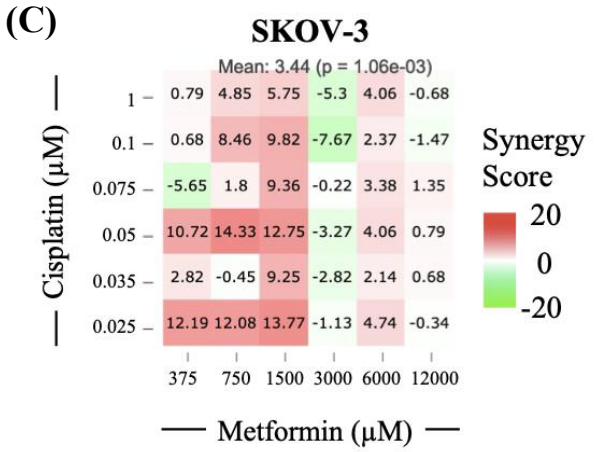

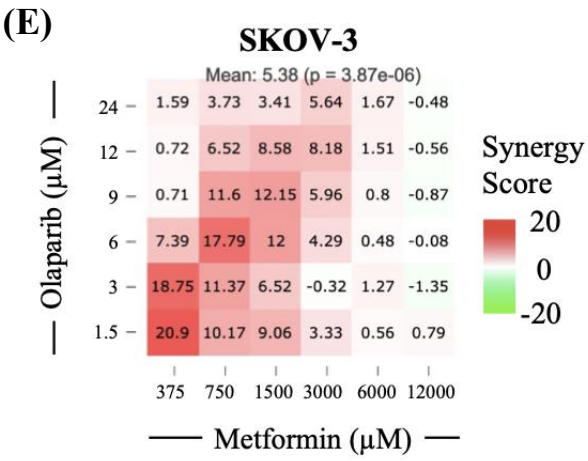

(D)

	SKOV-3
Cisplatin : Metformin (μM)	0.025-1 : 375-6000
Combination Index	0.45 – 0.90

(F)

	SKOV-3
Olaparib : Metformin (μM)	1.5-12 : 375-6000
Combination Index	0.64 – 0.93

Figure 14. Dual drug synergistic ratios in SKOV-3 cells. (A) Cell viability following treatment with cisplatin, metformin and the two agents in combination for 72 hours plotted either against cisplatin concentration (top) or metformin concentration (bottom) (n=1). (B) Cell viability following treatment with olaparib, metformin and the two agents in combination for 72 hours plotted either against olaparib concentration (top) or metformin concentration (bottom) (n=1). Data measured by MTT assays. Synergistic ratio of cisplatin and metformin shown by (C) Synergy Finder or (D) CompuSyn. Synergistic ratio of olaparib and metformin shown by (E) Synergy Finder or (F) CompuSyn. Data was obtained from MTT assays shown in (A) and (B) and inputted into either software (n=1). Cis, cisplatin; Met, metformin; Ola, olaparib.

	SKOV-3	ID8; $p53^{-/-}$; $BRCA1^{-/-}$	A2780-S	A2780-CP
Cisplatin : Olaparib : Metformin (μM)	0.0125-0.2 : 1.5-12 : 50-100	0.156-0.625 : 0.3-1.25 : 3000-6000	0.025-0.1 : 1.5-6 : 250-1000	5-20 : 6-24 : 3000-6000
Combination Index	0.73 – 0.93	0.73 – 0.96	0.50 – 0.94	0.49 – 0.96

Figure 15. Synergistic ratio between cisplatin, olaparib, and metformin across different ovarian cancer cell lines. MTT data was inputted into CompuSyn to obtain combination index (CI) values for SKOV-3, ID8 $p53^{-/-}$; $BRCA1^{-/-}$, A2780-S, and A2780-CP cells. CI<1 indicates synergy, whereas CI>1 represents antagonism (n=1).

3.4 Synthesis and characterization of cisplatin-olaparib-metformin PLGA-PEG NPs

From the developed cisplatin prodrug library, DTB Polymer and AA Polymer were selected to move forward for NP encapsulation given the dual-purpose potential of DTB Polymer. PLGA-PEG was selected as the polymeric system due to its biodegradability and advantageous attributes, including desirable sizes and better drug encapsulation. PLGA-PEG NPs encapsulating cisplatin in the form of DTB or AA Polymer, olaparib, and/or metformin in the form of C_{16}-Met or C_6-Met were synthesized by self-assembly nanoprecipitation as described in section 2.6 (**Figure 16A**). The various NPs synthesized include, E-NP (Empty-NP), AA-NP, DTB-NP, Ola-NP, C_{16}-Met-NP, C_6-Met-NP, DTB-Ola-NP, DTB-C_{16}-Met-NP, Ola-C_{16}-Met-NP, DTB-Ola-C_{16}-Met-NP, and DTB-Ola-C_6-Met-NP. The uniform round morphology of DTB-Ola-C_{16}-Met-NP (representative for all NPs) was confirmed by TEM images at 84.2k magnification (**Figure 16B**). Particle size (nm) and PDI of all NPs were measured using the dynamic light scattering technique (**Figure 16C and D**). The mean size and PDI between all NPs were fairly consistent, ranging between 85.4-125.6nm, and 0.069-0.11, respectively. All values were considered ideal[72,76,77]. The surface potential of AA-NP, DTB-NP, DTB-Ola-C_{16}-Met-NP, and E-NP were also determined using dynamic light scattering (**Figure 16E**). DTB-NP revealed a negative surface chemistry of -7.96±2.24 mV, while DTB-Ola-C_{16}-Met-NP displayed a near-neutral charge of 0.51±0.25 mV. Moreover, cisplatin and olaparib EE were measured by ICP-MS and HPLC, respectively (**Figure 16F and G**). DTB-Ola-C_{16}-Met-NP was shown to have the highest cisplatin EE of 30.31±3.54%, notably higher than DTB-Ola-C_6-Met-NP EE of 12.01%, although just measured once. The only difference between these two NPs is the hydrocarbon chain length of the metformin derivative, suggesting increased chain length fosters better cisplatin EE. Olaparib EE revealed broad variability between measurements, requiring further investigation. Nonetheless, the data suggests that both DTB Polymer and a

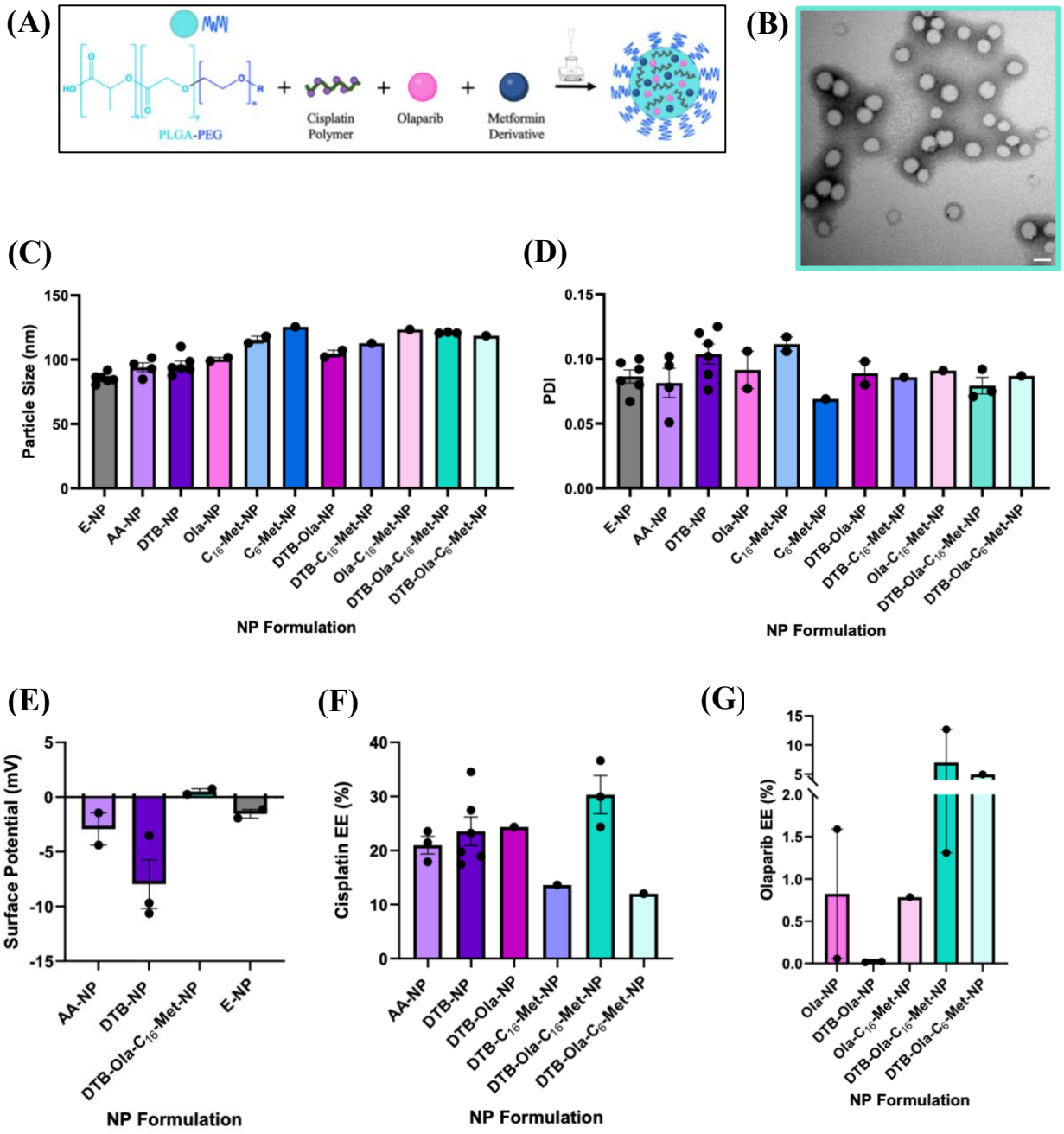
(A)
PLGA-PEG
Cisplatin Polymer
Olaparib
Metformin Derivative
(B)
(C)
Particle Size (nm)
150
100
50
0
E-NP
AA-NP
DTB-NP
Ola-NP
C16-Met-NP
C6-Met-NP
DTB-Ola-NP
DTB-C16-Met-NP
Ola-C16-Met-NP
DTB-Ola-C16-Met-NP
DTB-Ola-C6-Met-NP
NP Formulation
(D)
PDI
0.15
0.10
0.05
0.00
NP Formulation
(E)
Surface Potential (mV)
5
0
-5
-10
-15
AA-NP
DTB-NP
DTB-Ola-C16-Met-NP
E-NP
NP Formulation
(F)
Cisplatin EE (%)
40
30
20
10
0
AA-NP
DTB-NP
DTB-Ola-NP
DTB-C16-Met-NP
DTB-Ola-C16-Met-NP
DTB-Ola-C6-Met-NP
NP Formulation
(G)
Olaparib EE (%)
15
10
5
2.0
1.5
1.0
0.5
0.0
Ola-NP
DTB-Ola-NP
Ola-C16-Met-NP
DTB-Ola-C16-Met-NP
DTB-Ola-C6-Met-NP
NP Formulation

Figure 16. Synthesis and characterization of cisplatin-olaparib-metformin NPs. (A) Synthetic scheme of cisplatin polymer, olaparib, and metformin derivative loaded PLGA-PEG NPs by nanoprecipitation. Created with BioRender.com. (B) TEM image of DTB-Ola-C_{16}-Met-NP at 84.2k magnification. Scale bar: 50nm. (C) Particle size (nm) and (D) PDI of empty (E), single, dual, and triple drug NP formulations measured by dynamic light scattering (n=6,4,3,2 or 1). (E) Surface potential (mV) of AA-, DTB-, DTB-Ola-C_{16}-Met-, and E-NP determined by dynamic light scattering (n=2 or 3). (F) Cisplatin EE in all cisplatin containing NPs quantified by ICP-MS (n=6,3 or 1). (G) EE of olaparib in all olaparib containing NPs quantified by HPLC (n=1 or 2). Data presented as means ± SEM. PLGA-PEG, poly lactic-co-glycolic acid-polyethylene glycol; NP, nanoparticle; TEM, transmission electron microscopy; PDI, polydispersity index; EE, encapsulation efficiency, ICP-MS, inductively coupled plasma mass spectrometry; HPLC, high pressure liquid chromatography.

metformin derivative are necessary for improving olaparib encapsulation.

3.5 DTB-Ola-C_{16}-Met- and E-NP are stable across temperature and FBS conditions

To assess long term storage stability of DTB-Ola-C_{16}-Met- and E-NP at 4°C, size and PDI measurements were made immediately after synthesis and again after 60 days of storage (**Figure 17A**). Data revealed no significant change of either size or PDI, indicating long term storage does not alter these two NP characteristics. DTB-Ola-C_{16}-Met- and E-NP size and PDI stability in 0, 5, or 10% FBS in water incubated at both 37°C (**Figure 17B**) and 25°C (**Figure 17C**) was evaluated as a representative model for NP transport in the bloodstream. Measurements were taken at 0-, 4-, and 24-hour time points. Across the 24-hour time interval within each condition, there was no observable change in size (**Figure 17B and C, left**) or PDI (**Figure 17B and C, right**). As percent FBS increased, size trended downwards, whereas PDI gradually increased. Both NPs displayed the same stability trends irrespective of the starting size. Between temperature settings, PDI showed no difference, whereas NP size at each condition was slightly greater at 37°C compared to measurements taken at 25°C. Taken altogether, both NPs showed only modest changes in size across percent FBS, time, and temperature, demonstrating size stability in FBS across a period of 24 hours.

3.6 Cisplatin release from DTB-NP in response to pH stimuli

To understand the rate at which DTB-NP releases cisplatin from the NP and drug-polymer, drug release kinetics studies were performed using dialysis. Given the acidic nature of the tumor environment, dialysis membranes were prepared using 1x PBS adjusted to either neutral pH (7.4) or acidic pH (5.5), mimicking in vivo conditions, to determine the difference in drug release (**Figure 18**). PBS was collected over a period of 72 hours to measure cisplatin content by ICP-MS.

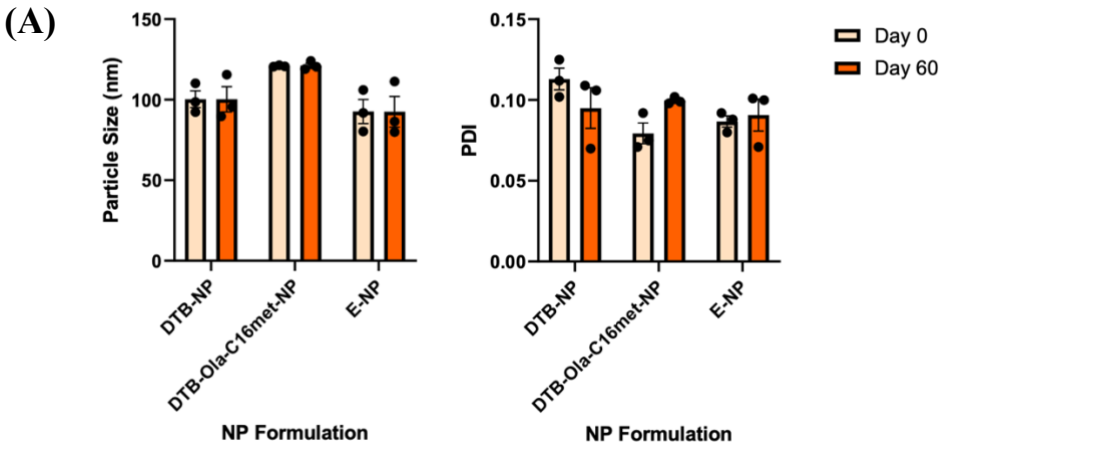
(A)
Particle Size (nm)
150
100
50
0
DTB-NP
DTB-Ola-C16met-NP
E-NP
NP Formulation
PDI
0.15
0.10
0.05
0.00
DTB-NP
DTB-Ola-C16met-NP
E-NP
NP Formulation
Day 0
Day 60

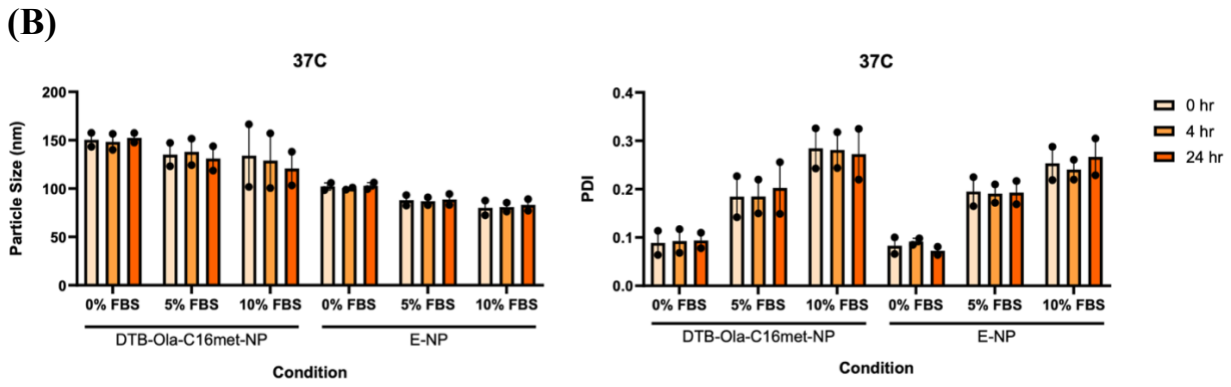
(B)
37C
Particle Size (nm)
200
150
100
50
0
0% FBS
5% FBS
10% FBS
0% FBS
5% FBS
10% FBS
DTB-Ola-C16met-NP
E-NP
Condition
37C
PDI
0.4
0.3
0.2
0.1
0.0
0% FBS
5% FBS
10% FBS
0% FBS
5% FBS
10% FBS
DTB-Ola-C16met-NP
E-NP
Condition
0 hr
4 hr
24 hr

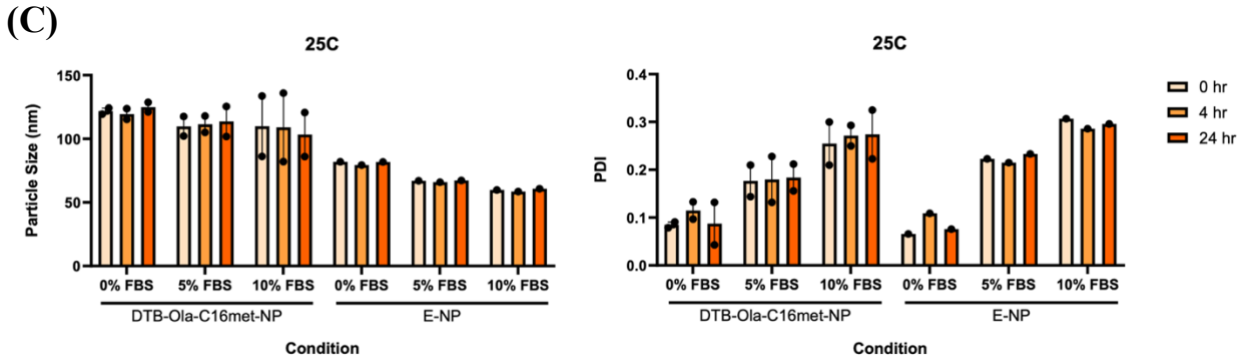
(C)
25C
Particle Size (nm)
150
100
50
0
0% FBS
5% FBS
10% FBS
0% FBS
5% FBS
10% FBS
DTB-Ola-C16met-NP
E-NP
Condition
25C
PDI
0.4
0.3
0.2
0.1
0.0
0% FBS
5% FBS
10% FBS
0% FBS
5% FBS
10% FBS
DTB-Ola-C16met-NP
E-NP
Condition
0 hr
4 hr
24 hr

Figure 17. Size and PDI stability of DTB-Ola-C_{16}-Met- and E-NP. (A) Particle size (nm) and PDI of DTB-, DTB-Ola-C_{16}-Met-, and E-NP measured by dynamic light scattering immediately after synthesis (Day 0) and again after 60 days of storage at 4°C. Data is presented as means ± SEM (n=3), *P<0.05 determined by paired t test. (B, C) Particle size (nm) and PDI stability of DTB-Ola-C_{16}-Met- and E-NP following incubation at either (B) 37°C or (C) 25°C in 0, 5 and 10% FBS measured at 0, 4 and 24 hours. Data is presented as means ± SEM (n=2). PDI, polydispersity index; NP, nanoparticle; FBS, fetal bovine serum.

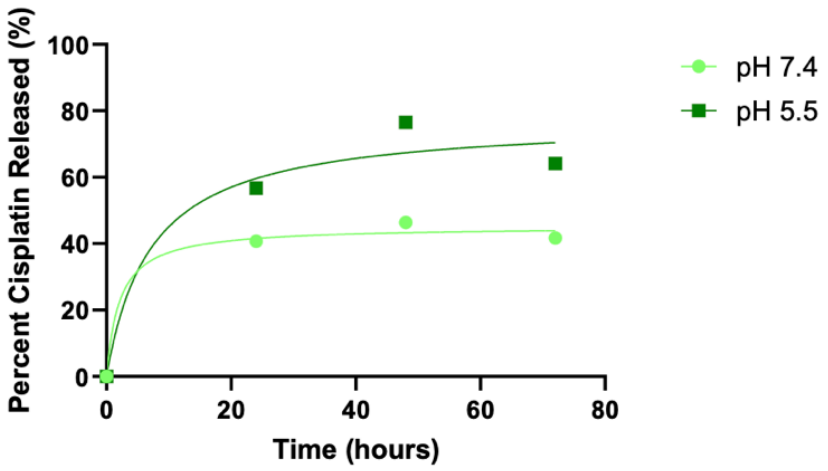
Percent Cisplatin Released (%)
100
80
60
40
20
0
0
20
40
60
80
Time (hours)
pH 7.4
pH 5.5

Figure 18. Drug Release Kinetics of DTB-NP. Percent cisplatin released from DTB-NP into 1x PBS incubated at 37°C at pH 7.4 compared to pH 5.5 measured across 72 hours by ICP-MS. Nonlinear regression analysis fitted to the data (n=1). PBS, phosphate buffered saline; ICP-MS, inductively coupled plasma mass spectrometry.

Across the time interval, incubation at pH 5.5 conferred greater cisplatin release compared to dialysis at pH 7.4. Particularly, cisplatin release increased by approximately 20% at 72 hours.

3.7 Cisplatin polymers induce DNA damage denoted by γH2AX

The individual drug effects in the NP system were evaluated to ensure the contribution of all three to the overall therapeutic effect. Firstly, following pH-mediated PLGA-PEG breakdown, AA and DTB Polymer are reduced in the hypoxic environment of the cell[105,106]. The reduction reaction causes the conversion of cisplatin from Pt(IV) to Pt(II). It is Pt(II) that can become activated to form DNA adducts (**Figure 19A**). To assess DNA damage induced by cisplatin, γH2AX was examined following treatment with DTB-, AA-, DTB-Ola-C_{16}-Met- and E-NP for 24 hours in SKOV-3 cells. We observed a similar increase in median fluorescence intensity of the second peak following both AA- and DTB-NP treatment, compared to E-NP (**Figure 19B**). The second peak is believed to be caused by pronounced DNA damage induced by cisplatin, whereas the first observable peak is suggested to correspond to physiological DNA damage levels. Additionally, there was a greater observed shift in the second peak toward higher intensity following DTB-Ola-C_{16}-Met-NP treatment (**Figure 19C**). Although it was only a modest increase compared to E-NP, the cisplatin concentration corresponding to cisplatin within the DTB Polymer in the DTB-Ola-C_{16}-Met-NP (0.25μM) was 32-fold lower than the cisplatin concentration of AA-NP, DTB-NP, and cisplatin control (8μM). A higher concentration could not be assessed since toxicity was too high.

3.8 Olaparib induces PARP and caspase-3 cleavage upon NP release

To validate pharmacological activity of encapsulated olaparib, SKOV-3 cells were first treated with olaparib, Ola-, DTB-Ola-C_{16}-Met- and E-NP for 72 hours. Cleaved PARP and caspase-3 expression were observed by western blot analysis (**Figure 20**). Preliminary results suggest

(A)

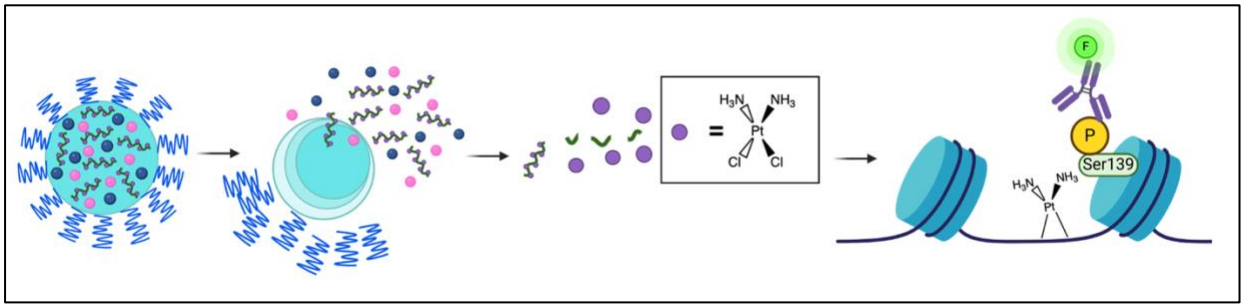
F
P
Ser139

(B)

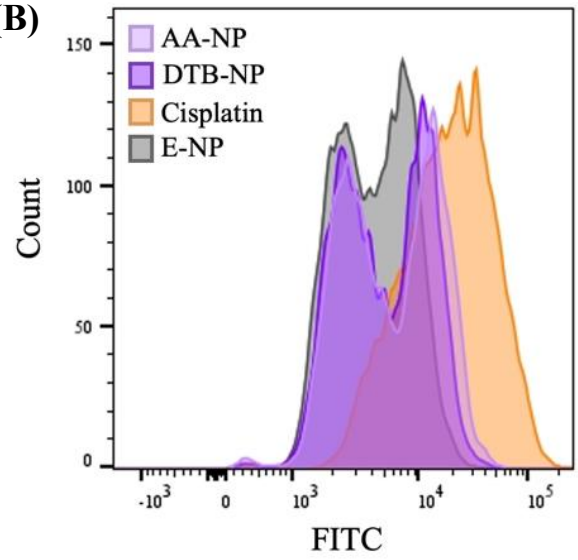
AA-NP
DTB-NP
Cisplatin
E-NP
Count
FITC

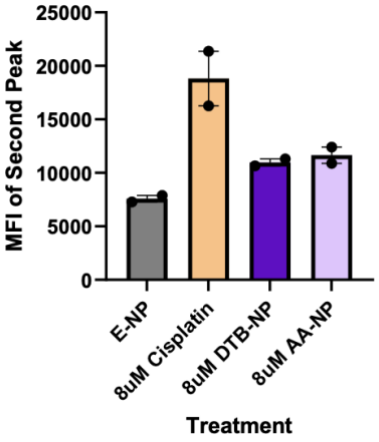
MFI of Second Peak
E-NP
8uM Cisplatin
8uM DTB-NP
8uM AA-NP
Treatment

(C)

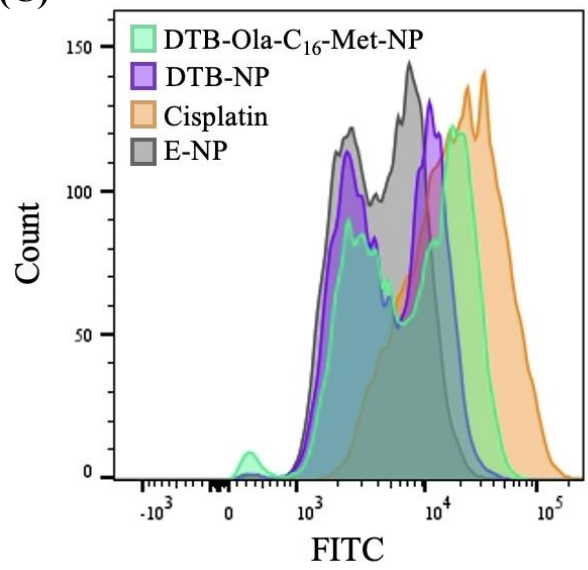
DTB-Ola-C16-Met-NP
DTB-NP
Cisplatin
E-NP
Count
FITC

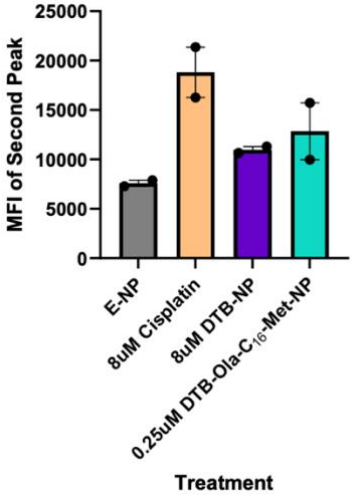
MFI of Second Peak
E-NP
8uM Cisplatin
8uM DTB-NP
0.25uM DTB-Ola-C16-Met-NP
Treatment

Figure 19. Cisplatin polymers induce DNA damage in SKOV-3 cells. (A) Schematic representation of DTB-Ola-C_{16}-Met-NP and DTB Polymer break down releasing cisplatin, which can then form DNA adducts. Ser139 on Histone 2AX becomes phosphorylated following adjacent DNA damage which is tagged with a FITC-IgG antibody. Created with BioRender.com. (B) Representative flow cytometry histogram of 1 of the 2 biological replicates of FITC-tagged γH2AX induced by cisplatin in SKOV-3 cells (left) and MFI (right) following E-NP, 8μM cisplatin, 8μM DTB-NP and 8μM AA-NP treatment for 24 hours. (C) Representative flow cytometry histogram of FITC-tagged γH2AX induced by cisplatin in SKOV-3 cells (left) and MFI (right) following E-NP, 8μM cisplatin, 8μM DTB-NP or 0.25μM DTB-Ola-C_{16}-Met-NP treatment for 24 hours. Data is presented as means ± SEM (n=2). γH2AX, phosphorylated H2AX; MFI, median fluorescence intensity.

(A)

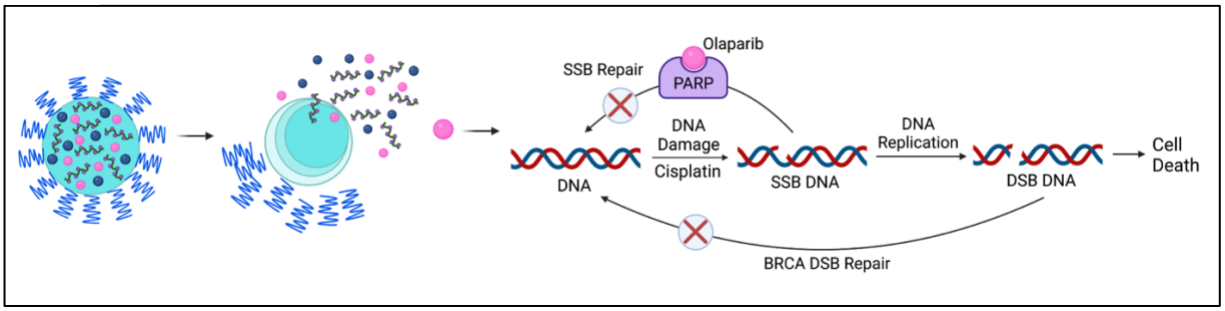
Olaparib
SSB Repair
PARP
DNA Damage
Cisplatin
DNA
SSB DNA
DNA Replication
DSB DNA
Cell Death
BRCA DSB Repair

(B)

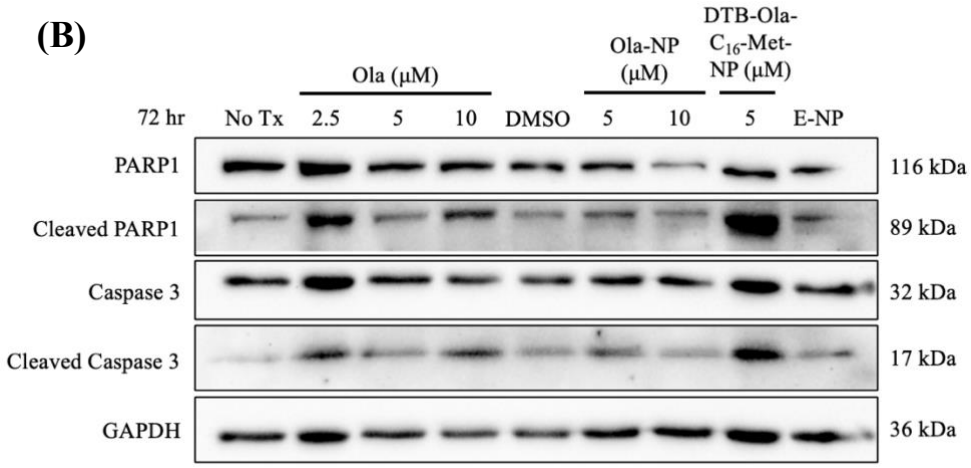
Ola (μM)
Ola-NP (μM)
DTB-Ola-C16-Met-NP (μM)
72 hr
No Tx
2.5
5
10
DMSO
5
10
5
E-NP
PARP1
116 kDa
Cleaved PARP1
89 kDa
Caspase 3
32 kDa
Cleaved Caspase 3
17 kDa
GAPDH
36 kDa

(C)

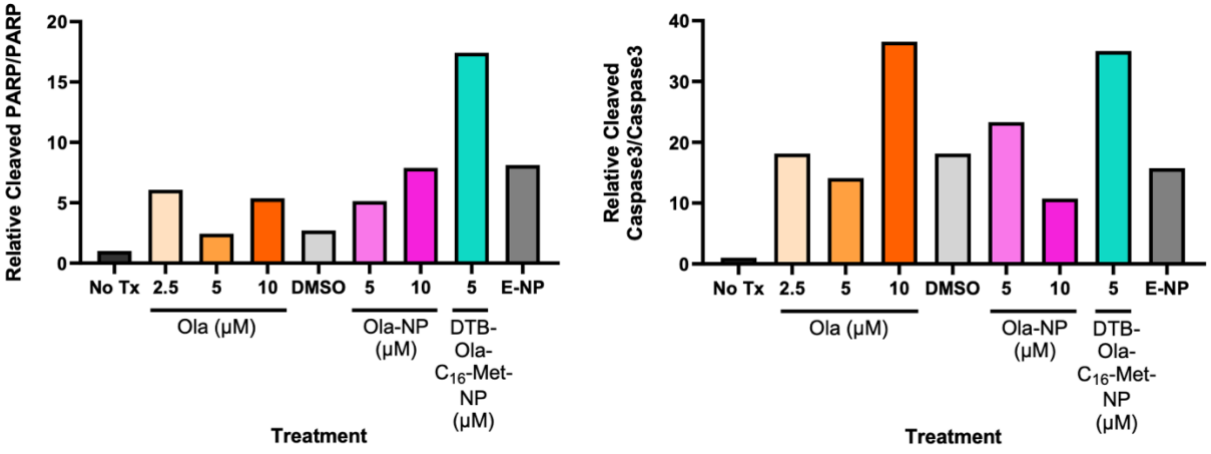
Relative Cleaved PARP/PARP
20
15
10
5
0
No Tx
2.5
5
10
DMSO
5
10
5
E-NP
Ola (μM)
Ola-NP (μM)
DTB-Ola-C16-Met-NP (μM)
Treatment
Relative Cleaved Caspase3/Caspase3
40
30
20
10
0
No Tx
2.5
5
10
DMSO
5
10
5
E-NP
Ola (μM)
Ola-NP (μM)
DTB-Ola-C16-Met-NP (μM)
Treatment

Figure 20. Validation of olaparib-induced PARP cleavage after NP release. (A) Schematic representation of DTB-Ola-C_{16}-Met-NP break down releasing olaparib to undergo its mechanism of action. Olaparib inhibits PARP preventing SSB repair of cisplatin induced DNA damage. PARP inhibition coupled with mutated BRCA DSB repair causes synthetic lethality, leading to cell death. Created with BioRender.com. (B) Western blot of PARP1 and caspase 3 and their cleaved counterparts in SKOV-3 cells after Ola-, DTB-Ola-C_{16}-Met-, and E-NP treatment for 72 hours. (C) Quantification of relative cleaved PARP1/PARP1 and cleaved caspase 3/caspase 3 ratios. Data normalized to No Tx control, which is set to 1. Data analyzed by Fiji (n=1). PARP, poly-ADP ribose polymerase; SSB, single strand break; BRCA, Breast Cancer gene; DSB, double strand break; Ola, olaparib; DMSO, dimethyl sulfoxide; NP, nanoparticle; Tx, treatment.

PARP and caspase-3 cleaved products are more abundant following DTB-Ola-C_{16}-Met-NP treatment compared to Ola- and E-NP. However, further studies are required to validate the data.

3.9 C_{16}-Met and C_6-Met derivatives can activate AMPK

To ensure the two metformin derivatives, C_{16}-Met and C_6-Met, retain the same pharmacological effect as pure metformin, western blot analysis was conducted in SKOV-3 cells following treatment with free C_{16}-Met and C_6-Met (0.0001-1μM) for 24 hours (**Figure 21**). Phenformin was used as a positive control instead of metformin, given metformin's potential non-consistent cell entry through the OCT1 transporter. In contrast, phenformin does not require OCT1 for cellular uptake, as is predicted for C_{16}-Met and C_6-Met when delivered unencapsulated[57]. We observed a concentration dependent increase in pAMPK expression induced by both derivatives when treated freely, without encapsulation in the NP. However, a drop in pAMPK was noticed at the highest concentration (1μM). Moreover, although phosphorylation increased with concentration, relative pAMPK/AMPK expression was lower than the no treatment control following C_6-Met treatment. Only when a concentration of 0.01μM was reached, did the ratio increase above the control.

3.10 Preliminary cytotoxicity

Lastly, preliminary cytotoxicity following treatment with AA-, DTB-, and DTB-Ola-C_{16}-Met-NPs was observed in SKOV-3 cells (**Figure 22**). However, there was no observed drastic cell death following NP treatments.

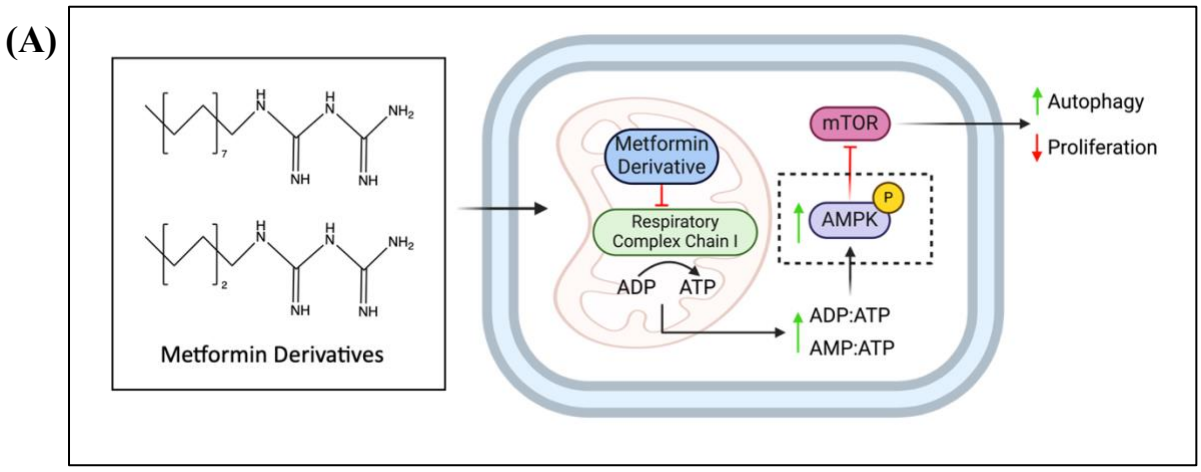
(A)
Metformin Derivatives
Metformin Derivative
Respiratory Complex Chain I
ADP
ATP
mTOR
AMPK
P
ADP:ATP
AMP:ATP
Autophagy
Proliferation

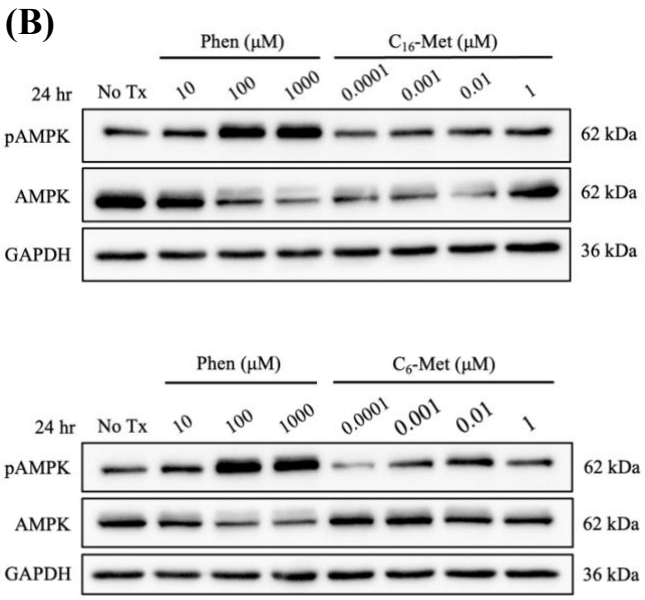
(B)
Phen (μM)
C16-Met (μM)
24 hr
No Tx
10
100
1000
0.0001
0.001
0.01
1
pAMPK
AMPK
GAPDH
62 kDa
62 kDa
36 kDa
Phen (μM)
C6-Met (μM)
24 hr
No Tx
10
100
1000
0.0001
0.001
0.01
1
pAMPK
AMPK
GAPDH
62 kDa
62 kDa
36 kDa

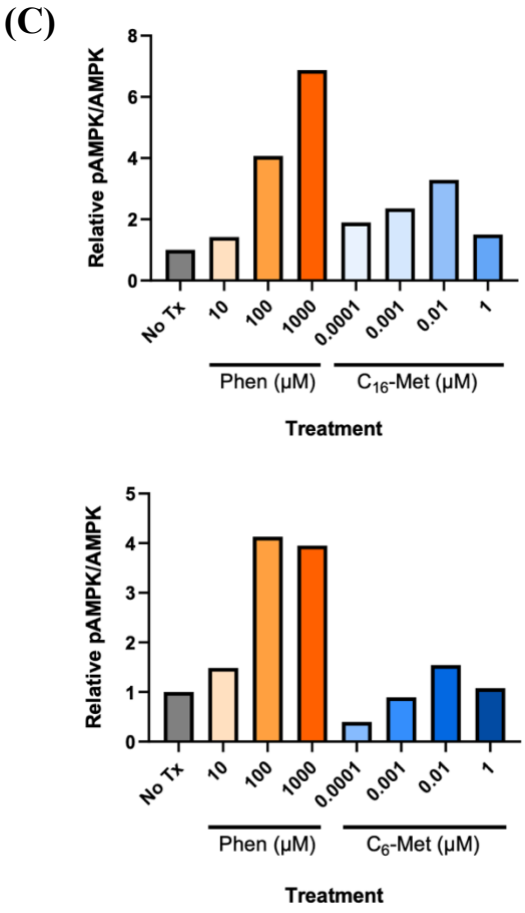
(C)
Relative pAMPK/AMPK
0
2
4
6
8
No Tx
10
100
1000
0.0001
0.001
0.01
1
Phen (μM)
C16-Met (μM)
Treatment
Relative pAMPK/AMPK
0
1
2
3
4
5
No Tx
10
100
1000
0.0001
0.001
0.01
1
Phen (μM)
C6-Met (μM)
Treatment

Figure 21. C_{16}-Met and C_6-Met derivatives activate AMPK in SKOV-3 cells. (A) Schematic representation of either free C_{16}-Met or C_6-Met derivative proposed mechanism of action. The metformin derivative inhibits respiratory complex chain I, thereby increasing the ratio of ADP and AMP to ATP, leading to AMPK activation, inhibition of mTOR and ultimately increased autophagy and decreased cell proliferation. The dotted box shows the step in the pathway for which has been blotted in (B) and (C). Created with BioRender.com. (B) Western blot of phosphorylated AMPK (pAMPK) in SKOV-3 cells after C_{16}-Met (top) and C_6-Met (bottom) treatment for 24 hours. Phenformin was used as a positive control. (C) Quantification of relative pAMPK/AMPK ratio of the blot directly to the left. Data normalized to No Tx control, which is set to 1. Data analyzed by Fiji (n=1). AMPK, AMP-activated protein kinase; mTOR, mammalian target of rapamycin; Phen, phenformin; Tx, treatment.

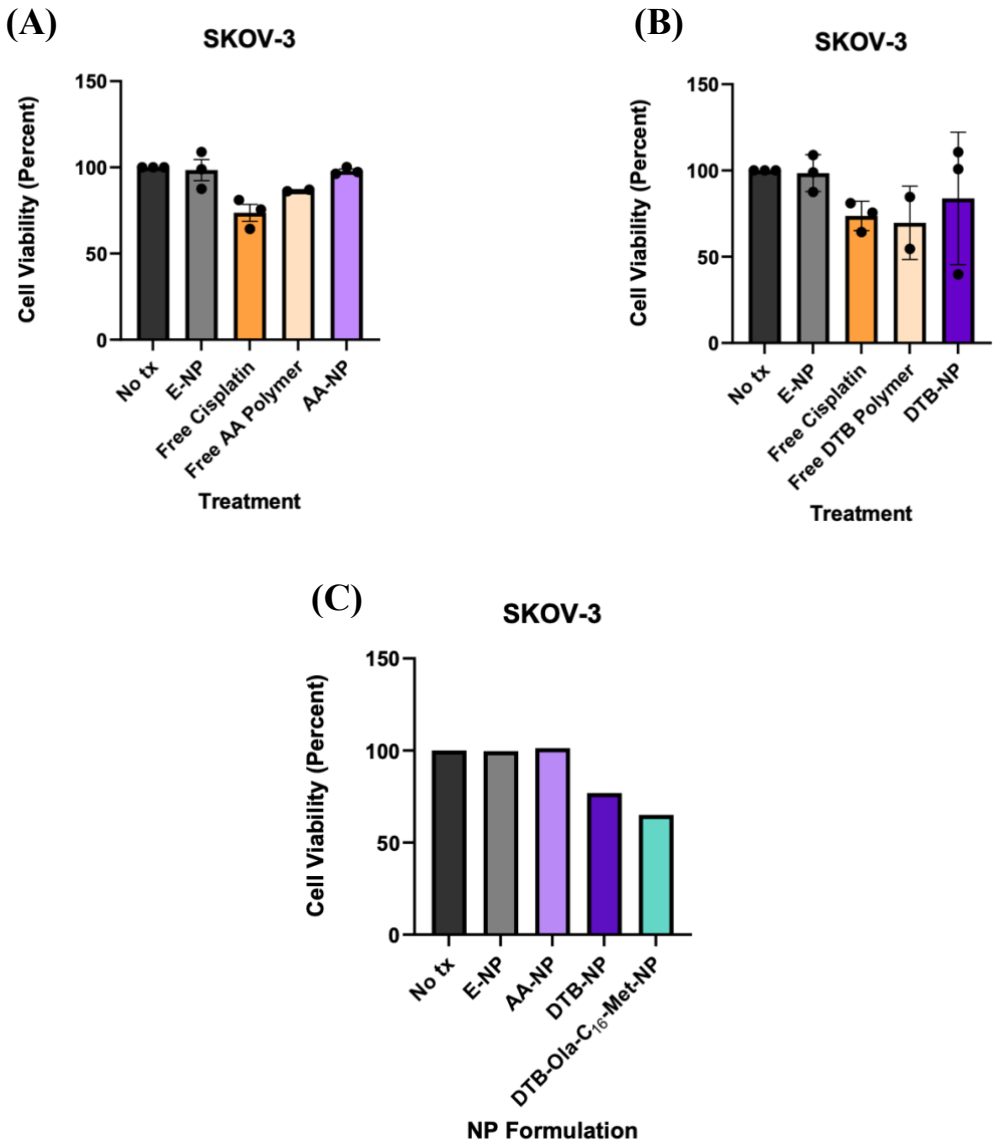
(A)
SKOV-3
Cell Viability (Percent)
150
100
50
0
No tx
E-NP
Free Cisplatin
Free AA Polymer
AA-NP
Treatment
(B)
SKOV-3
Cell Viability (Percent)
150
100
50
0
No tx
E-NP
Free Cisplatin
Free DTB Polymer
DTB-NP
Treatment
(C)
SKOV-3
Cell Viability (Percent)
150
100
50
0
No tx
E-NP
AA-NP
DTB-NP
DTB-Ola-C16-Met-NP
NP Formulation

Figure 22. Cytotoxicity of AA-, DTB- and DTB-Ola-C_{16}-Met-NPs in SKOV-3 cells. SKOV-3 cells were treated with (A) free AA polymer and AA-NP and (B) free DTB polymer and DTB-NP, free cisplatin, and E-NP for 72h. Cisplatin concentration in each treatment was 100nM. Data is presented as means ± SEM (n=3 or 2). (C) SKOV-3 cell viability following treatment with E-, AA-, DTB-, and DTB-Ola-C_{16}-Met-NP for 72h, with dosing every 24 hours (n=1). Cisplatin concentration in each treatment was 100nM. Viability was measured by MTT assays. Treatments were normalized to No tx (treatment) control cells.

4.0 Discussion

4.1 Overview

Ovarian cancer is the most fatal gynecological cancer amongst women[1]. Cytoreductive surgery and platinum-based chemotherapy remain the standard treatment regimen for patients. However, chemotherapy resistance, particularly cisplatin resistance, and systemic distribution limit treatment effectiveness and tolerability[1,5]. There are a multitude of cisplatin resistance mechanisms that either prevent DNA adduct formation or prevent apoptosis after DNA adduct formation. Namely, PARP-mediated DNA repair is well established as a mechanism of cisplatin resistance in ovarian cancer[34]. Olaparib is a small molecule drug in clinical use that inhibits PARP preventing single strand break repair of cisplatin-induced damage. More pronounced effects are observed when this combination is used in BRCA-mutated ovarian cancer, or more broadly ovarian cancer with any homologous recombination mutation, since synthetic lethality is achieved[49]. Several strategies have been explored to overcome resistance by using combination therapy approaches with olaparib or different targeting drugs[47,63]. Particularly, metformin has garnered attention for its anticancer effects by indirectly inhibiting mTOR, thereby altering metabolism toward a catabolic state to ultimately cause autophagy[58,60]. Improvements to combination therapy using NP delivery systems have also been investigated for preventing off target effects. Nanotechnology offers several advantages, including improved drug pharmacokinetic profiles, synergy maintenance, less toxicity, and tumor accumulation[65]. Several studies have explored cisplatin, olaparib or metformin encapsulation using different NP platforms with desirable results favouring the use of a NP[96–99]. Nonetheless, current research efforts are still required to improve therapeutic outcome. Here, we sought to develop a novel NP-based therapy encapsulating a

cisplatin polymer prodrug, olaparib, and a metformin derivative in a single nanocarrier for a triple therapeutic effect for ovarian cancer treatment.

4.2 Cisplatin, doxorubicin, and metformin prodrug/derivative validation

We first synthesized a library of polymer and small molecule cisplatin prodrugs for increased encapsulation inside the hydrophobic core of PLGA-PEG NPs, following similar synthesis procedures found in the literature[16,82]. We have successfully synthesized 7 different cisplatin prodrugs demonstrated by NMR and mass spectrometry data (**Figures 4-7**). Each compound was synthesized with a different intended purpose based on the functional groups found in the linker reagent, such as a disulfide bond for GSH scavenging or carboxylic acid for hydrogen bonding. Firstly, the hydrogen bond between carboxylic acid groups with guanidine groups, specifically found on metformin, is well established in the literature[107,108]. To test the hydrogen bonding capability, Dox Polymer was synthesized (**Figure 8**) to exploit the doxorubicin absorbance. Our results suggest that both metformin and C_{16}-Met can hydrogen bond to Dox Polymer due to the slower rate approaching equilibrium when compared to the solvent control (**Figure 11**). Although this finding requires further investigation for confirmation, it aligns with absorbance data shown in the literature to model hydrogen bonding[109]. This model is difficult to assess with cisplatin, given its lack of absorbance, therefore it was assumed the same binding property is seen in CBTA and PIMA Polymer since they both possess the same carboxylic functional group.

Previous studies in the literature have also targeted GSH-mediated deactivation and efflux of cisplatin by combining a disulfide bond component to the NP delivery system[27,92,93]. Researchers showed an increase in cisplatin release when these GSH-responsive NPs were incubated with increasing concentrations up to 10mM GSH. Additionally, studies also revealed

decreased GSH/GSSG levels in cisplatin-sensitive and cisplatin-resistant A2780 cells[27,92,93]. Taken together, these studies confirm incorporating disulfide bonds into NP design can target GSH, diminishing availability for cisplatin deactivation. Here we synthesized a cisplatin polymer, DTB Polymer, in which the disulfide bond was found in the linker moiety connecting cisplatin units together. Although we did not observe the results seen in the literature with our experimental conditions (data not shown), the GSH scavenging potential of our DTB Polymer could still be proven using different methods. It is possible the slow rate of PLGA-PEG degradation, afforded by the high molecular weight of PLGA (50 kDa), prevents full access of DTB Polymer to GSH in the 72-hour period used here, causing an unnoticeable difference in cisplatin release or GSH/GSSG levels compared to AA-NP[110]. Additionally, both DTB and AA Polymer molecular weight could not be confirmed due to the inability of polymer dissolution into tetrahydrofuran for measurement by gel permeation chromatography. Alternative methods to determine polymer size were attempted but were unsuccessful. A potential difference in DTB versus AA Polymer size could potentially result in different rates of reduction, thereby altering cisplatin release. For example, if there is a variable size difference between the polymers and the size of AA Polymer favours a faster rate of reduction, then it cannot be an adequate control for determining GSH-mediated cisplatin release from DTB Polymer[111,112].

In addition to the cisplatin and doxorubicin prodrugs, we also synthesized 2 metformin derivatives to increase hydrophobicity for better encapsulation efficiency. Structure and purity were confirmed by NMR and mass spectrometry (**Figures 9 and 10**). Unlike cisplatin and doxorubicin prodrugs, in which we used cisplatin and doxorubicin as the starting reagents, the metformin derivatives were synthesized using dicyandiamide and an amine compound given the requirement for reactive functional groups, which are absent on metformin. The 2 derivatives have

varying hydrocarbon chain lengths offering different levels of hydrophobicity. However, the encapsulation efficiency of the 2 derivatives inside our PLGA-PEG system remain undetermined. Further HPLC studies are required to determine which metformin derivative confers better encapsulation.

4.3 Drug synergy permits lower concentrations

To ensure the proposed drug combination displays synergy in different ovarian cancer cells, MTT assays were first performed followed by data analysis using synergy software, CompuSyn and Synergy Finder. All possible drug combinations were assessed using the unmodified version of each agent. Results demonstrate a range of concentrations for each drug that display synergy when in combination (**Figures 12-15**). Here our focus was to determine synergistic concentrations between cisplatin, olaparib, and metformin in order to achieve sufficient cytotoxicity while minimizing concentrations that normally result in severe side effects. Variable cisplatin IC50 values have been reported in the literature following treatment for 72 hours in SKOV-3 cells, ranging from around 4-26 μM[113,114]. Our results suggest we can achieve roughly 50% inhibition using much lower concentrations of cisplatin when combined with olaparib and/or metformin. Altogether, the data provided guidance for NP synthesis to ensure drug encapsulation maintains the synergistic ratio for later use in cytotoxicity studies with NP treatments.

4.4 Assessment of NP parameters

After numerous rounds of optimization, final PLGA-PEG NP formulations encapsulating either AA or DTB Polymer, olaparib and/or C_{16}-Met or C_6-Met were established based on parameters including morphology, size, PDI, surface charge and EE (**Figure 16**). All size and PDI values obtained are in accordance with literature values considered as ideal[72,76,77]. More specifically, across all NP formulations, the size ranged from 85.4-125.6nm, suitable for cellular

uptake and escape from glomerular filtration and immune recognition[72,76,77]. Additionally, the PDI of each NP was <0.2, indicative of a narrow size distribution despite multidrug encapsulation and multiple components/polymer systems. Additionally, both cisplatin and olaparib EE were assessed using ICP-MS and HPLC, respectively. Given the large distribution across olaparib EE measurements within the same NP formulation, further analysis is required.

NP administration occurs intravenously in the clinic. A key factor that can affect the biodistribution and cellular uptake of NPs is the adsorption of serum proteins forming a protein corona on the surface of the NP during transport[79]. Although the impact of the protein corona on cellular entry is not fully understood, it has been proposed to affect size-dependent uptake[79,115]. Here we performed a preliminary study to assess size and PDI stability of both DTB-Ola-C_{16}-Met- and E-NP when incubated with up to 10% FBS for a period of 24 hours (**Figure 17**). FBS was used as a representation of blood serum. Results showed only slight changes in size with increasing FBS and across time, measured at both physiological (37°C) and room (25°C) temperature, suggesting NP size is stable in solutions with up to 10% FBS. However, PDI positively correlated with increasing FBS. It is possible that protein sizes are also contributing to the measurement, thereby inadvertently expanding the size distribution of NPs.

To evaluate cisplatin release kinetics, DTB-NP was dialysed in PBS calibrated to pH 7.4 compared to pH 5.5 (**Figure 18**). Dialysis performed at pH 5.5 conferred a faster rate of cisplatin release. Although only performed once, the data aligns with the literature, in which the ester bonds found in PLGA are less stable and more readily degradable at pH 5.5[91]. To confirm the rate of cisplatin release is not impacted by the release of olaparib and metformin, drug release kinetic studies using DTB-Ola-C_{16}-Met-NP, measuring the release rate of all 3, needs to be evaluated.

4.5 In vitro NP treatments

Given the 3-in-1 design of our final NP system, we tested individual drug effects to confirm cisplatin, olaparib, and metformin contribution to cytotoxicity. We showed cisplatin-induced DNA damage measured by γH2AX, validating the reduction of cisplatin prodrugs, DTB and AA Polymer, to active cisplatin (**Figure 19**). More notably, treatment with DTB-Ola-C_{16}-Met-NP resulted in a slightly increased MFI compared to DTB-NP treatment. The cisplatin concentration of DTB-Ola-C_{16}-Met-NP was also 0.25μM compared to DTB-NP and cisplatin treatment of 8μM, suggesting the synergistic relationship between all three drugs confers a substantial reduction in concentration that achieves maximal effect. In the future, this finding should be validated using alternative methods, such as immunofluorescent staining of the NP system alongside γH2AX[16]. Preliminary results also revealed PARP and caspase-3 cleavage following both Ola- and DTB-Ola-C_{16}-Met-NP treatment by western blot analysis (**Figure 20**). To validate the contribution and pharmacological activity of the metformin derivatives, conditions were first optimized with free C_{16}-Met and C_6-Met treatments. We showed a concentration-dependent increase of pAMPK, suggesting both derivatives behave like metformin, in which pharmacological activity is assessed by AMPK activation (**Figure 21**). Concentrations of both derivatives that resulted in pAMPK were much lower than the positive control phenformin, suggesting both C_{16}-Met and C_6-Met have a higher potency. Higher concentrations of either C_{16}-Met or C_6-Met could not be tested as they were too toxic to the cells. Further validation of AMPK activation by NP delivery of the metformin derivatives is required.

Finally, preliminary cytotoxicity results following treatment with DTB-, AA-, and DTB-Ola-C_{16}-Met-NPs in SKOV-3 cells were obtained from MTT assays (**Figure 22**). However, results did not demonstrate high cytotoxicity. It is important to note that cisplatin concentrations used in these studies (100nM) are greatly below reported IC50 values[113,114]. The 100nM cisplatin

concentration was chosen based on the synergy findings. Since the formulated NP follows a 3-in-1 design, the individual drug concentrations cannot be adjusted without altering the others. Therefore, careful optimization is required to ensure final encapsulated concentrations maintain the synergistic ratio, otherwise the desired combinatorial effect will not be observed. Further studies need to be conducted to determine final encapsulated olaparib and metformin concentrations to confirm they are within the concentration range that is synergistic with 100nM cisplatin, the chosen concentration for the presented cytotoxicity studies. If results indicate otherwise, NP synthesis adjustments should be made. All things considered, it is possible that the current DTB-Ola-C_{16}-Met-NP lacks synergy, preventing low cisplatin concentration from reaching a more maximal effect. Although the 3-in-1 approach has constraints on drug concentration adjustments, the advantage of this strategy as opposed to three separate NPs dosed together, is vehicle homogeneity[65]. The slightest difference in any parameter (size, surface charge, morphology, for example) between three separate NPs could alter the uniform in vitro and in vivo behaviour, including distribution, serum protein interaction, and cellular uptake[65]. Optimizing only one NP system ensures identical pharmacokinetics for all three drugs.

Additionally, as evidenced by the cisplatin release studies, only about 65% of cisplatin can contribute to cytotoxicity at pH 5.5 after 72-hours. Therefore, dosing modifications should also be considered to ensure the desired concentration is obtained when 65% of cisplatin is released rather than 100%. Lastly, the 72-hour time frame used for all cytotoxicity studies may not be sufficient to observe substantial cell death. Our DNA damage, PARP cleavage, and pAMPK expression data does provide supporting evidence that cytotoxicity from DTB-Ola-C_{16}-Met-NP should be attainable; however, this may only be possible with longer treatment times.

4.6 Future directions

Since the initial purpose of these studies was to determine proof of concept, all experiments were performed in SKOV-3 cells, a common cell line to broadly study ovarian cancer. Future studies should be conducted in ID8;$p53^{-/-}$;$BRCA1^{-/-}$ and cisplatin-sensitive (A2780-S) versus cisplatin-resistant (A2780-CP) cells to validate DTB-Ola-C_{16}-Met-NP efficacy at inducing synthetic lethality and targeting resistant cells, respectively.

Moreover, DTB-Ola-C_{16}-Met-NP biodistribution and tumor-inhibiting efficacy should be evaluated using in vivo models. Specifically, mice bearing orthotopic tumors provides the most clinically relevant model[116]. Biodistribution of fluorescently tagged NPs can be assessed using In Vivo Imaging System to confirm preferential distribution to the tumor as opposed to common organs targeted by free drug, including liver, spleen, heart, and kidney[117]. Tumor volume and weight measurements will help determine tumor burden post treatment.

Finally, the synthesized cisplatin prodrug library fosters future exploration of diverse NP synthesis. Although additional studies are required to understand the full potential of DTB and AA Polymer, the focus of this project, NPs encapsulating CBTA versus PIMA Polymer should also be evaluated. The higher cisplatin content measured in these polymers, 27% and 40% respectively, increases the attractiveness for further studies.

5.0 Conclusion

Ovarian cancer affects approximately 3000 Canadian women every year[2]. However, response to treatment remains limited due to chemotherapy resistance and systemic toxicities. Here, we sought to develop a novel nanotherapeutic-based combinatorial treatment involving cisplatin, olaparib, and metformin. We successfully synthesized a library of cisplatin prodrugs and metformin derivatives to ensure adequate encapsulation inside PLGA-PEG NP hydrophobic core. Our synergy findings demonstrated that all three agents operate synergistically when combined at certain concentrations. PLGA-PEG NPs encapsulating AA or DTB Polymer, olaparib, and/or C_{16}-Met or C_6-Met were formulated while considering the identified synergistic ratio. Final formulations were optimized according to morphology, size, PDI, surface charge, and EE. However, additional efforts are required to solidify olaparib and metformin EE. Nonetheless, using the presented formulations, individual drug effects were demonstrated. DNA damage induced by cisplatin from encapsulated AA or DTB Polymer was shown by using γH2AX flow cytometry assays. Additionally, we revealed preliminary evidence of PARP and caspase-3 cleavage as well as pAMPK expression caused by encapsulated olaparib and free C_{16}-Met or C_6-Met, respectively, by western blot analysis. Finally, further research should focus to improve in vitro DTB-Ola-C_{16}-Met-NP cytotoxicity.

References

1. Lengyel E. Ovarian cancer development and metastasis. *Am J Pathol*. 2010;177(3):1053. doi:10.2353/AJPATH.2010.100105

2. The impact of ovarian cancer. Cure Our Ovarian Cancer. Accessed May 9, 2024. https://cureourovariancancer.org/ovarian-cancer-day/

3. Ovarian cancer statistics. Canadian Cancer Society. Updated November 2023. Accessed May 9, 2024. https://cancer.ca/en/cancer-information/cancer-types/ovarian/statistics

4. Momenimovahed Z, Tiznobaik A, Taheri S, Salehiniya H. Ovarian cancer in the world: epidemiology and risk factors. *Int J Womens Health*. 2019;11:287. doi:10.2147/IJWH.S197604

5. Helm CW, States JC. Enhancing the efficacy of cisplatin in ovarian cancer treatment – could arsenic have a role. *J Ovarian Res*. 2009;2(1):2. doi:10.1186/1757-2215-2-2

6. Köbel M, Kang EY. The evolution of ovarian carcinoma subclassification. *Cancers (Basel)*. 2022;14(2). doi:10.3390/CANCERS14020416

7. Zamwar UM, Anjankar AP. Aetiology, epidemiology, histopathology, classification, detailed evaluation, and treatment of ovarian cancer. *Cureus*. 2022;14(10). doi:10.7759/CUREUS.30561

8. Ricci F, Affatato R, Carrassa L, Damia G. Recent insights into mucinous ovarian carcinoma. *Int J Mol Sci*. 2018;19(6). doi:10.3390/IJMS19061569

9. Eisenkop SM, Friedman RL, Wang HJ. Complete cytoreductive surgery is feasible and maximizes survival in patients with advanced epithelial ovarian cancer: A prospective study. *Gynecol Oncol*. 1998;69(2):103-108. doi:10.1006/GYNO.1998.4955

10. Munnell EW. The changing prognosis and treatment in cancer of the ovary. *CA Cancer J Clin*. 1968;18(5):298-299. doi:10.3322/CANJCLIN.18.5.298

11. Griffiths C. Surgical resection of tumor bulk in the primary treatment of ovarian carcinoma. *Natl Cancer Inst Monogr*. Published online 1975.

12. Rosenberg B, VanCamp L, Trosko JE, Mansour VH. Platinum compounds: a new class of potent antitumour agents. *Nature*. 1969;222(5191):385-386. doi:10.1038/222385A0

13. Dasari S, Bernard Tchounwou P. Cisplatin in cancer therapy: molecular mechanisms of action. *Eur J Pharmacol*. 2014;740:364. doi:10.1016/J.EJPHAR.2014.07.025

14. Podhorecka M, Skladanowski A, Bozko P. H2AX phosphorylation: Its role in DNA damage response and cancer therapy. *J Nucleic Acids*. 2010;2010. doi:10.4061/2010/920161

15. Collins PL, Purman C, Porter SI, et al. DNA double-strand breaks induce H2Ax phosphorylation domains in a contact-dependent manner. *Nature Communications 2020 11:1*. 2020;11(1):1-9. doi:10.1038/s41467-020-16926-x

16. Zheng YR, Suntharalingam K, Johnstone TC, et al. Pt(IV) prodrugs designed to bind non-covalently to human serum albumin for drug delivery. *J Am Chem Soc*. 2014;136(24):8790-8798. doi:10.1021/JA5038269/SUPPL_FILE/JA5038269_SI_001.PDF

17. Harries M, Kaye SB. Recent advances in the treatment of epithelial ovarian cancer. *Expert Opin Investig Drugs*. 2001;10(9):1715-1724. doi:10.1517/13543784.10.9.1715

18. Thorn CF, Oshiro C, Marsh S, et al. Doxorubicin pathways: pharmacodynamics and adverse effects. *Pharmacogenet Genomics*. 2011;21(7):440. doi:10.1097/FPC.0B013E32833FFB56

19. Tacar O, Sriamornsak P, Dass CR. Doxorubicin: an update on anticancer molecular action, toxicity and novel drug delivery systems. *Journal of Pharmacy and Pharmacology*. 2013;65(2):157-170. doi:10.1111/J.2042-7158.2012.01567.X

20. McGuire WP, Hoskins WJ, Brady MF, et al. Cyclophosphamide and cisplatin compared with paclitaxel and cisplatin in patients with stage III and stage IV ovarian cancer. *New England Journal of Medicine*. 1996;334(1):1-6. doi:10.1056/NEJM199601043340101/ASSET/EB131B7D-88E6-41D8-87A8-821A885A5529/ASSETS/IMAGES/LARGE/NEJM199601043340101_F1.JPG

21. Omura GA, Bundy BN, Berek JS, Curry S, Delgado G, Mortel R. Randomized trial of cyclophosphamide plus cisplatin with or without doxorubicin in ovarian carcinoma: A gynecologic oncology group study. *J Clin Oncol*. 1989;7(4):457-465. doi:10.1200/JCO.1989.7.4.457

22. Neijt JP, Van Der Burg MEL, Vriesendorp R, et al. Randomised trial comparing two combination chemotherapy regimens (Hexa-CAF vs CHAP-5) in advanced ovarian carcinoma. *Lancet*. 1984;2(8403):594-600. doi:10.1016/S0140-6736(84)90594-4

23. Ushijima K. Treatment for recurrent ovarian cancer—at first relapse. *J Oncol*. 2010;2010. doi:10.1155/2010/497429

24. Pignata S, Cecere SC, Du Bois A, Harter P, Heitz F. Treatment of recurrent ovarian cancer. *Ann Oncol*. 2017;28(suppl_8):viii51-viii56. doi:10.1093/ANNONC/MDX441

25. Howell SB, Safaei R, Larson CA, Sailor MJ. Copper transporters and the cellular pharmacology of the platinum-containing cancer drugs. *Mol Pharmacol*. 2010;77(6):887. doi:10.1124/MOL.109.063172

26. Maryon EB, Zhang J, Jellison JW, Kaplan JH. Human copper transporter 1 lacking O-linked glycosylation is proteolytically cleaved in a Rab9-positive endosomal compartment. *J Biol Chem*. 2009;284(41):28104-28114. doi:10.1074/JBC.M109.044925

27. Ling X, Chen X, Riddell IA, et al. Glutathione-scavenging poly(disulfide amide) nanoparticles for the effective delivery of Pt(IV) prodrugs and reversal of cisplatin resistance. *Nano Lett*. 2018;18(7):4618-4625. doi:10.1021/ACS.NANOLETT.8B01924/SUPPL_FILE/NL8B01924_SI_001.PDF

28. Kelland L. The resurgence of platinum-based cancer chemotherapy. *Nature Reviews Cancer 2007 7:8*. 2007;7(8):573-584. doi:10.1038/nrc2167

29. Li S, Li C, Jin S, et al. Overcoming resistance to cisplatin by inhibition of glutathione S-transferases (GSTs) with ethacraplatin micelles in vitro and in vivo. *Biomaterials*. 2017;144:119-129. doi:10.1016/J.BIOMATERIALS.2017.08.021

30. Kuo MT, Chen HHW. Role of glutathione in the regulation of cisplatin resistance in cancer chemotherapy. *Met Based Drugs*. 2010;2010. doi:10.1155/2010/430939

31. Armstrong RN. Structure, catalytic mechanism, and evolution of the glutathione transferases. *Chem Res Toxicol*. 1997;10(1):2-18. doi:10.1021/TX960072X/ASSET/TX960072X.FP.PNG_V03

32. Lewis AD, Hayes JD, Wolf CR. Glutathione and glutathione-dependent enzymes in ovarian adenocarcinoma cell lines derived from a patient before and after the onset of drug resistance: intrinsic differences and cell cycle effects. *Carcinogenesis*. 1988;9(7):1283-1287. doi:10.1093/CARCIN/9.7.1283

33. Pasello M, Michelacci F, Scionti I, et al. Overcoming glutathione S-transferase P1-related cisplatin resistance in osteosarcoma. *Cancer Res*. 2008;68(16):6661-6668. doi:10.1158/0008-5472.CAN-07-5840

34. Plummer R. Poly(ADP-ribose) polymerase inhibition: a new direction for BRCA and triple-negative breast cancer? *Breast Cancer Res*. 2011;13(4):218. doi:10.1186/BCR2877

35. Heale JT, Ball AR, Schmiesing JA, et al. Condensin I interacts with the PARP-1-XRCC1 complex and functions in DNA single-strand break repair. *Mol Cell*. 2006;21(6):837-848. doi:10.1016/J.MOLCEL.2006.01.036

36. Ben Ali F, Qmichou Z, Oukabli M, et al. Alteration of glucose metabolism and expression of glucose transporters in ovarian cancer. *Open Exploration 2019 5:2*. 2024;5(2):384-399. doi:10.37349/ETAT.2024.00224

37. Pan Z, Zhang H, Dokudovskaya S. The role of mTORC1 pathway and autophagy in resistance to platinum-based chemotherapeutics. *Int J Mol Sci*. 2023;24(13). doi:10.3390/IJMS241310651

38. Alabdullah ML, Ahmad DA, Moseley P, Madhusudan S, Chan S, Rakha E. The mTOR downstream regulator (p-4EBP1) is a novel independent prognostic marker in ovarian cancer. *J Obstet Gynaecol*. 2019;39(4):522-528. doi:10.1080/01443615.2018.1534091

39. Lu H, Hu H, Li S. Diagnostic value of beclin-1 and mTOR in ovarian cancer. *Int J Clin Exp Pathol*. 2021;14(2):238. Accessed November 27, 2023. /pmc/articles/PMC7868785/

40. Gremke N, Polo P, Dort A, et al. mTOR-mediated cancer drug resistance suppresses autophagy and generates a druggable metabolic vulnerability. *Nature Communications 2020 11:1*. 2020;11(1):1-15. doi:10.1038/s41467-020-18504-7

41. Janku F, Yap TA, Meric-Bernstam F. Targeting the PI3K pathway in cancer: are we making headway? *Nature Reviews Clinical Oncology 2018 15:5*. 2018;15(5):273-291. doi:10.1038/nrclinonc.2018.28

42. Hudes G, Carducci M, Tomczak P, et al. Temsirolimus, interferon alfa, or both for advanced renal-cell carcinoma. *New England Journal of Medicine*. 2007;356(22):2271-2281. doi:10.1056/NEJMOA066838/ASSET/7C776AAE-DC6F-47D2-B27B-EE9896392140/ASSETS/IMAGES/LARGE/NEJMOA066838_T4.JPG

43. Zhang C, Xu C, Gao X, Yao Q. Platinum-based drugs for cancer therapy and anti-tumor strategies. *Theranostics*. 2022;12(5):2115. doi:10.7150/THNO.69424

44. Wright AA, Cronin A, Milne DE, et al. Use and effectiveness of intraperitoneal chemotherapy for treatment of ovarian cancer. *Journal of Clinical Oncology*. 2015;33(26):2841. doi:10.1200/JCO.2015.61.4776

45. Ward BG, Mather SJ, Hawkins LR, et al. Localization of radioiodine conjugated to the monoclonal antibody HMFG2 in human ovarian carcinoma: assessment of intravenous and intraperitoneal routes of administration. *Cancer Res*. 1987;47(17):4719-4723.

46. Balmaña J, Tung NM, Isakoff SJ, et al. Phase I trial of olaparib in combination with cisplatin for the treatment of patients with advanced breast, ovarian and other solid tumors. *Annals of Oncology*. 2014;25(8):1656-1663. doi:10.1093/annonc/mdu187

47. Gao J, Wang Z, Fu J, A. J, Ohno Y, Xu C. Combination treatment with cisplatin, paclitaxel and olaparib has synergistic and dose reduction potential in ovarian cancer cells. *Exp Ther Med*. 2021;22(3). doi:10.3892/ETM.2021.10367

48. Li X, Ng ASN, Mak VCY, Chan KKL, Cheung ANY, Cheung LWT. Strategic combination therapies for ovarian cancer. *Curr Cancer Drug Targets*. 2020;20(8):573-585. doi:10.2174/1568009620666200511084007

49. Chen A. PARP inhibitors: its role in treatment of cancer. *Chin J Cancer*. 2011;30(7):463. doi:10.5732/CJC.011.10111

50. Hou Z, Cui Y, Xing H, Mu X. Down-expression of poly(ADP-ribose) polymerase in p53-regulated pancreatic cancer cells. *Oncol Lett*. 2018;15(2):1943. doi:10.3892/OL.2017.7500

51. Passaro C, Volpe M, Botta G, et al. PARP inhibitor olaparib increases the oncolytic activity of dl922-947 in in vitro and in vivo model of anaplastic thyroid carcinoma. *Mol Oncol*. 2015;9(1):78-92. doi:10.1016/J.MOLONC.2014.07.022

52. Liu PF, Hu YC, Kang BH, et al. Expression levels of cleaved caspase-3 and caspase-3 in tumorigenesis and prognosis of oral tongue squamous cell carcinoma. *PLoS One*. 2017;12(7). doi:10.1371/JOURNAL.PONE.0180620

53. Tang S, Shen Y, Wei X, Shen Z, Lu W, Xu J. Olaparib synergizes with arsenic trioxide by promoting apoptosis and ferroptosis in platinum-resistant ovarian cancer. *Cell Death & Disease 2022 13:9*. 2022;13(9):1-14. doi:10.1038/s41419-022-05257-y

54. Arnaudeau C, Lundin C, Helleday T. DNA double-strand breaks associated with replication forks are predominantly repaired by homologous recombination involving an exchange mechanism in mammalian cells. *J Mol Biol*. 2001;307(5):1235-1245. doi:10.1006/JMBI.2001.4564

55. Helleday T. The underlying mechanism for the PARP and BRCA synthetic lethality: clearing up the misunderstandings. *Mol Oncol*. 2011;5(4):387. doi:10.1016/J.MOLONC.2011.07.001

56. Manchana T, Phoolcharoen N, Tantbirojn P. BRCA mutation in high grade epithelial ovarian cancers. *Gynecol Oncol Rep*. 2019;29:102. doi:10.1016/J.GORE.2019.07.007

57. Segal ED, Yasmeen A, Beauchamp MC, Rosenblatt J, Pollak M, Gotlieb WH. Relevance of the OCT1 transporter to the antineoplastic effect of biguanides. *Biochem Biophys Res Commun*. 2011;414(4):694-699. doi:10.1016/J.BBRC.2011.09.134

58. Yang C, Zhao N, Li D, Zou G, Chen Y. Metformin improves the sensitivity of ovarian cancer cells to chemotherapeutic agents. *Oncol Lett*. 2019;18(3):2404. doi:10.3892/OL.2019.10564

59. Rena G, Hardie DG, Pearson ER. The mechanisms of action of metformin. *Diabetologia*. 2017;60(9):1577. doi:10.1007/S00125-017-4342-Z

60. Rattan R, Graham RP, Maguire JL, Giri S, Shridhar V. Metformin suppresses ovarian cancer growth and metastasis with enhancement of cisplatin cytotoxicity in vivo. *Neoplasia*. 2011;13(5):483. doi:10.1593/NEO.11148

61. Zou G, Bai J, Li D, Chen Y. Effect of metformin on the proliferation, apoptosis, invasion and autophagy of ovarian cancer cells. *Exp Ther Med*. 2019;18(3):2086. doi:10.3892/ETM.2019.7803

62. Zheng Y, Zhu J, Zhang H, Liu Y, Sun H. Metformin inhibits ovarian cancer growth and migration in vitro and in vivo by enhancing cisplatin cytotoxicity. *Am J Transl Res*. 2018;10(10):3086. Accessed May 12, 2024. /pmc/articles/PMC6220222/

63. Ricci F, Brunelli L, Affatato R, et al. Overcoming platinum-acquired resistance in ovarian cancer patient-derived xenografts. *Ther Adv Med Oncol*. 2019;11. doi:10.1177/1758835919839543

64. Tallarida RJ. Quantitative methods for assessing drug synergism. *Genes Cancer*. 2011;2(11):1003. doi:10.1177/1947601912440575

65. Gadde S. Multi-drug delivery nanocarriers for combination therapy. *Medchemcomm*. 2015;6(11):1916-1929. doi:10.1039/C5MD00365B

66. Foretz M, Guigas B, Viollet B. Metformin: update on mechanisms of action and repurposing potential. *Nature Reviews Endocrinology 2023 19:8*. 2023;19(8):460-476. doi:10.1038/s41574-023-00833-4

67. Zoń A, Bednarek I. Cisplatin in ovarian cancer treatment—known limitations in therapy force new solutions. *Int J Mol Sci*. 2023;24(8). doi:10.3390/IJMS24087585

68. Lynparza : EPAR – Product Information. European Medicines Agency. January 9, 2015. Updated January 4, 2024. Accessed May 14, 2024. https://www.ema.europa.eu/en/medicines/human/EPAR/lynparza

69. Torchilin VP. Recent advances with liposomes as pharmaceutical carriers. *Nature Reviews Drug Discovery 2005 4:2*. 2005;4(2):145-160. doi:10.1038/nrd1632

70. Cortes JE, Goldberg SL, Feldman EJ, et al. Phase II, multicenter, randomized trial of CPX-351 (cytarabine:daunorubicin) liposome injection versus intensive salvage therapy in adults with first relapse AML. *Cancer*. 2015;121(2):234-242. doi:10.1002/CNCR.28974

71. Gabizon A, Shmeeda H, Barenholz Y. Pharmacokinetics of pegylated liposomal doxorubicin: review of animal and human studies. *Clin Pharmacokinet*. 2003;42(5):419-436. doi:10.2165/00003088-200342050-00002/METRICS

72. Pridgen EM, Langer R, Farokhzad OC. Biodegradable, polymeric nanoparticle delivery systems for cancer therapy. *Nanomedicine*. 2007;2(5):669-681. doi:10.2217/17435889.2.5.669

73. Cheng J, Teply BA, Sherifi I, et al. Formulation of functionalized PLGA-PEG nanoparticles for in vivo targeted drug delivery. *Biomaterials*. 2007;28(5):869-876. doi:10.1016/J.BIOMATERIALS.2006.09.047

74. Kamaly N, Yameen B, Wu J, Farokhzad OC. Degradable controlled-release polymers and polymeric nanoparticles: mechanisms of controlling drug release. *Chem Rev*. 2016;116(4):2602. doi:10.1021/ACS.CHEMREV.5B00346

75. Hrkach J, Von Hoff D, Ali MM, et al. Preclinical development and clinical translation of a PSMA-targeted docetaxel nanoparticle with a differentiated pharmacological profile. *Sci Transl Med*. 2012;4(128). doi:10.1126/SCITRANSLMED.3003651

76. Longmire M, Choyke PL, Kobayashi H. Clearance properties of nano-sized particles and molecules as imaging agents: considerations and caveats. *Nanomedicine (Lond)*. 2008;3(5):703. doi:10.2217/17435889.3.5.703

77. Desai MP, Labhasetwar V, Walter E, Levy RJ, Amidon GL. The mechanism of uptake of biodegradable microparticles in Caco-2 cells is size dependent. *Pharm Res*. 1997;14(11):1568-1573. doi:10.1023/A:1012126301290

78. Aggarwal P, Hall JB, McLeland CB, Dobrovolskaia MA, McNeil SE. Nanoparticle interaction with plasma proteins as it relates to particle biodistribution, biocompatibility and therapeutic efficacy. *Adv Drug Deliv Rev*. 2009;61(6):428. doi:10.1016/J.ADDR.2009.03.009

79. Chan WCW. Principles of nanoparticle delivery to solid tumors. *BME Front*. 2023;4. doi:10.34133/BMEF.0016

80. Kolishetti N, Dhar S, Valencia PM, et al. Engineering of self-assembled nanoparticle platform for precisely controlled combination drug therapy. *Proc Natl Acad Sci U S A*. 2010;107(42):17939-17944. doi:10.1073/PNAS.1011368107

81. Valencia PM, Pridgen EM, Perea B, et al. Synergistic cytotoxicity of irinotecan and cisplatin in dual-drug targeted polymeric nanoparticles. *Nanomedicine (Lond)*. 2013;8(5):687-698. doi:10.2217/NNM.12.134

82. Dhar S, Gu FX, Langer R, Farokhza OC, Lippard SJ. Targeted delivery of cisplatin to prostate cancer cells by aptamer functionalized Pt(IV) prodrug-PLGA - PEG nanoparticles. *Proc Natl Acad Sci U S A*. 2008;105(45):17356-17361. doi:10.1073/PNAS.0809154105/SUPPL_FILE/0809154105SI.PDF

83. Chou TC. Drug combination studies and their synergy quantification using the Chou-Talalay method. *Cancer Res*. 2010;70(2):440-446. doi:10.1158/0008-5472.CAN-09-1947

84. Pavillard V, Kherfellah D, Richard S, Robert J, Montaudon D. Effects of the combination of camptothecin and doxorubicin or etoposide on rat glioma cells and camptothecin-resistant variants. *Br J Cancer*. 2001;85(7):1077. doi:10.1054/BJOC.2001.2027

85. Raitanen M, Rantanen V, Kulmala J, Helenius H, Grénman R, Grénman S. Supra-additive effect with concurrent paclitaxel and cisplatin in vulvar squamous cell carcinoma in vitro. *Int J Cancer*. 2002;100(2):238-243. doi:10.1002/IJC.10472

86. Lancet JE, Uy GL, Newell LF, et al. CPX-351 versus 7+3 cytarabine and daunorubicin chemotherapy in older adults with newly diagnosed high-risk or secondary acute myeloid leukaemia: 5-year results of a randomised, open-label, multicentre, phase 3 trial. *Lancet Haematol*. 2021;8(7):e481-e491. doi:10.1016/S2352-3026(21)00134-4

87. Mayer LD, Tardi P, Louie AC. CPX-351: a nanoscale liposomal co-formulation of daunorubicin and cytarabine with unique biodistribution and tumor cell uptake properties. *Int J Nanomedicine*. 2019;14:3819. doi:10.2147/IJN.S139450

88. Lancet JE, Uy GL, Cortes JE, et al. CPX-351 (cytarabine and daunorubicin) liposome for injection versus conventional cytarabine plus daunorubicin in older patients with newly diagnosed secondary acute myeloid leukemia. *Journal of Clinical Oncology*. 2018;36(26):2684. doi:10.1200/JCO.2017.77.6112

89. Sengupta S, Eavarone D, Capila I, et al. Temporal targeting of tumour cells and neovasculature with a nanoscale delivery system. *Nature 2005 436:7050*. 2005;436(7050):568-572. doi:10.1038/nature03794

90. Lanao RPF, Jonker AM, Wolke JGC, Jansen JA, Van Hest JCM, Leeuwenburgh SCG. Physicochemical properties and applications of poly(lactic-co-glycolic acid) for use in bone regeneration. *Tissue Eng Part B Rev*. 2013;19(4):380. doi:10.1089/TEN.TEB.2012.0443

91. Kenley RA, Lee MO, Mahoney TR, Sanders LM. Poly(lactide-co-glycolide) decomposition kinetics in vivo and in vitro. *Macromolecules*. 1987;20(10):2398-2403. doi:10.1021/MA00176A012/ASSET/MA00176A012.FP.PNG_V03

92. Liping Y, Jian H, Zhenchao T, et al. GSH-responsive poly-resveratrol based nanoparticles for effective drug delivery and reversing multidrug resistance. *Drug Deliv*. 2022;29(1):229. doi:10.1080/10717544.2021.2023700

93. Iyer R, Nguyen T, Padanilam D, et al. Glutathione-responsive biodegradable polyurethane nanoparticles for lung cancer treatment. *J Control Release*. 2020;321:363. doi:10.1016/J.JCONREL.2020.02.021

94. Matsumura Y, Maeda H. A new concept for macromolecular therapeutics in cancer chemotherapy: mechanism of tumoritropic accumulation of proteins and the antitumor agent smancs. *Cancer Res*. Published online 1986.

95. Maeda H, Tsukigawa K, Fang J. A retrospective 30 years after discovery of the enhanced permeability and retention effect of solid tumors: next-generation chemotherapeutics and photodynamic therapy—problems, solutions, and prospects. *Microcirculation*. 2016;23(3):173-182. doi:10.1111/MICC.12228

96. Bortot B, Mongiat M, Valencic E, et al. Nanotechnology-based cisplatin intracellular delivery to enhance chemo-sensitivity of ovarian cancer. *Int J Nanomedicine*. 2020;15:4793. doi:10.2147/IJN.S247114

97. Cheng L, Jin C, Lv W, Ding Q, Han X. Developing a highly stable PLGA-mPEG nanoparticle loaded with cisplatin for chemotherapy of ovarian cancer. *PLoS One*. 2011;6(9):e25433. doi:10.1371/JOURNAL.PONE.0025433

98. Mensah LB, Morton SW, Li J, et al. Layer-by-layer nanoparticles for novel delivery of cisplatin and PARP inhibitors for platinum-based drug resistance therapy in ovarian cancer. *Bioeng Transl Med*. 2019;4(2). doi:10.1002/BTM2.10131

99. Faramarzi L, Dadashpour M, Sadeghzadeh H, Mahdavi M, Zarghami N. Enhanced anti-proliferative and pro-apoptotic effects of metformin encapsulated PLGA-PEG nanoparticles on SKOV3 human ovarian carcinoma cells. *Artif Cells Nanomed Biotechnol*. 2019;47(1):737-746. doi:10.1080/21691401.2019.1573737

100. Saber MM, Al-mahallawi AM, Nassar NN, Stork B, Shouman SA. Targeting colorectal cancer cell metabolism through development of cisplatin and metformin nano-cubosomes. *BMC Cancer*. 2018;18(1):1-11. doi:10.1186/S12885-018-4727-5/FIGURES/7

101. Xiong Y, Zhao Y, Miao L, Lin CM, Huang L. Co-delivery of polymeric metformin and cisplatin by self-assembled core-membrane nanoparticles to treat non-small cell lung cancer. *J Control Release*. 2016;244(Pt A):63-73. doi:10.1016/J.JCONREL.2016.11.005

102. Yadav B, Wennerberg K, Aittokallio T, Tang J. Searching for drug synergy in complex dose–response landscapes using an interaction potency model. *Comput Struct Biotechnol J*. 2015;13:504. doi:10.1016/J.CSBJ.2015.09.001

103. Miller MA, Zheng YR, Gadde S, et al. Tumour-associated macrophages act as a slow-release reservoir of nano-therapeutic Pt(IV) pro-drug. *Nature Communications 2015 6:1*. 2015;6(1):1-13. doi:10.1038/ncomms9692

104. Kamaly N, Fredman G, Subramanian M, et al. Development and in vivo efficacy of targeted polymeric inflammation- resolving nanoparticles. *Proc Natl Acad Sci U S A*. 2013;110(16):6506-6511. doi:10.1073/PNAS.1303377110/-/DCSUPPLEMENTAL/PNAS.201303377SI.PDF

105. Kim J, Pramanick S, Lee D, Park H, Kim WJ. Polymeric biomaterials for the delivery of platinum-based anticancer drugs. *Biomater Sci*. 2015;3(7):1002-1017. doi:10.1039/C5BM00039D

106. Gabano E, Pinton G, Balzano C, et al. Unsymmetric cisplatin-based Pt(IV) conjugates containing a PARP-1 inhibitor pharmacophore tested on malignant pleural mesothelioma cell lines. *Molecules 2021, Vol 26, Page 4740*. 2021;26(16):4740. doi:10.3390/MOLECULES26164740

107. Feng WQ, Wang LY, Gao J, et al. Solid state and solubility study of a potential anticancer drug-drug molecular salt of diclofenac and metformin. *J Mol Struct*. 2021;1234:130166. doi:10.1016/J.MOLSTRUC.2021.130166

108. Zhou WX, Zhao HW, Chen HH, Zhang ZY, Chen DY. Characterization of drug–drug salt forms of metformin and aspirin with improved physicochemical properties. *CrystEngComm*. 2019;21(25):3770-3773. doi:10.1039/C9CE00377K

109. Zhang Q, Lv Q, Zhang D, Jiang W, Zhang H, Zhang W. Influence of hydrogen bonding on the photophysical properties of diethylamino hydroxybenzoyl hexyl benzoate. *Processes 2023, Vol 11, Page 2077*. 2023;11(7):2077. doi:10.3390/PR11072077

110. Makadia HK, Siegel SJ. Poly lactic-co-glycolic acid (PLGA) as biodegradable controlled drug delivery carrier. *Polymers (Basel)*. 2011;3(3):1377. doi:10.3390/POLYM3031377

111. Yang J, Liu W, Sui M, Tang J, Shen Y. Platinum (IV)-coordinate polymers as intracellular reduction-responsive backbone-type conjugates for cancer drug delivery. *Biomaterials*. 2011;32(34):9136-9143. doi:10.1016/J.BIOMATERIALS.2011.08.022

112. Lopez-Sanchez A, Bertrand HC. Pt(IV) anticancer prodrugs bearing an oxaliplatin scaffold: what do we know about their bioactivity? *Inorg Chem Front*. 2024;11(6):1639-1667. doi:10.1039/D3QI02602G

113. Wintzell M, Löfstedt L, Johansson J, Pedersen AB, Fuxe J, Shoshan M. Repeated cisplatin treatment can lead to a multiresistant tumor cell population with stem cell features and sensitivity to 3-bromopyruvate. *Cancer Biol Ther*. 2012;13(14):1454. doi:10.4161/CBT.22007

114. Smith JA, Ngo H, Martin MC, Wolf JK. An evaluation of cytotoxicity of the taxane and platinum agents combination treatment in a panel of human ovarian carcinoma cell lines. *Gynecol Oncol*. 2005;98(1):141-145. doi:10.1016/J.YGYNO.2005.02.006

115. Chithrani BD, Ghazani AA, Chan WCW. Determining the size and shape dependence of gold nanoparticle uptake into mammalian cells. *Nano Lett*. 2006;6(4):662-668. doi:10.1021/NL052396O

116. Lwin TM, Hoffman RM, Bouvet M. Advantages of patient-derived orthotopic mouse models and genetic reporters for developing fluorescence-guided surgery. *J Surg Oncol*. 2018;118(2):253. doi:10.1002/JSO.25150

117. Sulaiman A, McGarry S, El-Sahli S, et al. Co-targeting bulk tumor and CSCs in clinically translatable TNBC patient-derived xenografts via combination nanotherapy. *Mol Cancer Ther*. 2019;18(10):1755-1764. doi:10.1158/1535-7163.MCT-18-0873/87369/AM/CO-TARGETING-BULK-TUMOR-AND-CSCS-IN-CLINICALLY

Contribution of Collaborators

Sean McGrath (PhD student) from Dr. Naomi Matsuura's lab at the University of Toronto performed all ICP-MS runs for cisplatin EE (Figure 13F) and drug release kinetic (Figure 15) measurements. Esha Gahunia (Honours student) performed surface charge measurements for Figure 13E.